Complexity of Ca^{2+} signals in astrocytes

-Contribution of astroglial $GABA_B$ receptors-

Dissertation

zur Erlangung des akademischen Grades des Doktors

der Naturwissenschaften (Dr. rer. nat.)

der Medizinischen Fakultät, Institut für Physiologie,

der Universität des Saarlandes

vorgelegt von

Laura Stopper

(geb. Schlosser)

Geboren in Wadern

Homburg, September 2018

The experimental work depicted in this thesis has been carried out at the Center for Integrative Physiology and Molecular Medicine in the Department of Molecular Physiology at the University of Saarland, Germany. The work was done independently from November 2013 until September 2018 with no other sources than stated by me.

1. Referee:
Prof. Dr. Frank Kirchhoff
University of Saarland
Center for Physiology and Molecular Medicine
Department of Molecular Physiology
Building 48
66421 Homburg

2. Referee:
Prof. Dr. Carola Meier
University of Saarland
Institute of Anatomy and Cell biology
Building 61
66421 Homburg

Day of defense: _____

FÜR MEINE LIEBEN

CONTENT

Abbreviation

AMPA	α-amino-3-hydroxy-5-methly-4-isoxazolpropionat
bp	base pair
cAMP	cyclic adenosine monophosphate
cb	cerebellum
cl	contralateral
CNS	central nervous system
ctx	cortex
cKO	conditional knock out
con	Control
DNA	deoxyribonucleic acid
EDTA	ethylenediaminetetraacetic protein
lsl	fl/stop/fl
f.c.	final concentration
g	gravitation
FOV	field of view
GABA	γ-amino butyric acid
GFP	green fluorescent protein
fl	floxed
HS	horse serum
HSP	Heat shock protein
ll	ipsilateral
kDa	kilo Dalton
KI	knock in
LoxP	locus of crossover of the bacteriophage P1
LSM	laser scanning microscopy
mc	monoclonal
mRNA	messenger ribonucleic acid
NMDA	N-methyl-D-aspartate
OPC	oligodendrocyte precursor cell
p	p-value
pc	polyclonal
RNA	ribonucleic acid
ROI	region of interest
RT	room temperature
TAq	Thermophilus aquaticus
TgH	transgenic mouse generated by homologous recombination
Tris	tris(hydroxymethyl)aminoethane
UV	ultraviolet light
wt	wild type
%ile	percentile
2P	2 Photon

The dimensions of this thesis are consistent with international System of Units (SI).

List of Figures

List of Table

ZUSAMMENFASSUNG

Neben Neuronen sind Astrozyten an der Signalübertragung der Synapse beteiligt. Dafür sind sie mit einer Vielzahl von Rezeptoren ausgestattet. Einer dieser Rezeptoren ist der metabotrope $GABA_B$-Rezeptor, der durch den Transmitter GABA (ɣ-Aminobuttersäure) aktiviert wird. In Neuronen führt die Aktivierung des $GABA_B$-Rezeptors, bestehend aus $GABA_{B1}$- und $GABA_{B2}$-Untereinheit, zu einer Aktivierung des inhibitorischen G-Proteins. Abhängig von der Position des Rezeptors kommt es dadurch zu einer Inhibition von Kaliumkanälen oder zu einer Verlängerung der Öffnungswahrscheinlichkeit von Kalziumkanälen. Die Expression und auch die Funktionalität von $GABA_B$-Rezeptoren auf Astrozyten wurde bereits beschrieben, aber die nachgeschaltete Signalkaskade und die Funktion in der Interaktion mit Neuronen ist bisher noch nicht geklärt. Eine Veränderung des intrazellulären Kalziums wird vermutet. Daher haben wir eine Mauslinie generiert, in der die essentielle $GABA_{B1}$-Untereinheit spezifisch in Astrozyten deletiert wird. Hierfür wurde die Tamoxifen induzierbare GLAST-CreERT2-Mauslinie mit der gefloxten $GABA_{B1}$-Linie verpaart (GLAST-CreERT2x$GABA_{B1}^{fl/fl}$). Durch den Verlust der $GABA_{B1}$-Untereinheit kann kein $GABA_B$-Rezeptor mehr gebildet werden. Ein Teil der GLAST-CreERT2x$GABA_{B1}^{fl/fl}$-Linie exprimiert außerdem den genetisch codierten Kalziumindikator GCaMP3, um *in vivo* Kalziumsignale von Kontroll- und Knockout-Tieren zu analysieren. In einen ersten Schritt wurde die genomische DNA Rekombinationseffizienz des gefloxten *gabbr1* Alleles mittels quantitativer real-time PCR in verschiedenen Gehirnarealen drei Wochen nach Tamoxifen-Administration untersucht. Die Analyse der genomischen DNA in den verschiedenen Gehirnarealen; Hirnstamm, Zerebellum, Kortex, Hippocampus und optischer Nerv, zeigte eine Reduktion der gefloxten *gabbr1* Allele (30%, 25%, 25%, 29%, 38%). Diese Reduktion spiegelt auch das relative Verhältnis der Astrozyten in den verschiedenen Regionen wieder. Außerdem konnte eine Reduktion um 50% an gefloxten *gabbr1* Allelen in MACS-isolierten kortikalen Astrozyten beobachtet werden. Auf Grund der hohen Expression der $GABA_B$-Rezeptoren in Neuronen und anderen Zellentypen konnten keine $GABA_{B1}$ mRNA Reduktion in totalen Zellhomogenaten mittels RT-PCR identifiziert werden. In einer NGS-Analyse der $GABA_{B1}$ mRNA in MACS-isolierten Astrozyten aus Zerebellum und Kortex konnte eine Reduktion von 50-70% gezeigt werden. Mittels Fluoreszenz *in situ* Hybridisierung (FISH) konnte der Verlust der mRNA spezifisch in Astrozyten in Zerebellum, Hippocampus und Kortex nachgewiesen werden. Eine genaue Analyse der Expression des $GABA_{B1}$ Protein auf der Membran von Astrozyten mittels Immunhistochemie zeigte den Verlust des Proteins in Kortex, Hippocampus und Zerebellum.

Die Sprache der Astrozyten sind die Kalziumsignale. Um die Auswirkung des Verlustes der astrozytären GABA$_B$-Rezeptoren auf die Kalziumsignale zu evaluieren, wurden anästhesierten und wachen Mäusen mittels 2-Photonen-Mikroskopie untersucht. *In vivo* führt die Deletion von astrozytären GABA$_B$-Rezeptoren zu kleineren und kürzeren Kalziumsignalen im Gliapil von anästhesierten Mäusen. In wachen Tieren sind neben den Signalen im Gliapil, auch somatische Kalziumsignale kleiner und kürzer in der Abwesenheit von GABA$_B$-Rezeptoren in Astrozyten. Zusammenfassend konnte die Deletion der essentiellen GABA$_{B1}$-Untereinheit gezeigt werden. Außerdem konnte gezeigt werden, dass GABA$_B$-Rezeptoren einen Beitrag zu der Komplexität der Kalziumsignale beitragen.

ABSTRACT

Astrocytes are decisively involved in synaptic transmission and for this purpose equipped with transmitter receptors capable of sensing neuronal activity. One of these receptors is the metabotropic $GABA_B$ receptor, a target of the main inhibitory neurotransmitter γ-aminobutyric acid (GABA). In neurons, activation of $GABA_B$ receptors (formed by dimerization of $GABA_{B1}$ and $GABA_{B2}$ subunits) leads to an activation of inhibitory G proteins, resulting in prolonged of opening time of Ca^{2+} channels or inhibition of potassium channels, depending on the localization of the receptors. The presence and the functionality of astrocytic $GABA_B$ receptors are already described but the downstream signaling and the influence in communication of the astrocytes remains unclear. Recent publication suggest a link to intracellular Ca^{2+} signals. Therefore, we generated a genetically modified mouse model where an astroglia-specific deletion of the essential $GABA_B$ receptor subunit $GABA_{B1}$ could be induced by crossbreeding GLAST-CreERT2 with floxed $GABA_{B1}$ mice (GLAST-CreERT2 x $GABA_{B1}$ $^{fl/fl}$). After deleting the $GABA_{B1}$ subunit no functional receptor can be formed. A subset of GLAST-CreERT2 x $GABA_{B1}$ $^{fl/fl}$ also expressed the genetically encoded Ca^{2+} indicator GCaMP3 allowing *in vivo* Ca^{2+} imaging in cKO and control. First, we quantified the genomic DNA recombination efficiency of the floxed *gabbr1* alleles in different brain region by real-time PCR three weeks after the tamoxifen injection. Analysis of genomic DNA purified from brainstem, cerebellum, cortex, hippocampus and optic nerve revealed a significant reduction of floxed gabbr1 alleles (30%, 25%, 25%, 29%, and 38%, respectively). This reflects the relative proportion of astroglia in the respective regions. Furthermore, we could detect loss of 50% of floxed *gabbr1* alleles in MACS isolated cortical astrocytes.

Due to the high expression of neuronal $GABA_B$ receptors and the expression of $GABA_B$ receptors on other cell types a reduction of $GABA_{B1}$ mRNA could not be detected in brain homogenates by real-time PCR. However, using NGS we could detect a significant loss of the $GABA_{B1}$ mRNA on MACS isolated cerebellar and cortical astrocytes (50% and 70%, respectively). Futhermore by using fluorescence in situ hybridization (FISH) we could visualize the loss of mRNA specifically in astrocytes in the cerebellum, hippocampus and cortex. A detailed analysis of $GABA_{B1}$ protein expression in the astrocyte membrane revealed a loss of the protein on the membrane in cortex, hippocampus and cerebellum with immunohistochemistry.

Astrocytes communicate through Ca^{2+} signals. To reveal the impact of $GABA_B$ receptors on Ca^{2+} signals, signals in anesthetized and awake animals were analyzed with the two-photon laser scanning microscopy. *In vivo* the deletion of astrocytic $GABA_B$ receptors resulted in only smaller and shorter Ca^{2+} signals in the gliapil of awake and anesthetized animals.

In awake animals next to the signals in the gliapil, also somatic Ca^{2+} signals were smaller and shorter in the absence of astrocytic $GABA_B$ receptors. In summary, the deletion of the essential $GABA_{B1}$ subunit could be proven and furthermore $GABA_B$ receptors play an important in the complexity of Ca^{2+} signals.

1. INTRODUCTION

1.1 Transmitters and their pathways in the central nervous system

The ability of the central nervous system (CNS) to learn, to memorize, to perceive and to respond to the environment requires highly coordinated network activity of neurons and glia cells. The communication of this network is regulated by transmitters and their corresponding receptors. In the CNS, two main transmitters are responsible for this interaction; the excitatory transmitter glutamate (GLU) and the inhibitory transmitter γ-aminobutyric acid (GABA). The balance of these two transmitters is important for the control of the physiological transmission. Hypoactivity of the GABA signaling is connected to epilepsy, spasticity, depression, sleep disorders, anxiety and stress (Bettler *et al.*, 2004; Kim & Yoon, 2017). Hyperactivity of this system is discussed in the context of schizophrenia (Benes & Berretta, 2001; Schmidt & Mirnics, 2015). Glutamate can bind to the ligand-gated ion channels AMPA (α-amino-3-hydroxy-5-methly-4-isoxazolpropionate), NMDA (N-methyl-D-aspartate) and Kainate, which open fast and have high permeability for cations, or it can also bind to metabotropic glutamate receptors (mGLU). GABA as transmitter plays a central role in controlling neuronal activity (Petroff, 2002). The proportion of cortical GABAergic neurons is between 20% to 44% (Petroff, 2002). The transmitter GABA can be synthetized over two ways: decarboxylation of glutamate by glutamate decarboxylases (GAD) or monoacetylation of putrescine (Petroff, 2002; Yoon *et al.*, 2012). The synthesis over GAD is the most common way and the availability of GABA is dependent on the activity of this enzyme. The enzyme GAD has two different isoforms GAD65 and GAD67, which differ in their molecular weight (Erlander *et al.*, 1991). GAD67 is mainly involved in the synthesis for general metabolic activity, whereas GAD65 is activated by synaptic transmission (Petroff, 2002; Yoon *et al.*, 2012). Neurons express both isoforms but the ratio is region specific. Astrocytes also express both isoforms but less than neurons (Yoon *et al.*, 2012). As transmitter, GABA can also act on two different types of receptors: ionotropic GABA$_A$ and metabotropic GABA$_B$ receptors. Binding of GABA to GABA$_A$ receptors leads to an influx of chloride ions, hyperpolarizing the cell membrane, whereas binding to GABA$_B$ receptors results in an activation of the coupled G protein.

1.1.1 Neuronal GABA$_B$ receptors

Metabotropic GABA$_B$ receptors, discovered in 1980, are G protein coupled receptors (seven trans-membrane domain receptors) and have extremely diverse effects (Bowery *et al.*, 1980). The receptor consist of two subunits, GABA$_{B1}$ and GABA$_{B2}$ (Kaupmann *et al.*, 1998). The GABA$_{B1}$ subunit binds the transmitter through a flytrap, whereas the GABA$_{B2}$ subunit transduces the signal through the coupled G protein into the cell. Therefore, both subunits are essential for building a functional receptor. Through a retention signal in the C-terminus, the GABA$_{B1}$ subunit remains in the endoplasmatic reticulum (ER) until the 1:1 assembly with the GABA$_{B2}$ subunit (Couve *et al.*, 2000; Pagano *et al.*, 2001).

In vertebrates, the GABA$_{B1}$ subunit exist of two isoforms (GABA$_{B1a}$, GABA$_{B1b}$), which both are able to build a functional receptor with the GABA$_{B2}$ subunit (Kaupmann *et al.*, 1997; Benke *et al.*, 1999). Both isoforms are not splice variants, but have a different transcriptional start. The start of the GABA$_{B1b}$ isoform is located in the GABA$_{B1a}$ intron upstream of the exon VI and ends at 5´end of exon VI (Pfaff *et al.*, 1999; Martin *et al.*, 2001). The different transcriptional starts lead to a discrepancy in the N-terminus and in the sushi domains (also known as short consensus repeats), which play a role in protein interactions. The function of the isoforms is still unknown, but the expression pattern of both isoforms differs in location at the synapse and in the developing brain. GABA$_{B1a}$ expression is highly upregulated at birth, whereas in the adulthood GABA$_{B1b}$ is predominantly expressed compared to GABA$_{B1a}$ (Fritschy *et al.*, 2004). At the presynaptic site of excitatory synapses, GABA$_{B1a}$ is mostly expressed, while the GABA$_{B1b}$ isoform is located on spines opposite glutamate releasing sites (Vigot *et al.*, 2006; Chalifoux & Carter, 2011).

In neurons, after GABA binding the coupled G$_{i0}$/G$_o$ protein is separated into α-subunit and βγ-subunit. The α-subunit inhibits the adenylate cyclase resulting in decreased activity of protein kinase A (Xu & Wojcik, 1986; Bowery *et al.*, 2002). Presynaptic voltage- gated Ca^{2+} channels of the N or P/Q type are inhibited through the βγ-subunit (Benarroch, 2012). On the postsynaptic side the opening time of potassium channels are prolonged (Lüscher *et al.*, 1997; Schuler *et al.*, 2001).

GABA$_B$ receptors are also involved in the development of the brain. They can enhance migration of non-neuronal cells (Gaiarsa *et al.*, 2011). During development, there is the so-called GABA-shift. In the development the transmitter GABA provokes to a cell depolarization, while in the adult brain the cells are hyperpolarized. In the developing brain GABA$_A$ receptors are mainly responsible for excitatory activity. But they are controlled by GABA$_B$ receptors through depressing the rise of the intracellular Ca^{2+} (Wu & Sun, 2015).

1.1.2 GABA$_B$ receptors on astrocytes

Astrocytes are involved in neuronal transmission by expressing a variety of transmitter receptors and they release gliotransmitters. Mostly investigated are the role of glutamate and the corresponding receptors in the tripartite synapse.
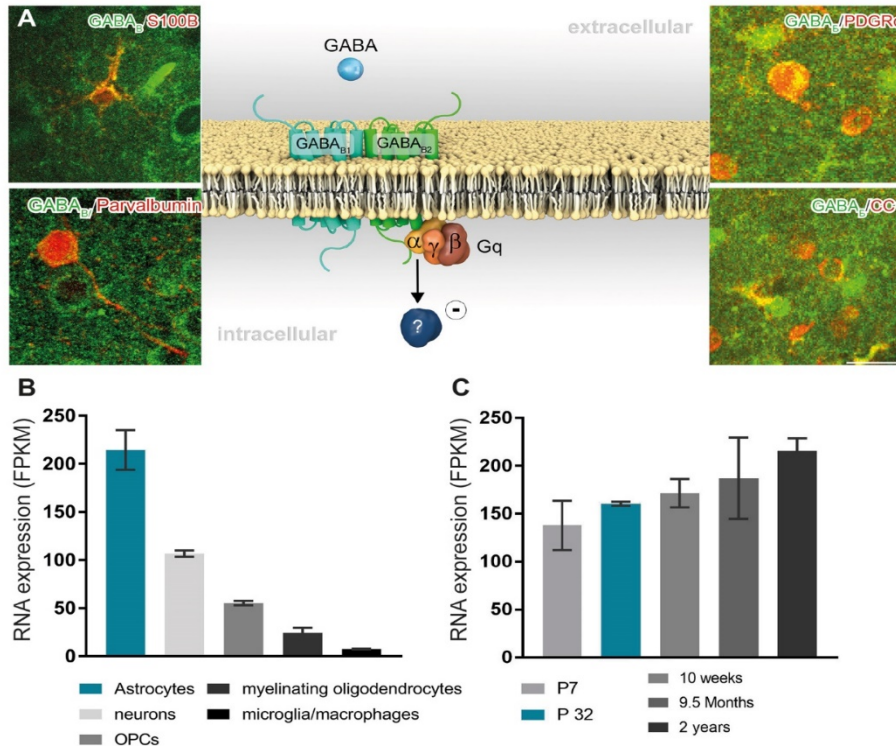
Figure 1: Astrocytic GABA$_B$ receptors

A: Astrocytic GABA$_B$ receptors expressed in neurons, astrocytes, NG2 cells and oligodendrocytes. B: Highest expression of GABA$_B$ in astrocytes compared to other cells analyzed by RNA sequencing. C: Time-dependent expression of the GABA$_{B1}$ mRNA analyzed with RNA sequencing (Zhang *et al.*, 2014)

However, the role of GABA as a transmitter for astrocytes is still unclear. Astrocytes are able to uptake GABA through the GABA transporter GAT1/3 and also express GAD for converting glutamate into GABA (Lee *et al.*, 2011a; Yoon *et al.*, 2012). Astrocytes express GABA$_A$ receptors (reviewed in (Yoon *et al.*, 2012)). Their activation leads to an efflux of chloride ions and to membrane depolarization (Yoon *et al.*, 2012). Astrocytic GABA$_A$ receptors seem to play an important role in development and their activation could lead to release of gliotransmitter through an increase of the intracellular Ca^{2+} concentration (Von Blankenfeld *et al.*, 1991; Nilsson *et al.*, 1992).

In the early 1980, first evidences of astrocytic $GABA_B$ receptors were found. In cell cultures of rodent astrocytes, a change in the intracellular calcium concentration after treatment with the $GABA_B$ receptor agonist baclofen was measured (Albrecht *et al.*, 1986). Electrophysiological studies on hippocampal astrocytes from rats have shown a hyperpolarization of the cell membrane after adding GABA or baclofen (Hösli *et al.*, 1990). The expression of astrocytic $GABA_B$ receptors could be proven with *in situ* hybridization (Calver *et al.*, 2000). First findings proved the expression of the different $GABA_B$ receptor subunits in cell culture and on slices (Charles *et al.*, 2003). Furthermore, $GABA_B$ receptors are functional, G protein coupled and associated with the adenylate cyclase system (Figure 1A (Oka *et al.*, 2006)). Not as assumed in neurons, $GABA_B$ receptors are mostly expressed on astrocytes as indicated by RNA-sequencing (Figure 1B). Their expression increased over the development of the animals (Figure 1C). However, the role in neuron-glia network and their function remains still unclear.

Astrocytic $GABA_B$ receptors might be antagonistic to glutamate. In the hippocampus, glial $GABA_B$ receptors are involved in the heterosypnatic depression (Serrano *et al.*, 2006; Haydon, 2009). Glutamate is released from Schaffer collaterals and binds to NMDA receptors on GABAergic neurons (Serrano *et al.*, 2006). This results in a GABA release and subsequently to an activation of astrocytic $GABA_B$ receptors, leading to rise of intracellular Ca^{2+}. This results in a release of ATP, inhibiting the purinergic A_1 receptors on Schaffer collaterals. Furthermore, astrocytic $GABA_B$ receptors transform inhibitory signals in excitatory signals by influencing Ɵ- and ɣ-waves (Perea *et al.*, 2016). Inhibitory transmission can be amplified trough $GABA_B$ receptors as observed in hippocampal slices. GABA, released from neurons, binds to astrocytic $GABA_B$ receptors and leads to a release of glutamate (Kang *et al.*, 1998). $GABA_B$ receptors might play protective role for astrocytes. The transmitter glutamate can be neurotoxic under pathological conditions. Astrocytes can take up glutamate as a protection for neurons (Chen *et al.*, 2003).

1.2 Neuron-glia interaction

In the human brain, neurons and glia cells are equally distributed (Nedergaard *et al.*, 2003; von Bartheld *et al.*, 2016). Astrocytes are one of the key player in the CNS. They provide metabolites and the scaffold for growing neurons and regulate the extracellular cation concentration through ion-selective uptake. Astrocytes are involved in healing and aging processes by forming the glia scar (Alberdi *et al.*, 2005). With their small peripheral processes they form the so called tripartite synapse influencing neuronal transmission (Perea *et al.*, 2009). This tripartite synapse consists of the pre- and post-synapse and the astrocytic processes (Araque *et al.*, 1999). A single astrocytes might able to contact around 100.000 synapses (Perea *et al.*, 2009). Neuronal transmission can be modulated through release of gliotransmitters, like glutamate, ATP and D-Serin (Araque *et al.*, 2014). Astrocytes can not only release gliotransmitter, they also express ionotropic and metabotropic receptors (Araque *et al.*, 2014).
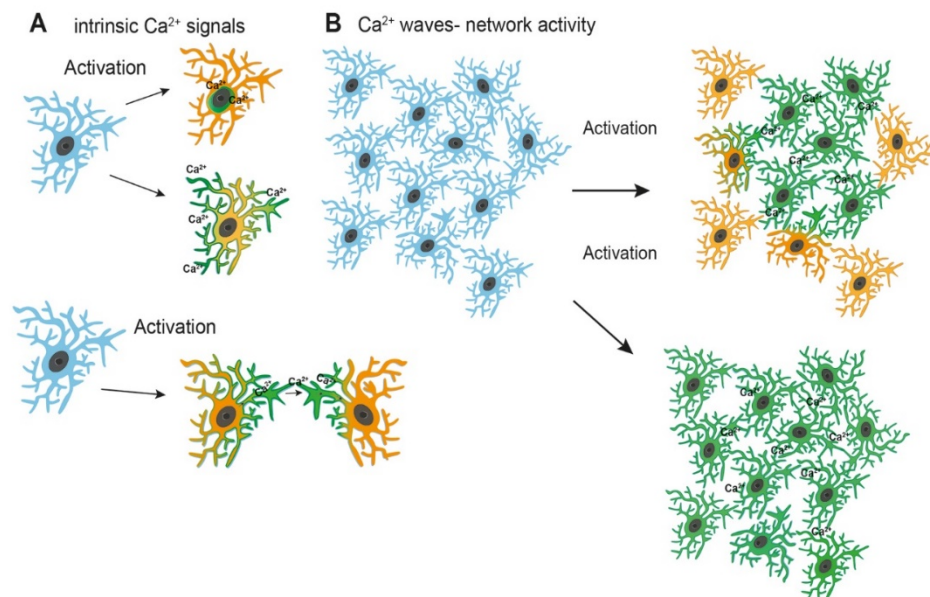
Figure 2: Types of astrocytic Ca^{2+} signals

A: Intrinsic Ca^{2+} signals regulate internal cell processes, like transmitter release. Information transfer over Ca^{2+} signals. B: Network activity of the astrocytic syncytium which incorporates different number of cells or cellular processes.

Neurons communicate over electrical signals whereas astrocytes convey their information over Ca^{2+} signals. The activation of metabotropic receptors leads to changes in the intracellular Ca^{2+}, which results in release of gliotransmitter. Over so called Ca^{2+} waves astrocytes can communicated with each other ((Charles *et al.*, 1991; Scemes & Giaume, 2006), Figure 2A). It is more intracellularly transporting IP3 (inositol trisphosphate) or extracellularly ATP conveying this signal transduction in the astrocytic syncytium.

Futhermore, astrocytes can show intrinsic Ca^{2+} fluctuations without external influences regulating intrinsic processes or signal transduction into other cell (Nett *et al.*, 2002; Berridge *et al.*, 2003). Astrocytic Ca^{2+} elevations can be triggered by physiological stimuli. Whisker stimulation results in Ca^{2+} wave in the mouse barrel cortex (Wang *et al.*, 2006). However, the language of these signals is not well understood. There are several approaches to translate the Ca^{2+} code of astrocytes. Nimmerjahn *et al*. divided the signals into three groups; sparkles, bursts and flares (Nimmerjahn *et al.*, 2009). Sparkles are small single signals, which could be only detected in individual cells. Burst are spontaneous but larger signals, which cover a radius of 55 µm. Flares are large, synchronous signals, which covers a whole network of astrocytes. Flares only occur in awake and moving animals (Wang *et al.*, 2006; Nimmerjahn *et al.*, 2009; Ding *et al.*, 2013). Sparkles could be the intrinsic Ca^{2+} fluctuation regulating cell intrinsic processes (Nimmerjahn *et al.*, 2009). The Ca^{2+} signals can be classified by their signal properties but also by their location on the astrocytes; in microdomains or in soma, process or endfeet (Bindocci *et al.*, 2017).

So far, the role of $GABA_B$ receptors in neuron-glia interaction is unsolved. Therefore, the $GABA_B$ receptor will be specifically deleted on astrocytes by using the Cre-LoxP-system. We take advantage of a $GABA_{B1}^{fl/fl}$ mouse line, were recombination of the floxed $GABA_{B1}$ subunit prevents functional receptor assembly (Haller *et al.*, 2004). Combination with the GLAST-CreERT2 mice ensure deletion in astrocyte specific and in a time-dependent deletion (Mori *et al.*, 2006). Only in the presence of tamoxifen, the CreERT2 is released from the heat shock protein HSP90 in the cytosol and can recombines in the nucleus floxed DNA sequence. By using the genetically encoded Ca^{2+} indicator GCaMP3 changes in Ca^{2+} signals in absence of the astrocytic $GABA_B$ receptor will be evaluated.

2. AIM

The aim of this thesis is to investigate the modulation of Ca^{2+} signals through astrocytic $GABA_B$ receptors.

Activation of neuronal $GABA_B$ receptors leads to inhibition of potassium channels or to a prolongation of the opening time of calcium channels, depending on the localization of the receptors (Bettler *et al.*, 2004). $GABA_B$ receptors are expressed *in vitro* in primary astrocytes (Oka *et al.*, 2006). However, the function of astroglial $GABA_B$ receptors and its modulation on Ca^{2+} signals is still unclear. By using the Cre/LoxP system a time dependent and cell specific knockout of $GABA_B$ receptors was generated. By crossbreeding with GLAST-CreERT2 mice, the deletion is limited to astrocytes.

Therefore, the following objectives are defined:

First: Confirmation of successful $GABA_B$ deletion specifically on astrocytes

The expression of the $GABA_{B1}$ subunit will be investigated on DNA, mRNA and protein level in three different brain regions by using different techniques (RT-PCR, FISH and IHC). Moreover, the impact of the loss of $GABA_B$ receptors on other astrocyte specific proteins will be investigate under physiological and pathophysiological conditions.

Second: Modulation of astroglia Ca^{2+} signals through $GABA_B$ receptors *in vivo*

Using the genetically encoded Ca^{2+} indicator GCaMP3, will enable us to investigate changes in the Ca^{2+} signal properties *in vivo*. Therefore, anesthetized and awake cKO and control mice will be repeatedly imaged with 2P-Microscopy and data will be analyzed with MSparkles.

Third: Pharmacokinetic modulation of astrocytic $GABA_B$ receptors

Acutely isolated brain slices of cKO and control mice will be treated with a $GABA_B$ agonist and antagonist to reveal the $GABA_B$ specific triggered Ca^{2+} responses.

3. MATERIALS AND METHODS

3.1 Materials

3.1.1 Reagents

Standard chemicals were not listed separately and were purchased from companies like Amersham Biosciences (Freiburg), Roche (Penzberg), Carl Roth (Karlsruhe), Eppendorf (Hamburg), Riedel de Haën (Hannover), Merck (Darmstadt), Sigma-Aldrich (Taufkirchen), BioRad (München), Invitrogen (Karlsruhe).

3.1.2 Consumables and Kits

Pipette tips, Sarstedt (Nümbrecht); glass pipettes, VWR International (Darmstadt); Falcontubes, Greiner Bio-One (Frickenhausen); Eppendorf reaction tubes, Eppendorf (Hamburg); Venomix canulas, Braun (Melsungen); 96-well-PCR-reaction-tubes, 4titude (Berlin); 24 well culture plates, Sarstedt (Nümbrecht); object slides, Karl Hecht Glaswarenfabrik (Sondheim); cover slips, Menzel-Gläser (Braunschweig); RT-PCR-96-well-plates, Axon (Kaiserslautern); Precellys homogenizing tubes, Precellys Ceramic Kit, peqlab (Erlangen).

The following kits were used: All prep DNA/RNA Mini and Micro Kit, Qiagen (Hilden); REDExtract-N-AmpTM Tissue PCR Kit, Sigma-Aldrich (Taufkirchen); Super Signal West Pico Chemiluminescent Substrate and Pierce BCA Protein Assay Kit, Thermo Scientific (Rockford, USA); Adult Brain Dissociation Kit, Anti-ACSA-2 MicroBead Kit, Miltenyi (Bergisch Gladbach).

3.1.3 Devices

Table 1: Devices

Device	Producer	City
Gel chambers and supplies for agarose gels	Workshop of the CIPMM	Homburg
Gel chambers for SDS-PAGE	Serva	Heidelberg
Western blotting system	Biorad	München
Confocal microscope LSM 710	Zeiss	Oberkochen
Precellys 24 (Homogenizer)	Peqlab Biotechnologie GmbH	Erlangen
Thermomixer comfort	Eppendorf	Hamburg
Vibratome VT1000S, VT1200S	Leica	Wetzlar
Centrifuges 5418,5804,5430R	Eppendorf	Hamburg
Infinite PRO 200 microplate reader	Tecan	Crailsheim
Preparations- and perfusion instruments	F.S.T., Pharmacia	Heidelberg
peqSTAR Thermo Cycler	Peqlab Biotechnologie GMBH	Erlangen
Quantum gel documentation system	Peqlab Biotechnologie GMBH	Erlangen
BioSpectrometer	Eppendorf	Hamburg
CFX96 Real-Time PCR Detection System	BioRad	München
Electrophoresis power supply	Consort	Turnhout
Vacuum pump	Integra Biosciences	Biebertal
Pipettes	Brand	Wertheim
Shaker DRS-12	neoLab	Heidelberg
Intelli Mixer	neoLab	Heidelberg
IKA C MAG HS 7 digital (magnetic mixer)	ChemLabz	Benzheim
Electronic scale CPA8201, CPA244S	Santorius	Göttingen
InSlide Out Hybridization Oven (241000)	Boekel	Feasterville
AxioScan.Z1	Zeiss	Oberkochen

3 1.4 Buffers

All buffers were prepared with deionized and RNAse-free H_2O from an ultrapure water system GenPure (Thermo Scientific, Rockford, USA) and MilliQ (Merck Millipore, Darmstadt). All stated concentrations are final concentration.

Phosphate buffered saline (PBS, 10x)

NACl	1.37	M
KCl	27	mM
Na_2HPO_4	100	mM
KH_2PO_4	18	mM

4 % FA in PBS

Paraformaldehyde	4 %	(w/v)
NaOH	10	M

some drops until paraformaldehyde is dissolved

Agarose gel electrophoresis

Tris acetate EDTA buffer (TAE, 50x)

Tris (Tris (hydroxylmethylaminomethan))	2	M
Acetic acid (100 %)	1	mM
EDTA (Ethylendiamintetraacetate, 0.5 M, pH 8)	1	mM

Agarose gel

Agarose powder in TAE buffer	1 %	(w/v)
Ethidium bromide (1%)	0.015 %	(v/v)

Immunohistochemistry (IHC)

Blocking-, primary antibody solution in PBS

Horse serum	5 %	(v/v)
Triton-X-100	0.3 %	(v/v)

Secondary antibody solution in PBS

Horse serum	2 %	(v/v)

Western blot buffers

Homogenization buffer

Sucrose	320	mM
Tris (pH 7.4)	10	mM
$NaHCO_3$	1	mM
$MgCl_2$	1	mM

Buffer was prepared freshly each time and protease inhibitor aliquots (Complete Mini protease inhibitor tablets, (Roche, Basel Schwitzerland)) were added before use.

10x SDS running buffer

Tris	250	mM
Glycine	1.92	M
SDS	1	%

4x SDS sample buffer

Tris HCL (1M, pH 6.8)	1 %	(v/v)
Glycerol (87 %)	8 %	(v/v)
SDS (10 %)	16 %	(v/v)
β-Mercaptoethanol	4 %	(v/v)
Bromphenol blue (1 %)	4 %	(v/v)

Stored in 1 ml aliquots at -20°C

1x transfer buffer

Glycine	38.63	mM
Tris	47.87	mM
Methanol	20	(v/v)
SDS	1.28	mM

Stripping buffer

Acetic acid	6 %	(v/v)
NaCl	428.5	mM

Blocking buffer

non-fat milk powder	5 %	(w/v)

dissolved in 1xPBS

Washing buffer (PBS-T)
1xPBS

Tween 20	0.05 %	(v/v)

Cortex buffer for cranial window

NaCl	125	mM
KCl	5	mM
Glucose	10	mM
HEPES	10	mM
$CaCl_2$	2	mM
$MgSO_4$	2	mM

Buffers for acute brain slices

Cutting solution

NaCl	126	mM
KCl	3	mM
Glucose	15	mM
$NaHCO_3$	25	mM
$MgSO_4$	3	mM
NaH_2PO_4	1.2	mM

aCSF (artificial cerebrospinal fluid)

NaCl	126	mM
KCl	3	mM
Glucose	15	mM
$NaHCO_3$	25	mM
$CaCl_2$	2	mM
$MgSO_4$	2	mM
NaH_2PO_4	1.2	mM

3.1.5 Antibodies

3.1.5.1 Primary antibodies

Table 2: Primary antibodies for immunohistochemistry and Western blot

Antibody	Company	Clonality	Species	Dilution	use
CC1	Calbiochem	mc	mouse	1:200	IHC
GABA$_{B1}$	Abcam	mc	mouse	1:1000	IHC
GABA$_{B2}$	Millipore	pc	guinea pig	1:100	IHC
GFAP	DakoCytomation	pc	rabbit	1:500/ 1:1000	IHC /WB
GFAP	Abcam	pc	goat	1:1000	IHC
GFP	Rockland	pc	goat	1:1000	IHC
GFP	Clontec	pc	rabbit	1:500	IHC
GLAST	Chemicon	pc	guinea pig	1:2000	IHC
IBA1	Abcam	pc	goat	1:1000	IHC
IBA1	Wako	pc	rabbit	1:1000	IHC
NeuN	Abcam	pc	rabbit	1:500	IHC
Parvalbumin	Swant	pc	rabbit	1:1000	IHC
PDGRalpha	BD Pharmaring	mc	rat	1:1000	IHC
S100B	Abcam	mc	rabbit	1:500	IHC
S100B	Abcam	mc	mouse	1:500	IHC
Tubulin	Sigma Aldrich	mc	mouse	1:10000	WB

3.1.5.2 Secondary antibodies

Most secondary antibodies for immunohistochemistry (from donkey) were purchased from Invitrogen (Molecular Probes, Carlsbad USA), diluted 1:1000 and are listed as followed: anti-mouse Alexa 488/543/555 conjugated; anti-rabbit Alexa 488/543/555/633 conjugated; anti-goat Alexa 488/633 conjugated. Additionally, the following secondary antibodies were used: donkey anti-guinea pig Cy3 conjugated (diluted 1:500) form Dianova (Hamburg); goat anti-guinea pig Alexa 488/633 conjugated (1:1000) from Invitrogen (Molecular Probes, Carlsbad USA). Secondary antibodies for Western blotting were purchased from Dianova and diluted 1: 2500: anti-rabbit, anti-mouse horseradish peroxidase.

17

3.1.6 Other dyes and chemical components

Ethidium bromide, Carl Roth (Karlsruhe)

EvaGreen, Axon (Kaiserslautern)

4′,6-Diamidin-2-phenylindol (DAPI), Sigma (Taufkirchen)

Easy ladder (100 Lanes), Bioline (Neunkirchen)

Precision Plus protein standard Dual Color, BioRad (München)

Tetrodotoxin (TTX), Alomone Labs (Jerusalem, Israel)

CGP 35348, Cayman Chemicals (Hamburg)

Baclofen, Cayman Chemicals (Hamburg)

3.1.7 Primer

Sense and anti-sense PCR primers were synthesized by Roche (Mannheim). The oligonucleotide stocks (50 pM) were diluted to 10 pM in deionized H_2O. All sequences are given in 5' $\rightarrow$ 3' direction.

Table 3: Genotyping primer

Line	Primer		Sequence	(bp)
GABA$_B$	24391	KI	5'-TGGGGTGTGTCCTACATGCAGCGGACGG-3'	742
	24392	WT	5'GCTCTTCACCTTTCAACCCAGCCTCAGGCAGGC-3'	526
GCaMP3	27490	KI	5'-GGACATTAAAGCAGCGTATCC-3'	245
	27632		5'-CACGTGATGACAAACCTTGG-3'	
GCaMP3	14025	WT	5'-CTCTGCTGCCTCCTGGCTTCT-3'	327
	14026		5'-CGAGGCGGATCACAAGCAATA-3'	
GLAC	11986	KI	5'-GAGGCACTTGGCTAGGCTCTGAGGA-3'	400
	11984		5'-GGTGTACGGTCAGTAAATTGGACAT-3'	
GLAC	11986	WT	5'-GAGGCACTTGGCTAGGCTCTGAGGA-3'	700
	11985		5'-GAGGAGATCCTGACCGATCAGTTGG-3'	
RATO	27490	KI	5'-GGCATTAAAGCAGCGTATCC-3'	196
	27491		5'-CTGTTCCTGTACGGCATGG-3'	
RATO	27488	WT	5'-AAGGGAGCTGCAGTGGAGTA 3'	297
	27489		5'-CCGAAAATCTGTGGGAAGTC 3'	

Table 4: RT-PCR primers

Gen	Primer		Sequence	bp	RNA/ DNA
β-Actin	9146	fwd	5'-CTTCCTCCCTGGAGAAGAGC-3'	124	RNA
	9147	rev	5'-ATGCCACAGGATTCCATACC-3'		
GABA$_B$	22603	fwd	5'-CGAAGCATTTCCAACATGAC-3'	126	RNA
	22604	rev	5'-CAAGGCCCAGATAGCATCATA-3'		
GFAP	11283	fwd	5'-TGGAGGAGGAGATCCAGTTC-3'	120	RNA
	11282	rev	5'-AGCTGCTCCCGGAGTTCT-3'		
NRGIII	4767	fwd	5'-GTGTGCGGAGAAGGAGAAAACT-3'	120	DNA
	4805	rev	5'-AGGCACAGAGAGGAATTCATTTCTTA-3'		
GABA$_B$	23518	fwd	5'-CAGTCGACAAGCTTAGTGGATCC-3'	82	DNA
	23519	rev	5'-TCCTCGACTGCAGAATTCCTG-3'		

3.1.8 Animals
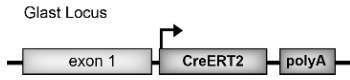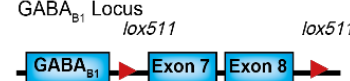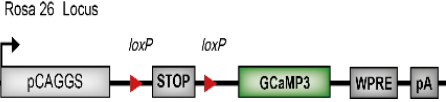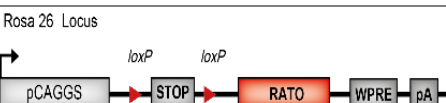
3.1.8.1 TgH (Glast-CreERT2)^{GLAST}

In this transgenic mouse line, CreERT2 is knocked into the locus of the l-glutamate/l-aspartate transporter (GLAST). CreERT2 replaced Exon II near the translation initiation side (Mori *et al.*, 2006). The Cre DNA recombinase is bound to the ligand binding domain of the modified estrogen receptor (ER) (Mori et al., (Metzger & Chambon, 2001). The fusion protein remains in the cytosol until tamoxifen is present (Metzger & Chambon, 2001). Then CreERT2 can translocate into the nucleus and mediate the recombination. For this study only heterozygous animals are used (see Table 5).

3.1.8.2 TgH (GABA$_{B1}$ $^{fl/fl}$)^{GABA}$_B$

The GABA$_{B1}$ receptor gene (subunit 1) is located on chromosome 17. If this subunit is deleted, no functional receptor can be formed because only the assembly of both subunits (B1 and B2) leads to a functional receptor (Bettler *et al.*, 2004). Exon VII and Exon VIII are flanked by Lox 511 sequence in the GABA$_{B1}$ receptor gene (Haller *et al.*, 2004). Homozygous floxed GABA$_B$ receptor mice are indicated as GABA$_B$ (see Table 5). Here this mouse line is crossbred to TgH (Glast-CreERT2) mice to ensure an astrocyte specific GABA$_B$ receptor deletion after tamoxifen administration. Furthermore, to visualize recombined cells the red fluorescent reporter tdTomato and for analysing Ca^{2+} dynamics the green fluorescent Ca^{2+} indicator GCAMP3 were crossbred.

Table 5: mouse construct

Mouse line	Construct	Reference
TgH (Glast-CreERT2)		(Mori *et al.*, 2006)
TgH (GABA$_{B1}$ $^{fl/fl}$)		(Haller *et al.*, 2004)
TgH (Rosa 26-CAG-lsl-GCAMP3)		(Paukert *et al.*, 2014)
TgH (Rosa 26-CAG-lsl-tdTomato)		(Madisen *et al.*, 2010)

3.1.8.3 TgH (Rosa 26-CAG-lsl-GCAMP3)[GCAMP3]

GCaMP3 is a Ca^{2+} indicator, consisting of an EGFP (enhanced green fluorescent protein), the M13 domain of the myosin light chain kinase as well as calmodulin. The M13 domain of the myosin light chain kinase is bound at the N-terminus of the EGFP and is the target sequence for the calmodulin. The calmodulin is fused to the C-terminus and is able to bind Ca^{2+}. In the presence of Ca^{2+} the conformation of the protein is changed and the fluorescence intensity of EGFP is thereby enhanced (Nakai *et al.*, 2001). The expression of Ca^{2+} indicator GCaMP3 is controlled by the CAGGS promoter, a fused promoter consisting of CMV *immediate early Enhancer* and the chicken β-actin promoter and is insert in the Rosa26 locus ((Niwa *et al.*, 1991), see Table 5). Through a floxed neomycin stop cassette, which is, located between the promoter and the Ca^{2+} indicator GCaMP3 a CreERT2 induced expression is ensured (see Table 5). A WPRE (hepatitis virus posttranscriptional regulatory element) element stabilizes the mRNA (Paukert *et al.*, 2014). For this study only homozygous animals were used.

3.1.8.4 TgH (Rosa 26-CAG-lsl-tdTomato)[RATO]

The TgH (Rosa26-CAG-lsl-tdTomato) reporter mouse expresses the red fluorescent protein tdTomato under control of a CAG promotor while crossbred to a TgH-GLAST-CreERT2 knock-in mouse line. Thereby, Cre activity leads to a deletion of the floxed STOP cassette positioned ahead of the fluorescent protein sequence (Madison *et al.*, 2009; Madisen *et al.*, 2010). In addition, a WPRE signal downstream of the tdTomato protein sequence enhances its RNA stability. For this study only homozygous animals were used.

3.1.9 Hard- und Software

All figures were generated using Adobe InDesign and Illustrator CS2018. The art of Figure1 was drawn by Jens Grosche (Effigos AG). Graphics and statistical analyses were performed with GraphPad Prism7. Confocal images were generated and exported using the LSM-Image-Software Zen and processed with ImageJ. The analysis of Ca^{2+} signals was process with ImageJ-plugin PureDenoised and Matlab-based Software MSparkles.

The evaluation of the real-time PCR dates were analyzed with the software CFX Manager 3.0 (Applied Biorad) and Excel 2016. Analysis of the injury model was done with ImageJ plugin LROI. Database research was done using the internet service PubMed of the "National Center for Biotechnology Information" (Internet address: http://www.ncbi.nlm.nih.gov/).

3.1.10 Statistics

All data sets were analyzed in GraphPad Prism 7. Before the statistical analysis, the data sets were tested for normality using the Shaprio-Wilk normality test and for outlier using the ROUT-test recommended by GraphPad Prism 7. The detected outliers were removed from the data sets. By passing the Shapiro-Wilk normality test the statistical analysis was done with an unpaired two-tailed t-test. Following p-values were assumed: * $p < 0.05$, ** $p < 0.005$, *** $p < 0.0001$, ****$p < 0.00001$. When not passing the Shapiro-Wilk normality test the data sets were analyzed with Mann-Witney-U-test. Following p-values were assumed: * $p = 0.01-0.05$, ** $p = 0.001-0.01$, *** $p = 0.0001-0.001$, ****$p < 0.00001$. The statistical analyses for the different data sets are listed in Table 6. For the statistical analysis of the injury model a two-way-ANOVA-test were used. In the case of normal distribution the mean with standard deviation was displayed, by not passing the normality test the median with 25% and 75% percentile (%ile) is displayed.

Table 6: Statistical test for the different data sets

Figure	Normality	Test
Figure 5	yes	two-tailed-t-test
Figure 6	yes	two-tailed-t-test
Figure 11	yes	tow-tailed-t-test
Figure 12	yes	two-tailed-t-test
Figure 15	yes	tow-tailed-t-test
Figure 17	yes	tow-Way-ANOVA
Figure 18	yes	two-tailed-t-test
Figure 19	no	Mann-Whitney-U-Test
Figure **20**	no	Mann-Whitney-U-Test
Figure 21	no	Mann-Whitney-U-Test
Figure 22	no	Mann-Whitney-U-Test
Figure 23	no	Mann-Whitney-U-Test
Figure 24	no	Mann-Whitney-U-Test
Figure 25	no	Mann-Whitney-U-Test
Figure 26	no	Mann-Whitney-U-Test
Figure 28	no	Mann-Whitney-U-Test
Figure 29	no	Mann-Whitney-U-Test
Figure 31	no	Mann-Whitney-U-Test
Figure 32	no	Mann-Whitney-U-Test
Figure 34	no	Two-tailed-Test
Figure 37	yes	two-tailed-t-test
Figure 38	yes	two-tailed-t-test
Figure 44	no	Mann-Whitney-U-Test
Figure 45	no	Mann-Whitney-U-Test

The analysis of hippocampal images were done with the ImageJ JACoP v2.0 colocalization plugin (Cordelieres & Bolte, 2014). The overlap coefficient and Mander's coefficient M2 between the GLAST and GABA$_B$ staining were determined. The statistical analysis was reported in (Perea *et al.*, 2016).

3.2 Methods

3.2.1 Genotyping

Tail biopsy

Tail biopsy of mice was conducted between two and three weeks of age, with weaning by the animal caretakers at the animal facility of the Center for Integrative Physiology and Molecular Medicine (CIPMM) in Homburg. Per mouse one piece of tail tissue (~ 0.5 cm) was removed and stored at -20 °C. The extracted DNA was used for genotyping of transgenic mice through PCR.

PCR

The polymerase chain reaction (PCR) allows the amplification of a specific DNA sequence (Mullis & Faloona, 1987). The genomic DNA extraction from mouse tails was performed with REDextract-N-Amp PCR KIT with some modifications. The tails were incubated with 62.5 µl of extraction solution for 10 min by shaking. Then the solution was incubated by 95ºC for 20 min for stopping the extraction reaction and 50 µl of neutralization solution was finally added. The genotyping was conducted through PCR. The primers for the genotyping are listed in Table 3: Genotyping primer. Gel electrophoresis was used to separate DNA fragments according to their molecular weight (1.5-2 % agarose gels with ethidium bromide (f.c. 0.015 %)). For documentation, the Quantum gel documentation system was used.

3.2.2 Whole body fixation of mice

The mouse was anesthetized with Ketamine/Xylacin (Ketamine, Xylacin, 0.9 % NaCl, 100 µl/10 µg body weight). The abdomen was opened from caudal to cranial up to the sternum. The peritoneum was cut from medial to lateral, the diaphragm was severed longitudinally. Through severing the costal up to the sternum, the pericardium was released carefully from the peritoneum. A butterfly needle was inserted into the left ventricle and the perfusion with 1xPBS was started by a pump. Simultaneously, an incision of the superior concave vein and let the blood drain off. After perfusion with PBS, the animal was perfused with 4 % FA (paraform-aldehyde) in 1xPBS. The brain was removed and post fixed in 4 % FA overnight at 4°C.The next day FA was exchanged to PBS and the fixed brain was used for vibratom slicing. For RNA, DNA, Protein and MACS extraction, the animals were only perfused with HBSS. The brains were removed and separated into different brain regions (brainstem, cerebellum, cortex, hippocampus and optic nerve). These samples were immediately frozen on dry ice at -80 ºC.

3.2.3 Preparation of vibratome slices

The fixed brain tissue was cut in PBS into sagittal sections (40 -70 µm) at a Leica VT1000S vibratome. These sections were collected in 24-well-tissue culture plates containing 1xPBS and were used for immunohistochemistry.

3.2.4 Immunohistochemistry

To block unspecific binding sections were incubated for 1 h in blocking buffer at RT, and then incubated with the primary antibody, diluted in blocking solution overnight at 4°C. After washing, slices were incubate with secondary antibody diluted in the secondary antibody buffer for 2 h at RT. After washing sections were mounted in Immu-Mount (Thermo Scientific). The used primary and secondary antibodies are listed in Table 2 and section 3.1.5.2. The analysis was performed at the confocal microscope and Axio Scan.Z1.

3 2.5 Fluorescence *in situ* hybridization (FISH)

Mice were perfused and the brains were dissected as described in 3.2.2 and 3.2.3. For FISH, the QuantiGene®ViewRNA ISH Cell Assay Kit (Affymetrix) and the GABA$_{B1}$ mRNA probe (#VX4-99999-01, type 4, Panomics/ Affymetrix) were used. All hybridisation steps are carried out at 40° C, in the Boekel InSlide Out ™ Hybridization Oven (model 241000). The procedure was performed by Laura C. Caudal (Department of Molecular Physiology, CIPMM).

3.2.5 Microscopy

Confocal laser scanning microscopy

For the figures LSM 710 with Aprochomat 40x/1, 4 Oil DIC (UV) VIS-IR M 27) and a Lasos Argon laser (454 nm, 514 nm)/Helium-Neon laser (543 nm, 633 nm) were uses. The following figures are all maximum intensity projections of z-stacks (1 µm step between layers).

Digital slice scanner AxioScan.Z1

The digital slice scanner AxioScan.Z1 (Zeiss) is an automated epifluorescence system to scan total object slides. A detailed description can be found in (Jahn *et al.*, 2018). The AxioScan was used to capture the stab wound injury.

3.2.6 Western blot

Tissue preparation

Samples of different brain regions were transferred into a Precellys tube filled with 300 or 600 µl freshly prepared homogenization buffer (3.1.4), depending on the brain region and homogenate in the Precellys. The homogenate was used for DNA/RNA and protein preparation. The protein concentration measurement was performed with Pierce BCA Protein Assay Kit according to manufacturer's micro plate´s procedure protocol. After incubation for 30 min at 37 ºC the samples were measured in the plate reader Infinte M 200pro (Tecan) at 562 nm.

Separation of proteins by discontinuous SDS Page

Protein samples were diluted to a final volume of 20 µl with ddH$_2$O and sample buffer containing 2-mercaptoethanol. As molecular weight standard, the Precision Plus Protein™ Dual Color Standard was used. The gel (SERVA*Gel*™ TG PRiME™ 10 %) was run in a chamber (BlueVertical™ PRiME™, Serva) filled with running buffer at 250 V (50 mA, 150 W) for 45 min.

Western blot and Immunodetection

Proteins were transferred with a semidry blotter (Bioenzym) and the membrane was incubated with blocking buffer (5 % milk powder in PBS) for 1 h at RT. After incubation, the membrane was cut into stripes corresponding to the predicted molecular weight of the analyzed proteins and incubated with primary antibodies solved in 5 % milk powder in PBS overnight at 4 ºC. After washing steps the corresponding secondary HRP (horseradish peroxidase) conjugated antibody was diluted in PBS-T and then applied to the membrane for 2 h at RT. After washing the membrane was incubated for 2 min in enhanced chemiluminescent detection solution (ECL) and developed. For densitometric analysis, films were analyzed with ImageJ.

3.2.7 Magnetic activated cell sorting (MACS)

For the isolation of astrocytes, mice were perfused with cold HBSS to remove blood. Brains were dissected into cortex and chopped into small tissue pieces. The tissue was transferred into Miltenyi C-Tubes and enzyme mix 1 and 2 were added. The dissociation of the tissue was done by the GentleMACS octo dissociator with heaters (37C_ABDK_01). After the incubation, the tissue was further dissociated using a 1000 µl pipette. The cell homogenate was passed through a strainer (70 µm) to remove tissue clots and centrifuged at 300 g for 10 min. The supernatant was discarded and cells were dissolved in 1xD-PBS (1xDulbecco´s PBS) plus debris removal solution and overlayed with 1xD-PBS.

The gradient was centrifuged at 3000 g for 10 min without break. After this step, three phases were formed and the upper two were removed completely. Cells were washed with D-PBS and centrifuged (1000 g, 10 min). The supernatant was removed completely and the cell pellet was dissolved in PBS with 0.5 % BSA. Cells were incubated for 10 min with the FcR blocking reagent and then the anti-ACSA-2 MicroBeads were added for 15 min. After the incubation, cells were washed with PBS-BSA buffer and centrifuged (300 g, 10 min). The pellet was dissolved in 500 µl PBS-BSA buffer and applied to a MACS MS-column that is placed in a magnetic field of the MACS separator. The flow-through contains all unlabelled cells. The column was washed 3x with PBS-BSA buffer and then removed from the separator for final elution of the labelled cells. The cells were directly eluted into reaction tubes and centrifuged at 500 g for 10 min. The supernatant was discarded and the cell pellet was immediately frozen at -80 °C until further processing. For next generation sequencing (NGS) the cell pellet was dissolved in 300 µl RLT buffer plus from the AllPrep DNA/RNA micro kit (Qiagen) and then frozen at -80 °C.

3.2.8 Next generation sequencing

For Next generation sequencing (NGS) GABA$_{B1}$ cKO and control mice (n=5) were perfused with HBSS and astrocytes were isolated via MACS (3.2.7). Astrocytes of the cortex and the cerebellum were dissolved in RLT buffer plus (Qiagen, Hilden) and directly frozen at – 80 °C. RNA was extracted using the Qiagen Micro-Rneasy Kit (Qiagen, Hilden) following manufacturer's instructions. cDNA was synthesized using RNA-Seq system v2 (ThermoFischer, Dreieich). For library preparation the IonXpress plus gDNA and Amplicon library preparation kit (ThermoFischer, Dreieich) was used. The library was size-selected using a 2 % electrophoresis gel, each sample library was further quantified using the KAPA Library Quantification Kit (Roche, Penzberg). Equal quantities of each sample were pooled and sequenced on an Illumina Sequencer. Sample processing and data analysis were performed at the Department of Psychiatry (Molecular Neurobiology) at the Ludwig Maximilian University, Munich, Germany for further processing and data analysis.

3.2.9 RT-PCR

Isolation of RNA, DNA and determination of concentration

For isolation of RNA and DNA, the AllPrep DNA/RNA Mini Kit from Qiagen was used. This kit was designed to purify genomic DNA and total RNA simultaneously from one tissue sample and is based on specific binding of RNAs (excluding 5S, 5.8S and tRNAs) and DNAs to separated columns: All steps were executed following the manufacturer's instructions.

Precipitation of RNA

For cDNA synthesis 500 to 1000 ng RNA were precipitated. The RNA was diluted, to a final concentration of 1 µg/50 µl and mixed with 1 µl pellet paint. Next, 25 µl of 7.5 M NH$_4$Ac (ammonium acetate) was added and vortexed. Followed by addition of 180 µl 100 % EtOH to the samples, the probes were vortexed and inverted. The supernatant was carefully discarded after centrifugation of 15 min. The pellet was washed with 200 µl of 70 % EtOH, followed by centrifugation for five min and removal of the supernatant. Subsequently the pellets were dried for ten min at room temperature and dissolved in 4 µl RNAse free water by putting the tubes five min on ice.

c-DNA synthesis

Through reverse transcription PCR fragile mRNA can be transcribed to cDNA by reverse transcriptase. This RNA dependent DNA polymerase needs oligonucleotide primers for the synthesis of cDNA. For the cDNA synthesis, RNA and RNA-free water (final volume of 12.2 µl and a final concentration of 1 µg) and master mix (7.8 µl) were added. After centrifugation, the PCR plate was incubated at 37 ºC for 1 hour. The amplified cDNA was directly diluted 1:10 with RNase free water and stored at -20 °C

Quantitative real time PCR for mRNA expression

Quantitative real time PCR is based on polymerase chain reaction. But it allows monitoring the amplification for a specific DNA fragment in real time and also the quantification of this fragment by using the fluorescent dye EvaGreen. The reaction was performed in Real-time System CFX 86 c1000 Thermal Cycler (Biorad). The evaluation was analyzed with software CFX Manager 3.0 (Biorad) and Excel 2013. All reactions were performed in quadruplets and β-actin were used as endogen. The selected primers are listed in Table 4.

Quantitative real time PCR for DNA recombination

The quantitative real time PCR for DNA is similar to the quantitative real time PCR for mRNA. However the position of the primers is in intron stretches to avoid contamination of mRNA. Neuregulin III was used as endogen. The reactions take place in 96-well plates (Axon) in the CFX96 Real-Time PCR Detection System (BioRad). All samples were carried out in quadruplets. Selective primers are listed in Table 4. The shown RT-PCR data were generated by Carmen V. Kasakow (Department of Molecular Physiology, CIPMM).

3.2.10 Tamoxifen protocol

Tamoxifen was diluted at a concentration of 10 mg/ml in Miglyol (Caesar & Loretz), aliquoted and stored at 4° C. The animals were injected intraperitoneal with tamoxifen. The daily dose was calculated by 100 mg/kg bodyweight. The injection was repeated three or five times once per day (Jahn *et al.*, 2018). The treatment was performed by the animal caretaker at the animal facility of CIPMM.

3.2.11.1 Surgery

For all described surgeries, animals were anesthetized with a mixture of 5 % isoflurane and 47.5 % O_2 and 47.5 % N_2O using Harvard Apparatus equipment. When the animal was sedated, the isoflurane was reduced to 2 % and the flow of the O_2 and the N_2O to 0.4 l/min (0.8 l/min in total) and placed on a heating plate. A temperature probe soaked in vaseline was inserted rectally to control the body temperature between 36.6-37.5 °C by an adjustable heat plate. The eyes were covered with Bepanthen (Bayer) to prevent the cornea from drying out. All procedures have to be performed under conditions as sterile as possible, and the wounds have to be kept as small and clean as possible.

3.2.11.1 Stab wound injury (SWI)

Stab wound injury (SWI) was performed in seven-week-old mice. After anesthetizing the animals the scalp was opened along the rostro-caudal axis and the craniotomy was performed with a hand drill (0.7 mm) above the somatosensory cortex (1.5 mm laterally and 2 mm caudally, referring to bregma as 0/0). The center of the craniotomy was stabbed with a surgical scalpel (#11, B/Braun, 78532 Tübingen, Germany), parallel to the midline and inserted to a depth of 1 mm from the cortical surface. Occurring bleedings were stopped by sponges (Gelastyp sponges, Sanofi aventi). Afterwards the wound was sutured and the animals received painkiller for three consecutive days (buprenorphine hydrochloride; 0.1 µl/10 g body weight). SWI was analyzed with a custom-made ImageJ plug-in LROI (Gebhard Stopper, Molecular Physiology, CIPMM). For each condition, three to four animals were analyzed. With LROI five slices were analyzed for each animals and the mean was calculated. Then the mean of each group (cKO and con) was calculated and compared.
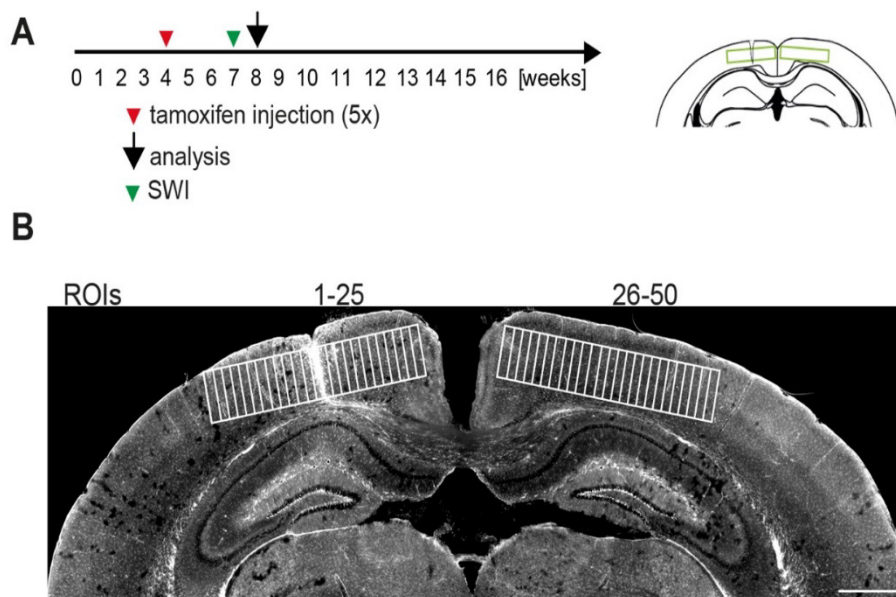
Figure 3: ImageJ plugin LROI used for SWI analysis

A: Experimental design. B: Coronal brain section with analyzed regions chosen with the plugin LROI (white boxes). Scale bar 500 μm.

LROI is designed to analyze uniform regions-of-interest (ROIs) with a specific width and height (Figure 3). LROI creates a set of neighboring, non-overlapping ROIs, along a user-drawn guidance line. It allows the user to specify a set of constraints, e.g. the number of LROIs and the ROI width. The ROI height is determined by dividing the length of the guidance line by the number of ROIs to create. For this reason, the exact length of the guidance is also user-adjustable (http://imagej.net/User:CIPMM-MolPhys).

3.2.11.2 Cranial window

The following procedure were adapted from Cupido and colleagues (Cupido *et al.*, 2014). The scalpel was disinfected with 70 % ethanol and used to remove all tissue (skin, hairs, and muscle). Afterwards the wound edges were disinfected with 70 % ethanol and Betaisodona solution (Mundipharma) three times with cotton swabs. The craniotomy was performed on the somatosensory cortex (lateral = 1.5 mm and longitudinal = 2 mm from the bregma). The diameter of the craniotomy ranged between 3 and 4 mm. The drilling procedure was performed with a driller (Hardware store) and burrs with a diameter of 0.9 mm (FST 19008-09, Fine Science Tools). It is important to stop in between the drilling process, remove the bone particles and cool down the surgery area with cortex buffer to prevent overheating of the subadjucent brain region. The remaining bone was removed from the window with a forcep (5 SF (FST 11252), 5S (FST 11254-20, Fine Science Tools) trying not to damage the dura. Small bleeding was stopped with sponges (Gelastypt, Sanofi aventis).

A coverslip was placed on the tissue and sealed with dental cement (RelyX®, 3M ESPE). A metal holder (5 mm diameter) was put over the coverslip and glued with dental cement onto the bone. After the surgery the animals were kept on the heating pad until they recovered completely. For three consecutive days the animals were treated with painkillers (buprenorphine hydrochloride; 0.1 µl/ 10 g body weight; dexamethasone hydrochloride 0.2 mg/kg body weight) and recovery was controlled by weight and mouse grimace scale. After five to seven days the first image session was done under the two-photon laser scanning microscope.

3.2.12 Two-photon laser scanning microscopy (2P-LSM)

In vivo 2P-LSM was performed using a custom-built microscope equipped with a 20x water-immersion objective lens (1.0 NA; Zeiss). Scanning and image acquisition were controlled using custom-written software ScanImage (Pologruto *et al.*, 2003). To minimize photo damage, the excitation laser intensity was kept at a minimum for a sufficient signal-to-noise ratio. Laser wavelength was set at 910 nm (Chameleon Ultra II, Ti:Sapphire Laser, Coherent). The emitted light was detected by a photomultiplier tube (R6357, Hamamatsu) (Cupido *et al.*, 2014).

3.2.13 Ca^{2+} imaging in acute brain slices

The animals were decapitated, the brain was dissected and placed in ice-cooled, carbogen-saturated (5 % CO2 - 95 % O2, pH~7.4) preparation solution. Sections were cut with a vibratome (Leica VT 1200S) and transferred to a nylon-basket as slice holder for incubation in aCSF at 35°C. The slices recovered in aCSF with continuous oxygenation for at least 1 h before recording. Subsequently, slices were transferred to an imaging chamber under the 2P-LSM and kept submerged by a platinum grid with nylon threads for mechanical stabilization. The imaging chamber were continuously perfused with aCSF with 1 $MgCl_2$ mM and 2.5 $CaCl_2$ mM (room temperature; 20–23 °C) at a flow rate of 2–5 ml/min. Astrocytes were labelled with the genetically encoded Ca^{2+} indicator GCaMP3. The chosen ROI covered a Ca^{2+} network with 15-25 astrocytes and was located in the somatosensory cortex. The imaging settings were selected every time equally: 512x512 pixel, frame rate 1.5 Hertz, pixel time 5.7 µs. For isolation of Ca^{2+} signals slices were incubated with the fast sodium channel blocker TTX (Tetrodotoxin (citrate)) for 10 min. For the investigation of the astrocytic $GABA_B$ receptors the specific $GABA_B$ antagonist CGP 35348 (5 µM, Cayman Chemicals) and agonist baclofen (10 µM, Cayman Chemicals) were applied by bath application on the slices. The application procedures are illustrated in the experimental design in the results part.

3.2.14 Ca^{2+} imaging *in vivo*

After recovery from the surgery the animals were anesthetized for the imaging session first with a mixture of 5 % isoflurane and 47.5 % O$_2$ and 47.5 % N$_2$O using Harvard Apparatus equipment. After sedation isoflurane was reduced to 2 % and the flow of the O$_2$ and the N$_2$O to 0.4 l/min (0.8 l/min in total) until the end of the imaging session. The animals were fixed with a metal holder on a custom made head restrainer (Figure 4B). The selected ROIs for Ca^{2+} imaging were located in the somatosensory cortex 100-120 μm beneath the dura to insure a healthy environment. The same imaging properties were used as in 3.2.12. The same image was recorded over 5 to 10 minutes to investigate the Ca^{2+} changes during this time period. The total duration of one image session ranged between 30-60 min. After the session the animals were kept on a heating pad until they recovered completely.

For Ca^{2+} imaging in awake animals they were habituated before the first imaging session. The habituation was adapted from (Guo *et al.*, 2014; Kislin *et al.*, 2014); first animals were accustomed to the scientist by running freely for 10 min every day on the hand until they showed normal behavior (max 7-10 days). In a second step the animals were head restricted but had the opportunity to run freely on a treat mill for 10-15 min on seven consequective days (Figure 4B) or were kept in a tube for 10-15 min on seven consequective days. Only animals that showed normal no aggressive behavior after this time period were used for imaging. The animals were slightly anesthetized with 0.5 % isoflurane (47.5 % O$_2$ and 47.5 % N$_2$O to 0.4 l/min (0.8 l/min in total) to fix with the metal holder in the custom made treat mill. A region of interest was selected with around 15-25 astrocytes and the anesthesia was stopped. The same imaging properties were used as described before (3.2.13). After 10-20 minutes, the animals were released in their home cage.

3.2.15 Analysis of Ca^{2+} signals using MSparkles

MSparkles is a custom-made MATLAB® application and develop by G. Stopper (Department of Molecular Physiology, CIPMM). It was specifically designed for the analysis of Ca^{2+} signals and provides two analysis modes, classical ROI analysis as well as morphological Ca^{2+} transient analysis. The ROI analysis itself provides four modes of operation. Automatic ROI detection, based on temporal derivatives, ROI grid analysis (Figure 4C), global ROI analysis and analysis of hand-drawn ROIs (Figure 4C). For each ROI, the signal trace is computed as the mean value per time-step. Then, for each trace a peak detection and classification algorithm is executed, which returns the full width at half maximum (FWHM) and signal-peaks, grouped by their deviation from the mean (μ) in orders of one, two and three standard deviations (σ).

In addition to classical ROI analysis, MSparkles offers morphological signal analysis. Here, the dynamic expansion and contraction of Ca^{2+} waves are computed using morphological operators such as opening, closing, erosion and dilation. Thereafter, the 2D time-dependent image space is treated as a 3D Euclidean space in which groups of three dimensionally connected objects are computed. Each group represents a spatially and temporally isolated Ca^{2+} signal. For purposes of visualization, each signal is assigned a unique color, which is scaled in its intensity by the corresponding signal's peak value.
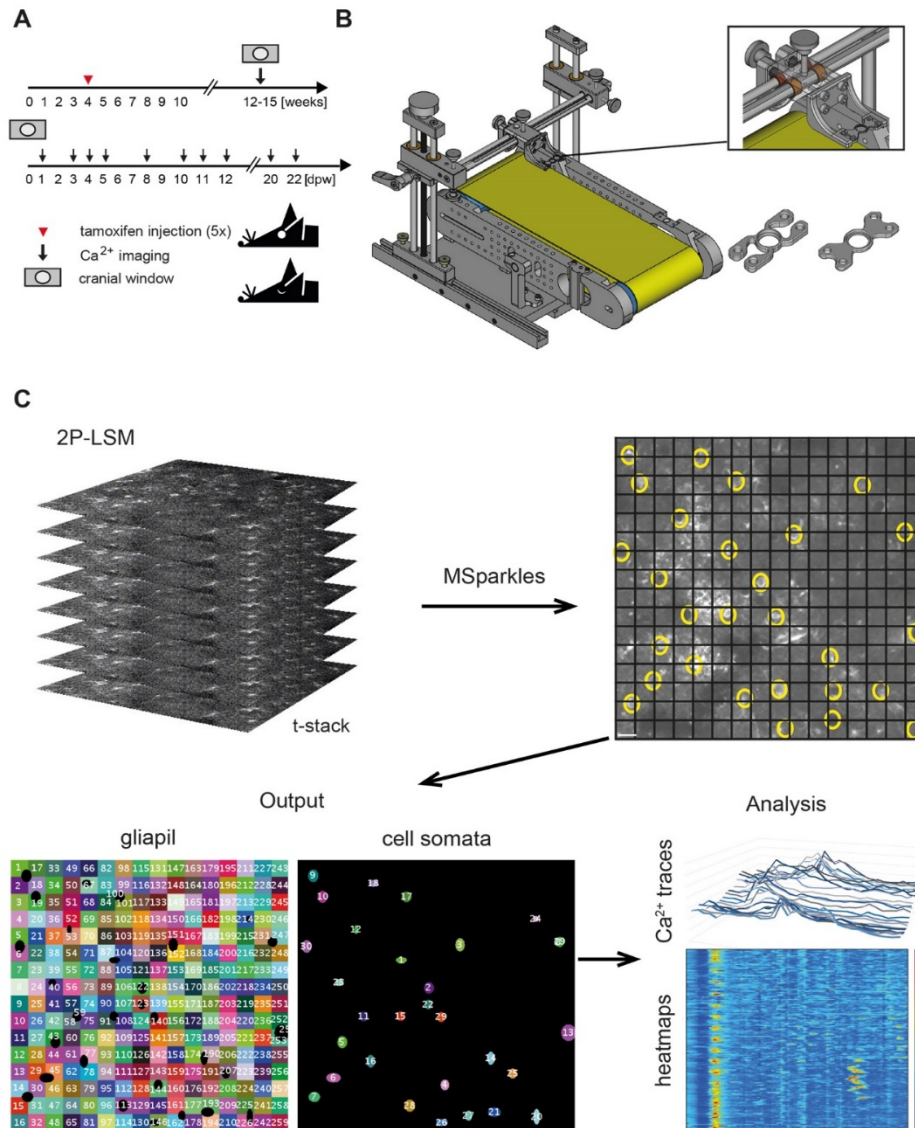
Figure 4: Illustration of the treat mill and data analysis procedure with MSparkles

A: Experimental design for the Ca^{2+} imaging. B: The costume-made treat mill with two different holders models C: The data processing with MSparkles. Two out of four analysis methods were used, grid analysis and the manual selected analysis.

Prior to any of these two analysis approaches, images are run through a pre-processing pipeline. This pipeline performs de-noising using the PURE-LET (Luisier *et al.*, 2010) algorithm, drift correction based on cross-correlation, and automatic background estimation and de-trended by fitting a low order polynomial in a least squares sense. The fitted polynomial is then used as approximation for basal $Ca^{2+}Ca^{2+}$level, F_0 which is then used for data normalization.

3.2.16 Mouse administration

For mouse administration the database PyRAT (Python based Relational Animal Tracking) from Scionics Computer Innovation GmbH (Dresden) was used. In this database all relevant information like mouse number (= earmark), date of birth, sex, pedigree, genotype and breeding behavior are saved. In addition, all types of surgeries, treatments, license and imaging session were added to each individual animal.

3.2.17 Veterinary licenses

All animals, which were used in this thesis, were kept at the animal facility of the Center for Physiology and Molecular Medicine (CIPMM) in Homburg. The animals were kept and bred in strict accordance with the recommendations to European and German guidelines for the welfare of experimental animals. Animal experiments were approved by the Saarland state's "Landesamt für Gesundheit und Verbraucherschutz" in Saarbrücken/Germany (animal license number: 71/2013, 72/2010, 34/2016 and 36/2016).

4. RESULTS

All numbers and statistical test results are listed in the appendix I. The statistical analysis and statistical tests are listed in sections 3.1.10 Statistics and table 6.

4.1 Recombination of floxed $GABA_B$ alleles after tamoxifen induction

The aim of this thesis is to investigate the modulation of Ca^{2+} signals through astrocytic $GABA_B$ receptors. For this purpose, $GABA_B$ receptors were specifically deleted on astrocytes by using the CreERT2/LoxP system.
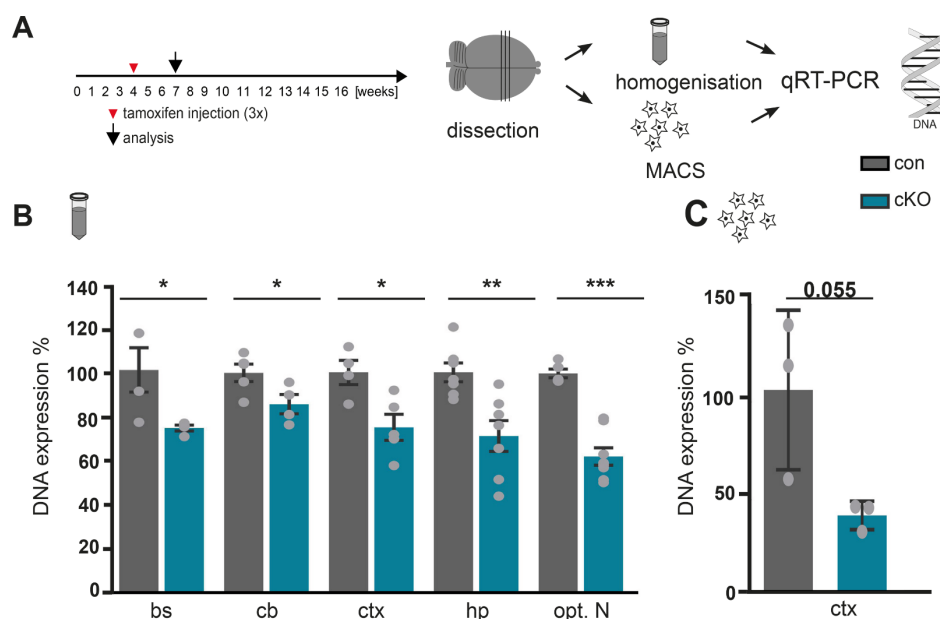
Figure 5: Reduction of $gaba_{B1}$ alleles in different brain regions

A: Tamoxifen injection at four weeks (3x) and analysis with seven weeks. The brain was dissected in the diffrent brain regions and qRT-PCR was performed on the homogenates. Furthermore qRT-PCR was performed on MACS isolated cortical astrocytes. B: Significant reduction of the GABAB1 alleles in different brain regions: brainstem (bs), cerebellum (cb), cortex (ctx), hippocampus (hp) and optic nerve (opt. N) comparing control (con, gray) and conditional cKO (cKO, turquoise) (n= 5-8 animals). C: A 50% reduction of GABAB1 floxed alleles was found in MACS isolated cortical astrocytes (n= 3-9 animals).

In a first step the loss of the $gabab_{B1,}$ alleles were investigated in different brain regions; brainstem (bs), cerebellum (cb), cortex (ctx), hippocampus (hp) and optic nerve (opt. N). The animals were injected with tamoxifen (3x) at an age of four weeks and analyzed 21 days later.

The brain was dissected into the different brain regions and qRT-PCR was performed (Figure 5A). Furthermore, from dissected cortex astrocytes were isolated over magnetic activated cell sorting (MACS).

In all brain regions, a significant loss of $gaba_{B1}$ alleles could be detected compared conditional knockout (cKO, turquoise) to control mice (con, gray) (Figure 5B). In bs and in ctx the reduction amounts to ~ 25% while in the hippocampus a reduction of ~ 29% was determined. The greatest reduction (~ 38%) was detected in opt. N and the smallest (~ 15%) in cb. Data were normalized to the mean of controls in the respective brain regions. Isolated cortical astrocytes showed not significant reduction of about 50% of the $GABA_{B1}$ alleles (Figure 5C).

4.2 Analysis of the GABAB receptor expression in the cerebellum

4.2.1 Reduction of mRNA in isolated astrocytes in cKO

In the cKO mice, the expression of $GABA_{B1}$ mRNA was investigated (Figure 6). Animals were either induced with four weeks and analyzed 21 days later or were induced with four, seven and ten weeks (every time 3x) and analyzed at an age of 13 weeks (Figure 6). The cerebellum was isolated and homogenized and qRT-PCR was performed. No reduction of $GABA_{B1}$ mRNA could be found with both induction protocols when cKO was compared to control mice (Figure 6B). But, by RNA sequencing in isolated astrocytes $GABA_{B1}$ mRNA expression was significantly reduced by 50 %. Data were normalized to the mean of control.
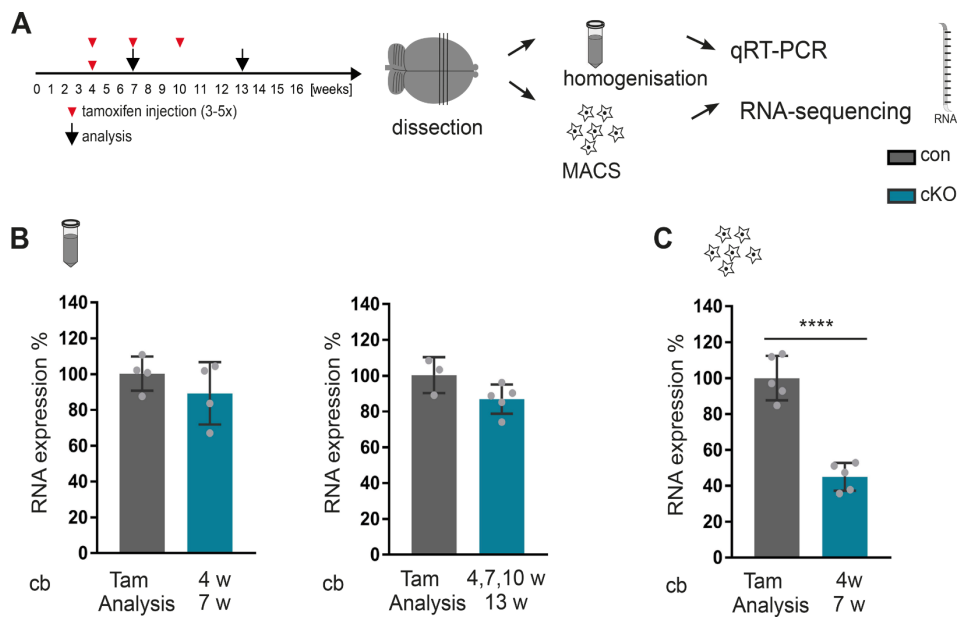
Figure 6: Reduction of mRNA in isolated astrocytes but not in total homogenates

A: Tamoxifen injection with four weeks (3x) and analysis with seven weeks or tamoxifen injection at four, seven and ten weeks (3x each time point) and analysis with 13 weeks. The cerebellum was dissected and qRT-PCR was performed. B: No significant reduction of GABA$_{B1}$ mRNA expression after different tamoxifen protocols. C: Significant reduction of GABA$_{B1}$ mRNA in MAC-sorting isolated astrocytes (n= 5-4 animals).

4.2.3 Astrocytic GABA$_{B1}$ mRNA reduction using Fluorescence *in situ* hybridization

By using Fluorescence *in situ* hybridization (FISH) GABA$_{B1}$ mRNA could be visualized on astrocytes. This allowed a detailed analysis of changes in GABA$_{B1}$ mRNA expression specifically on astrocytes. Astrocytes were marked with the astrocytic markers S100B (Ca^{2+} binding protein β, (Vives *et al.*, 2003)) and GFAP (glial fibrillary acid protein,(Eng *et al.*, 2000)). Furthermore astrocytes were marked intrinsically with the genetically encoded Ca^{2+} indicator GCaMP3 and restained with α-GFP (Paukert *et al.*, 2014). The specific expression of GCaMP3 in astrocytes was already investigated. The specificity of FISH staining was tested and used in the analysis of cKO and con (Figure 36, Appendix I). The Co-expression of the GABA$_{B1}$ mRNA and the GABA$_{B1}$ protein was shown in different cell types: neurons were stained with NeuN (Hirrlinger *et al.*, 2005) and S100B for astrocytes (Figure 36B, D).

To analyze changes of GABA$_{B1}$ mRNA, cKO animals were injected with tamoxifen at an age of four weeks and analyzed 21 days later (Figure 7A). Overall GABA$_{B1}$ mRNA expression was shown for all cerebellar layers (Figure 7B-E).

Furthermore, the localization of GABA$_{B1}$ mRNA in S100B/GFAP positive and S100B/GCaMP3 positive Bergmann glia could be detected (Figure 6B-C, arrowheads). After tamoxifen treatment expression of GABA$_{B1}$ mRNA was reduced on Bergmann glial cells positive for GFAP/S100B and S100B/GCaMP3 (Figure 7D, E, arrowheads).

Figure 7: GABA$_{B1}$ mRNA reduction on cerebellar astrocytes

A: Tamoxifen injection with four weeks and analysis with seven weeks. GABA$_{B1}$ mRNA on cerebellar Purkinje cells in the cerebellum, which is present in the control and cKO animals (open triangles, B-E). B-C: GABA$_{B1}$ mRNA is expressed on astrocytes positive for GFAP/S100B or S100B/GCaMP3, indicated by arrow heads. D-E: Loss of GABA$_{B1}$ mRNA on Bergmann glial cells (arrow heads). Bars indicate 20 μm (overview) and 10 μm (enlargement), respectively.

4.2.3 Loss of the GABA$_{B1}$ protein on Bergmann glia processes

The expression of the GABA$_{B1}$ protein was investigated on GFAP positive Bergmann glia (Figure 8B). After tamoxifen administration at an age of four weeks GFAP positive Bergmann glial processes lack GABA$_{B1}$ protein expression (Figure 8C), indicating that three weeks after induction of recombination GABA$_B$ receptors are decreased on cerebellar processes.
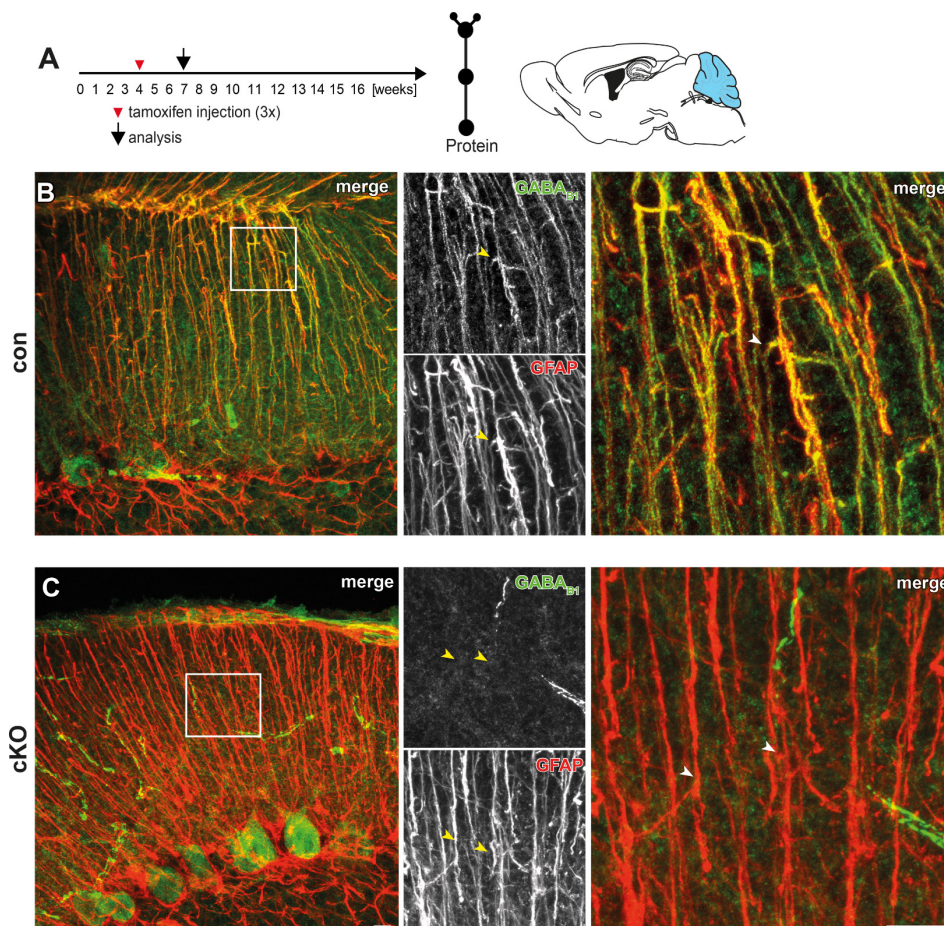
Figure 8: Lack of GABA$_{B1}$ protein on Bergmann glia processes in cKO

A: Tamoxifen injection with four weeks and analysis with seven weeks. B: GABA$_{B1}$ protein is expressed on GFAP positive Bergmann glia indicated by arrowheads. C: Loss of GABA$_{B1}$ receptors specifically on Bergmann glial cells (arrowheads). Bars indicate 20 µm (overview) and 10 µm (enlargement), respectively.

4.2.4 GABA$_{B2}$ subunit loss in cKO astrocytes

The GABA$_B$ receptor consists of two subunits GABA$_{B1}$ and GABA$_{B2}$ (Bettler *et al.*, 2004). By deleting one subunit no functional receptor can be formed (Haller *et al.*, 2004). Here the successful deletion of both subunits on astrocytes was investigated (Figure 9). The GABA$_{B1}$ und GABA$_{B2}$ subunits are co-localized in GCaMP3 positive Bergmann glial cells (Figure 9B). After tamoxifen administration with four weeks the expression of the GABA$_{B2}$ subunit was investigated 21 days later (Figure 9A). No GABA$_{B1}$ and GABA$_{B2}$ subunit expression were found on Bergmann glial cells (Figure 9C, arrowheads). Nevertheless, both subunits were expressed on parvalbumin positive interneurons (Figure 9D, open triangle).
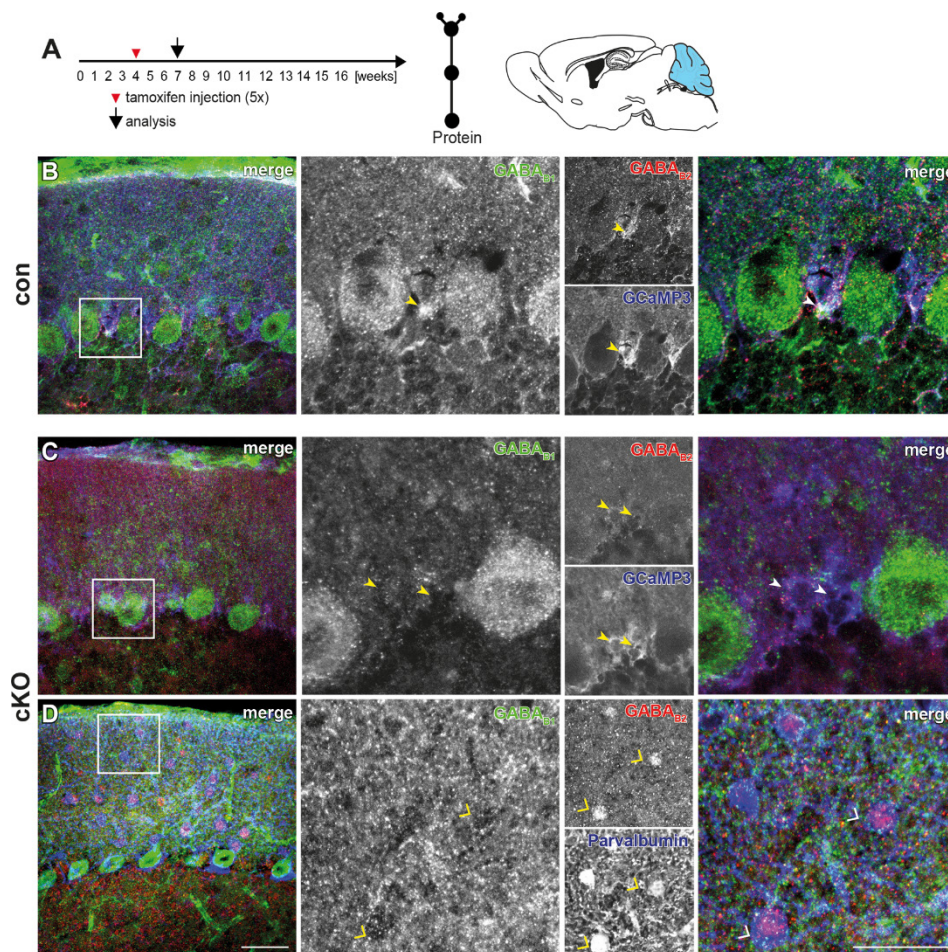
Figure 9: Loss of GABA$_{B2}$ subunit in Bergmann glial cells

A: Tamoxifen injection with four weeks and analysis with seven weeks. B: Visualization of the GABA$_{B1}$ and GABA$_{B2}$ subunits on GCaMP3 positive astrocytes (arrowheads). C: Loss of GABA$_{B1}$ and GABA$_{B2}$ subunit specifically on Bergmann glia cells in cKO (arrowheads). D: Both subunits were still present on interneurons (open triangle). Bars indicate 10 and 20 µm, respectively. Bars indicate 20 µm (overview) and 10 µm (enlargement), respectively.

4.3 Analysis of the GABA$_B$ receptor knockout in the hippocampus

4.3.1 Loss of the GABA$_{B1}$ mRNA in astrocytes confirmed by FISH
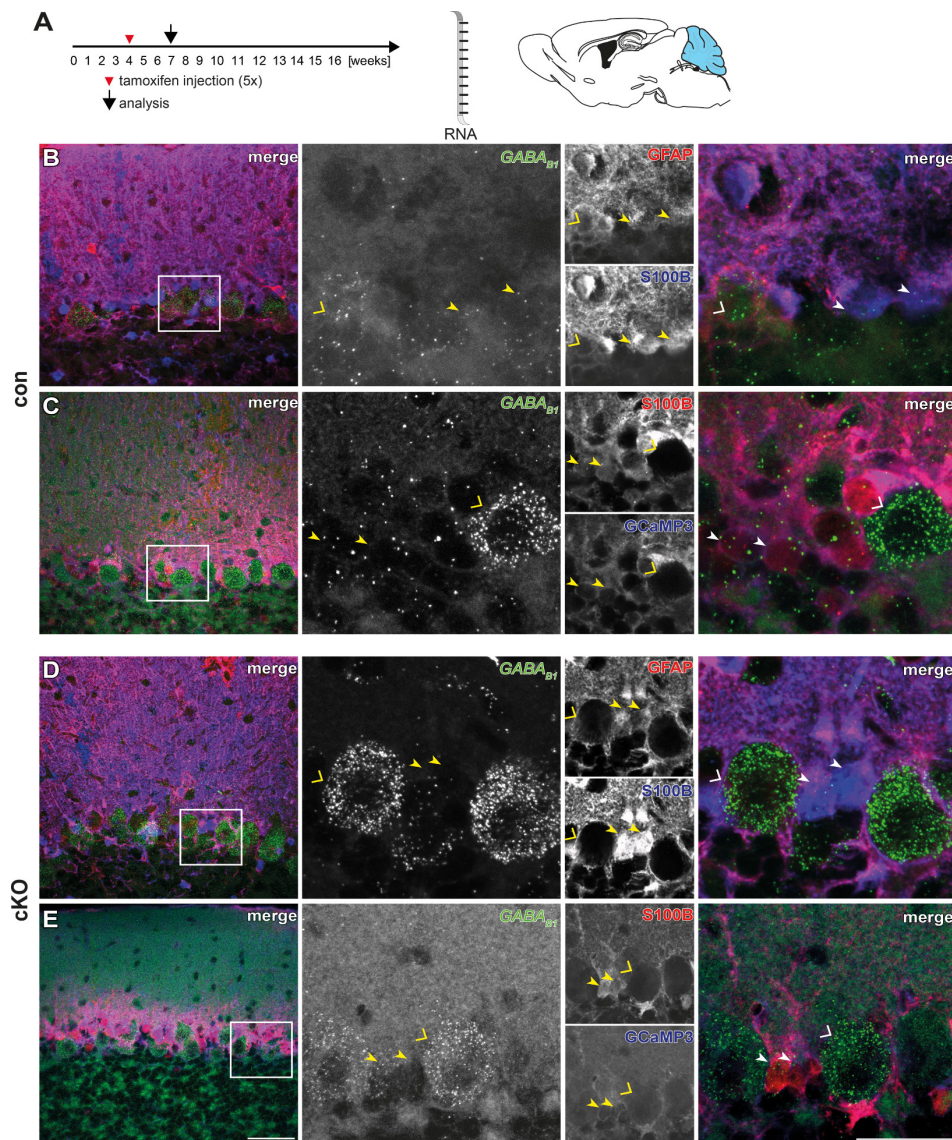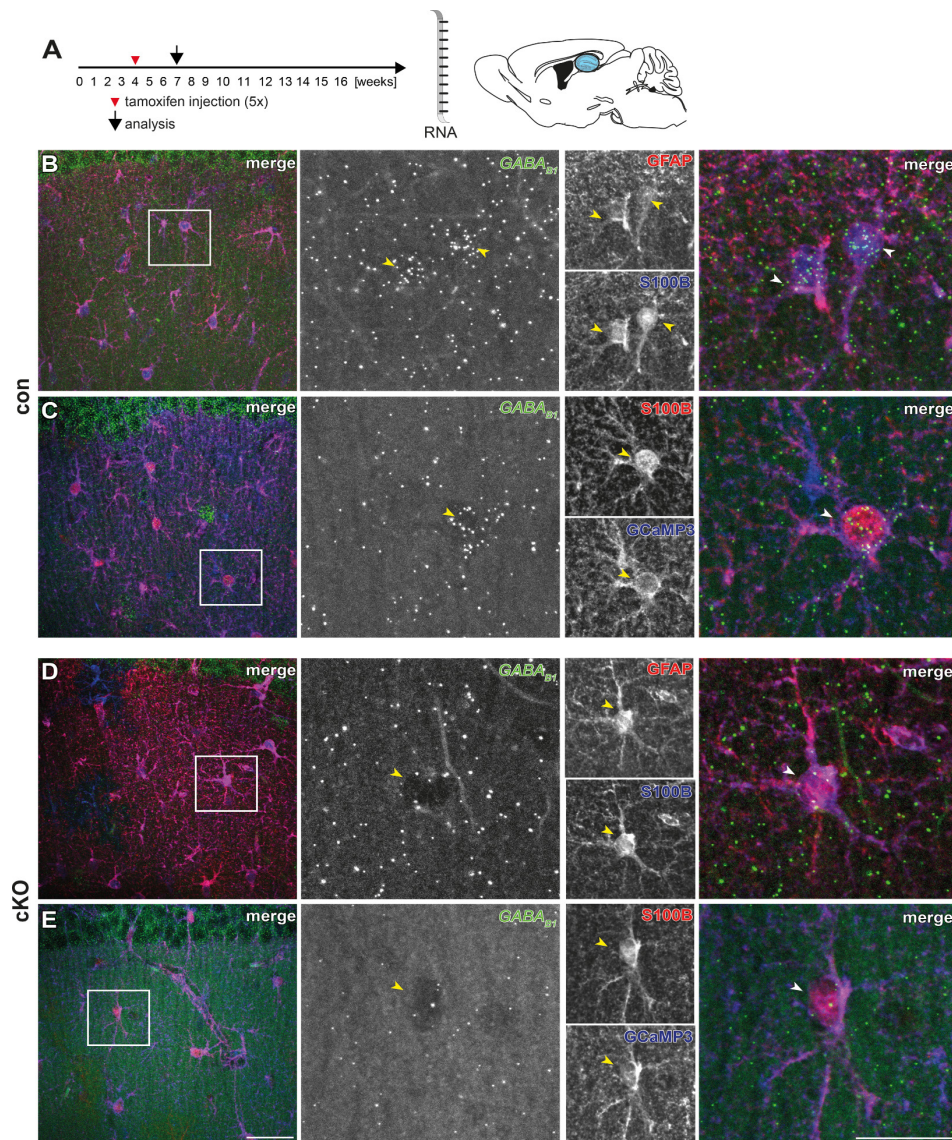

Figure 10: GABA$_{B1}$ mRNA reduction on hippocampal astrocytes

A: Tamoxifen injection with four weeks and analysis with seven weeks. B-C: Expression of GABA$_{B1}$ mRNA on GFAP/S100B or S100B/GCaMP3 positive astrocytes (arrow heads). D-E: Loss of GABA$_{B1}$ mRNA on astrocytes after TAM induction (arrowheads). Bars indicate 20 µm (overview) and 10 µm (enlargement), respectively.

Recombination was induced at an age of four weeks and mice were analyzed 21 days later (Figure 10A). GABA$_{B1}$ mRNA was expressed in S100B/GFAP or S100B/GCaMP3 positive astrocytes in control animals (Figure 10B, C arrowheads). After tamoxifen treatment, the expression of GABA$_{B1}$ mRNA was reduced on hippocampal astrocytes positive for GFAP/S100B and S100B/GCaMP3 (enlargement in Figure 10D, E, arrowheads).

4.3.2 Loss of the GABA$_{B1}$ protein in cKO hippocampal astrocytes

After successful loss of hippocampal GABA$_{B1}$ mRNA in astrocytes the expression of the protein was investigated. GABA$_{B1}$ receptor expression could be identified on GFAP/GLAST positive astrocytes (Perea *et al.*, 2016). After tamoxifen administration at an age of four weeks, the astrocyte processes lacked the GABA$_{B1}$ protein. This loss was quantified with two overlap coefficients (Figure 11D, Overlap and Manders coefficient), where the overlap between GLAST and GABA$_{B1}$ expression was measured and a significant reduction could be detected in cKO compared to control (con).
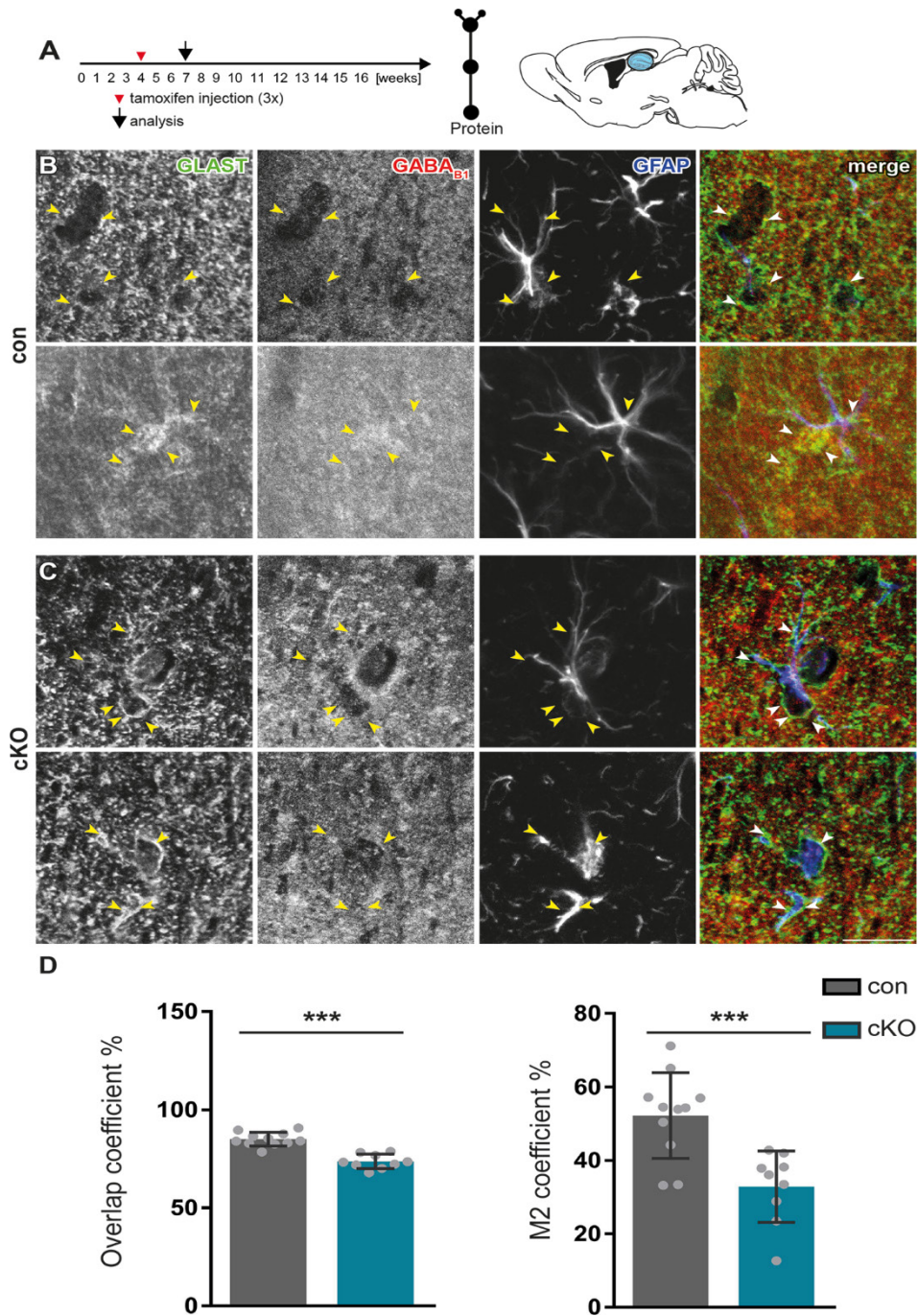
Figure 11: Significant reduction of the GABA$_{B1}$ protein in hippocampal astrocytes

A: Tamoxifen injection with four weeks and analysis with seven weeks. B: GABA$_{B1}$ protein is expressed on GFAP/GLAST positive astrocytes (closed arrowheads). C: Reduction of GABA$_{B1}$ protein specifically on astrocytes (arrowheads). D: Quantification of GABA$_{B1}$ protein in cKO and con showed a significant reduction in cKO (Overlap coefficient, Manders coefficient), Bar indicate 10 µm, respectively (n= 9-11 slices, 2 animals). Figure modified after (Perea *et al.*, 2016)

4.4 Analysis of the GABA$_B$ receptor knockout in cortical astrocytes

4.4.1 Reduced GABA$_{B1}$ mRNA expression in isolated astrocytes but in total homogenates

In cKO mice, the expression of GABA$_{B1}$ mRNA was investigated (Figure 12). Two different tamoxifen protocols were used (Figure 12A): tamoxifen injection at four weeks for three times and analyzed at seven weeks or three tamoxifen injections with four, seven and ten weeks and analysis with 13 weeks.
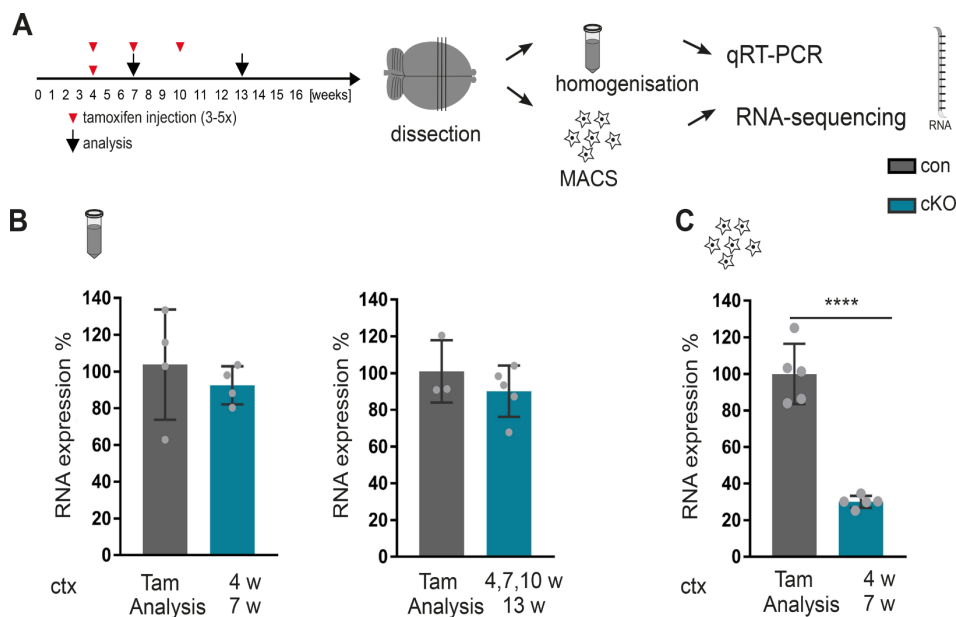
Figure 12: Reduction of GABA$_{B1}$ mRNA in isolated astrocytes but not in cortical homogenates

A: Tamoxifen injection with four weeks (3x) and analysis with seven weeks or tamoxifen injection at four, seven and ten weeks (3x each time point) and analysis with 13 weeks. The cortex was isolated and qRT-PCR was performed on total cortical homogenates or MACS isolated cortical astrocytes. B: No significant reduction of GABA$_{B1}$ mRNA expression after different tamoxifen protocols in cortical homogenates. C: Significant reduction in GABA$_{B1}$ mRNA expression of isolated astrocytes (n =3-5 animals).

The cortex was isolated, homogenized and the expression of the GABA$_{B1}$ mRNA was investigated. No significant reduction in GABA$_{B1}$ mRNA with both different tamoxifen protocols could be detected (Figure 12B). By using isolated astrocytes (MACS), a significant reduction of about 70% could be shown in GABA$_{B1}$ mRNA with RNA sequencing (Figure 12C).

4.4.2 Astrocyte specific deletion of GABA$_{B1}$ mRNA visualized with FISH

Cortical GABA$_{B1}$ mRNA was visualized with FISH specifically on S100B, GFAP and GCaMP3 positive astrocytes. After tamoxifen injection with four weeks, the expression of GABA$_{B1}$ mRNA was investigated in control and cKO animals (Figure 13).
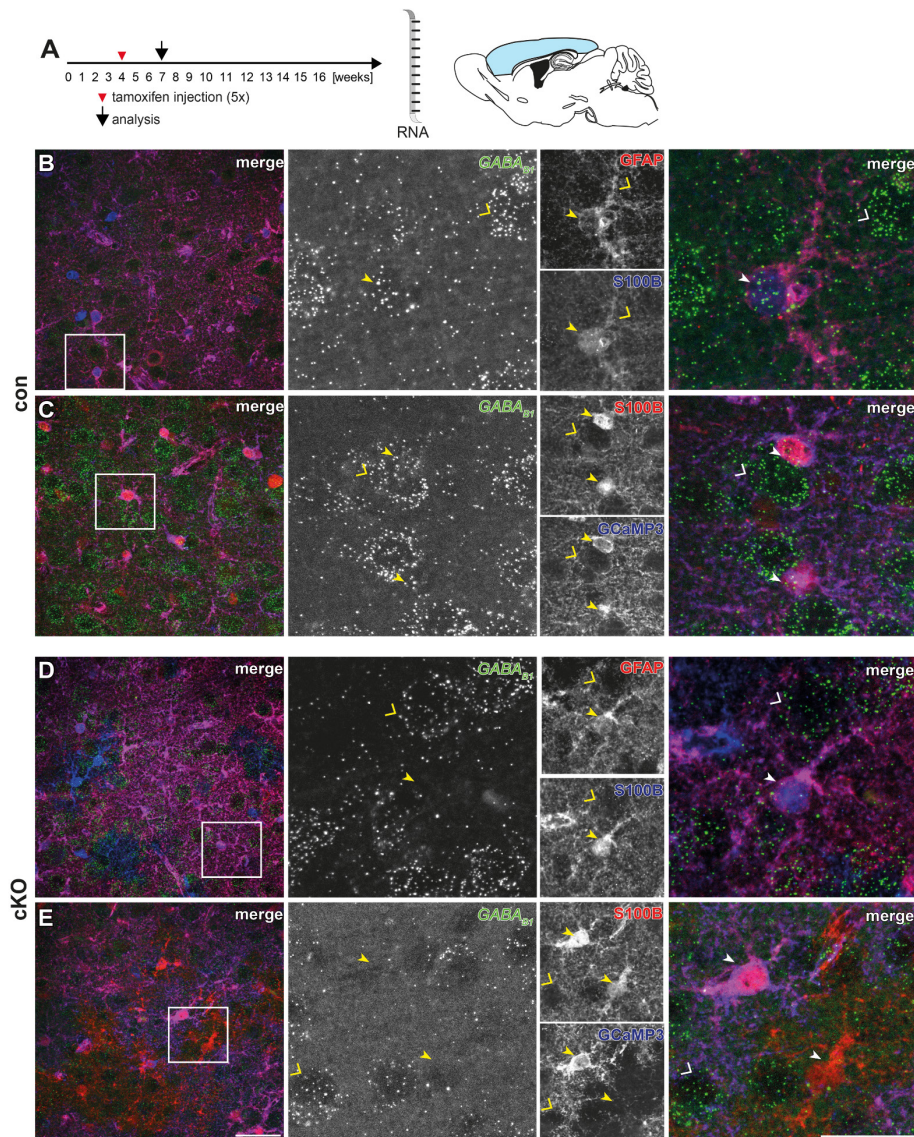
Figure 13: Reduced GABA$_{B1}$ mRNA in cortical astrocytes

A: Experimental design: Tamoxifen injection with four weeks and analysis with seven weeks. GABA$_{B1}$ RNA in cortical neurons in control and cKO (open triangle, B-E). B-C: GABA$_{B1}$ mRNA expression on GFAP$^+$/S100B$^+$ astrocytes or S100B$^+$/GCaMP3$^+$ astrocytes (arrow heads). D-E: Loss of GABA$_{B1}$ mRNA specifically on cKO astrocytes (arrow heads). Bars indicate 20 µm (overview) and 10 µm (enlargement), respectively.

In the control mice, S100B/GFAP positive astrocytes expressed $GABA_{B1}$ mRNA (Figure 13B), whereas mRNA was lacking in cKO (Figure 13D). GCaMP3/S100B positive astrocytes with $GABA_{B1}$ mRNA in control could be observed (Figure 13C) but not in cKO (Figure 13E).

4.4.3 Cortical $GABA_{B1}$ protein expression was reduced in cKO

Astrocytes, positive for S100B, expressed $GABA_{B1}$ protein in control animals (Figure 14B, closed arrowheads); whereas cKO astrocytes lacked $GABA_{B1}$ (Figure 14C, closed arrowheads).
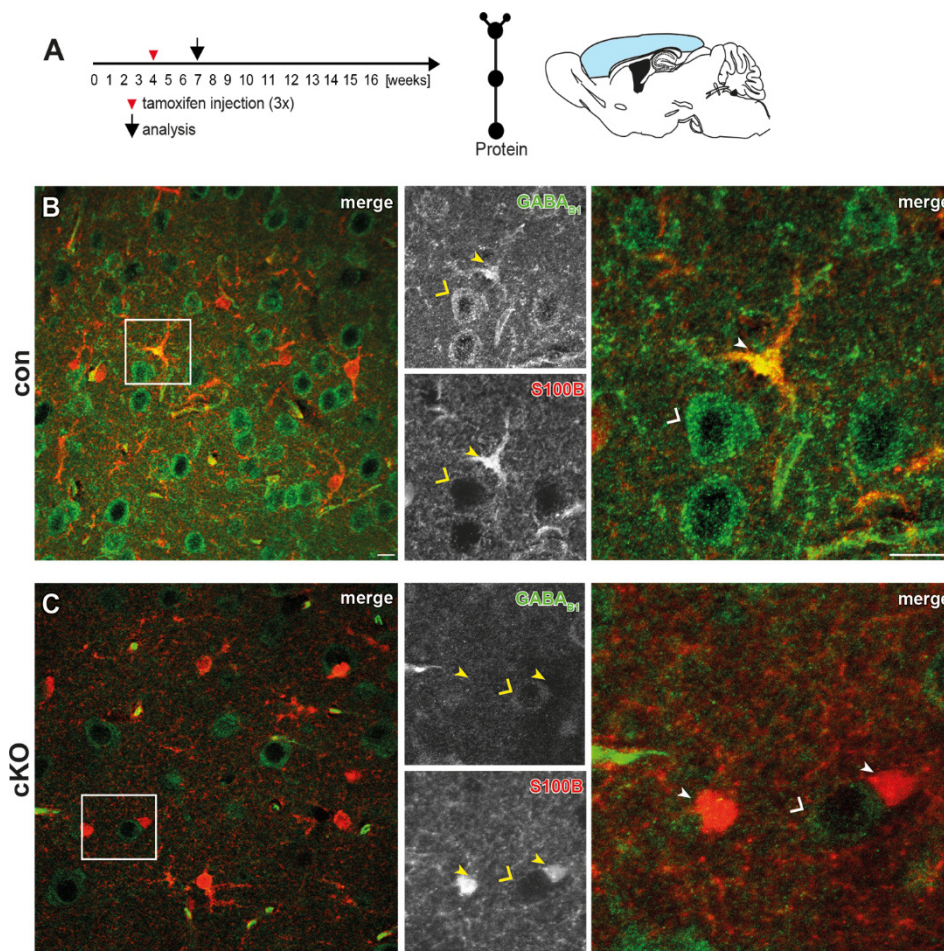
Figure 14: Loss of $GABA_{B1}$ expression in cortical astrocytes

A: Tamoxifen injection with four weeks and analysis with seven weeks. $GABA_{B1}$ protein expression on neurons in control and cKO (B-C, open triangle). B: $GABA_{B1}$ protein on S100B positive astrocytes (arrow heads). C: Loss of $GABA_{B1}$ protein specifically on cortical astrocytes (arrow heads). Bars indicate 20 μm (overview) and 10 μm (enlargement), respectively.

4.4.4 Quantification of GABA$_B$ receptor deletion on mRNA and protein

For quantification of GABA$_{B1}$ mRNA changes in cKO the standard tamoxifen protocol was used (Tam 4 weeks, analysis 7 weeks, Figure 15A). For quantification of the GABA$_{B1}$ protein expression, four different tamoxifen protocols were compared: 4-7 weeks; 4-10 weeks; 4-16 weeks; p13-14-7 weeks; 4, 7, 10-13 weeks (Figure 15A). Three confocal images of S100B$^+$ cortical astrocytes were taken and quantified with three individual slices per animal. Analysis of GABA$_{B1}$ mRNA in cortex indicated around 70% of the astrocytes expressed GABA$_{B1}$ mRNA in control animals, with only 40% in cKO animals (Figure 15B). On the protein level, in control animals ~ 60% of all analyzed astrocytes were GABA$_{B1}$ receptor positive. In cKO animals, a significant reduction about 50% in all different tamoxifen protocols could be found (Figure 15C). In the cKO 30% of all astrocytes expressing GABA$_{B1}$ receptor. With none of the tested protocols, this could be further reduced.
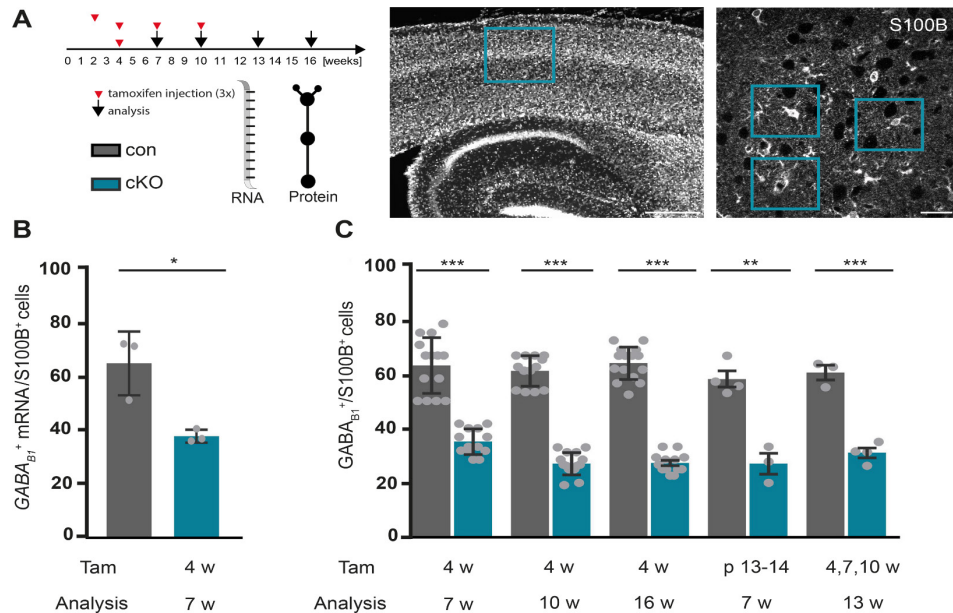
Figure 15: Quantification of the GABA$_{B1}$ mRNA/protein loss in cortical astrocytes

A: Tamoxifen protocol: 4-7weeks; 4-10 weeks; 4-16 weeks; p13, 14-7weeks; four, 7, 10-13 weeks. Images were taken in the somatosensory cortex with an enlargement of astrocytes. B: Reduction of GABA$_{B1}$ mRNA visualized with FISH in cKO compared to con. C: Quantification of the GABA$_{B1}$ protein deletion. loss of GABA$_{B1}$ protein expression with all tested tamoxifen protocols by 50%. Bars indicate 300 µm (overview) and 20 µm (enlargement), respectively (n= 3-15 animals).

4.4.5 Absence of GABA$_{B2}$ subunit in cortical astrocytes but not in neurons

To complete the expression study of GABA$_{B1}$ cKO GABA$_{B2}$ subunits were investigated in the absence and presence of astrocytic GABA$_{B1}$ subunit. The co-expression of GABA$_{B1}$ and GABA$_{B2}$ subunits in GCaMP3 positive control cortical astrocytes could be found (Figure 16B). No GABA$_{B1}$ and GABA$_{B2}$ subunit expression could be identified on cKO astrocytes (Figure 16C, arrowheads); while both subunits were still expressed on parvalbumin positive neurons (Figure 16D, open triangles).
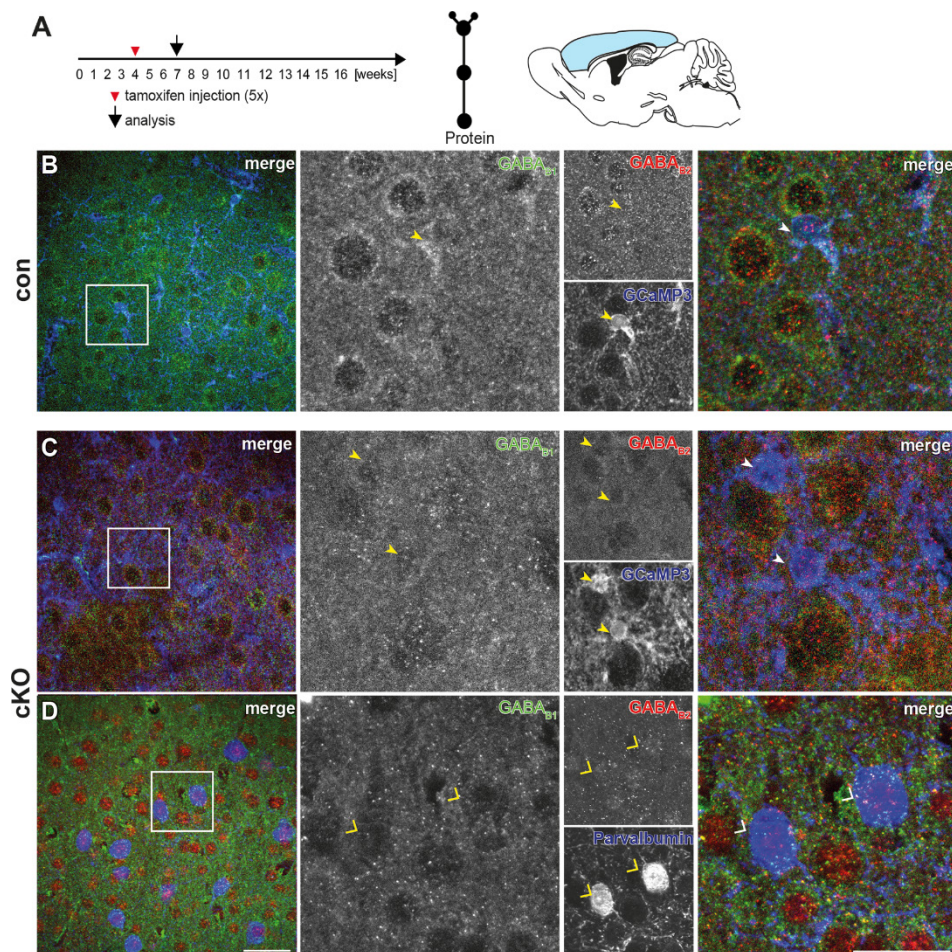
Figure 16: GABA$_{B1}$ and GABA$_{B2}$ subunit loss in cKO astrocytes

A: Tamoxifen injection with four weeks and analysis with seven weeks. B: Co-expression of GABA$_{B1}$ and GABA$_{B2}$ subunits on GCaMP3 positive astrocytes (arrowheads). C: Loss of GABA$_{B1}$ and GABA$_{B2}$ subunits specifically on astrocytes in cKO (arrowheads). D: Both subunits were still present on parvalbumin positive neurons in cKO (open triangles). Bars indicate 20 µm (overview) and 10 µm (enlargement), respectively.

4.4.6 GFAP expression changes under physiological and pathological conditions in cKO animals

Next changes in astrocyte-specific proteins after $GABA_{B1}$ receptor deletion were investigated. While no changes could be observed for glutamine synthetase (GS) or GLAST, GFAP was reduced in cKO (Figure 37, Appendix I). On mRNA and protein level GFAP was down-regulated in cKO compared to control (Figure 37B, C). Since cortical expression of GFAP is highly upregulated under pathological conditions (Burda & Sofroniew, 2014), expression changes of GFAP in the absence of GABAB receptors were investigated under pathological conditions (stab wound injury (SWI)). The animals were injected with tamoxifen at an age of four weeks. SWI was performed 21 days later and seven days after the injury (7dpi), the animals were analyzed (Figure 17). Here the red fluorescent reporter tdTomato was crossed to the $GABA_{B1}$ cKO mouse line.

A high expression of GFAP and tdTomato (tdT) at the injury site could be identified compared to the contralateral side (cl) (Figure 17B). Analysis of the fluorescence intensity of GFAP ipsilateral (il) displayed an upregulation of GFAP in cKO and control animals (Figure 17C) compared to physiological condition (cl). While expression of GFAP was increased at the injury site (il), this increase was reduced in the cKO (Figure17C). Also an increase in the tdTomato fluorescence intensity at the injury site could be detected. No difference between cKO and control animals could be observed (Figure 17D). Furthermore, no difference in tdTomato and GFAP expression between cKO and control could be detected contralaterally.
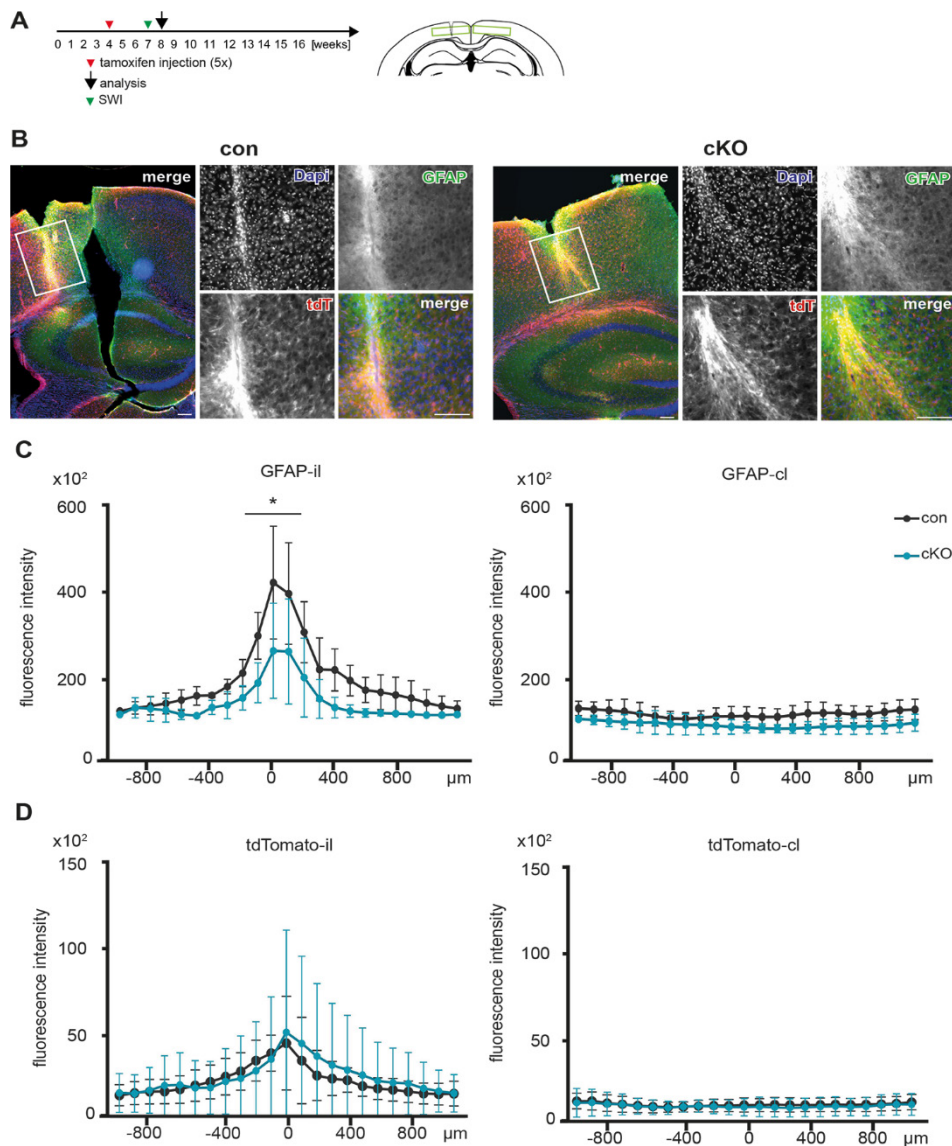
Figure 17: Reduced GFAP upregulation after acute injury in cKO animals

A: Tamoxifen injection with four weeks, stab wound injury (SWI) with seven weeks, analysis 7 d later. B: Overview of the injury side in the cKO and control animals. Close-up showed the high expression of GFAP and tdTomato (tdT) at the injury side. C: Increase in GFAP expression on the ipsilateral side (il). On cKO shows less increase of GFAP at the injury side compared to con. At the contralateral side no different between cKO and control in the GFAP fluorescence intensity. D: No difference in the tdTomato expression between cKO and con at the contra- and ipsilateral side. Bars indicate 500 µm (overview) and 200 µm (enlargement), respectively (n= 12-15 slices, 3-5 animals).

4.5 Analysis of astroglial Ca²⁺ properties *in vivo* and acutely isolated slices

After confirming the astroglial GABA_B receptor deletion on the molecular level, the functional consequences of the cKO were analyzed. Activation of GABA_B receptors leads to changes in intracellular Ca²⁺ concentrations, however this is a matter of debate (Albrecht *et al.*, 1986; Kang *et al.*, 1998; Mariotti *et al.*, 2016). Astrocytes communicate over Ca²⁺ signals with other cells (Volterra *et al.*, 2014; Bindocci *et al.*, 2017b). Therefore, we focused on the changes in Ca²⁺ signal properties in the absence of GABA_B receptors, *in vitro* with acutely isolated brain slices and *in vivo* in anesthetized and awake animals. Ca²⁺ signals were visualized with the genetically encoded Ca²⁺ indicator GCaMP3 (3.1.8.3 TgH (Rosa 26-CAG-lsl-GCAMP3)^GCAMP3).

All Ca²⁺ data were analyzed with MSparkles. Ca²⁺ signals were characterized by their location into gliapil or somatic signals (cell bodies) and by amplitude and duration of the signal. Furthermore signals were classified based on their amplitude greater or equal than the first standard deviation but smaller than the second standard deviation (1SD; small signals), higher or greater the second standard deviation but smaller than the third standard deviation (2SD, medium) and are greater or equal than third standard deviation (3SD, large signals) (Figure 18).
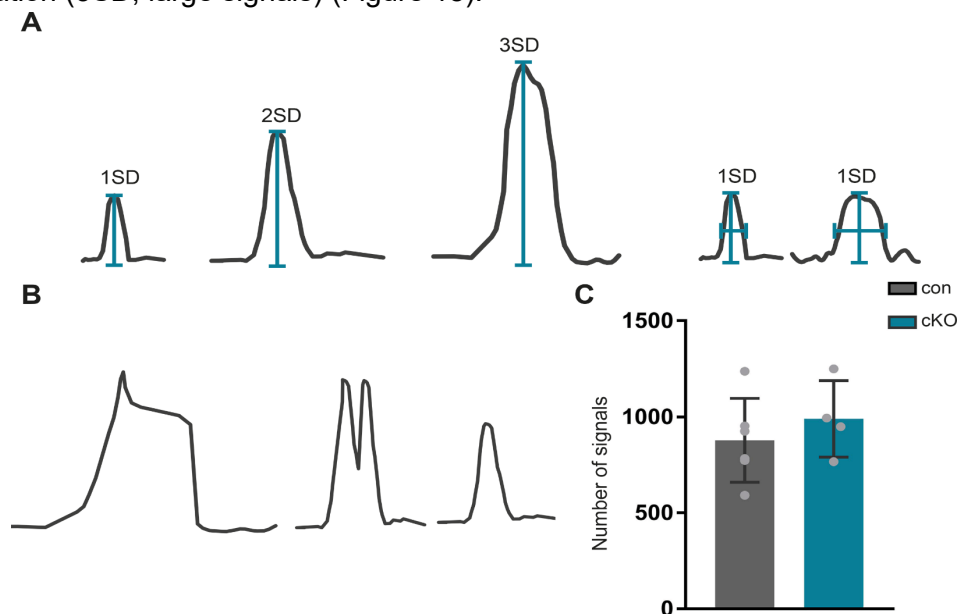
Figure 18: Example for Ca²⁺ signals sorted by their characteristics

A: Example of Ca²⁺ peak with different signal strength, sorted by MSparkles into 1, 2, and 3SD. The duration is dependent on the signal amplitude. B: Examples of different Ca²⁺ signals C: Pooled number of signals in cKO and control animals. No difference in the signal number due to the high variability (n= 4-5 ROIs).

The duration is dependent on the amplitude. The signals are sorted in the different groups (1,2,3SD) by their signal amplitude regardless their duration (Figure 18A).

All the following figures are a summary of different animals in different experiments. A large variance of individual ROIs could be found (Figure 39). The summary of the individual data is plotted as a boxplot, which can even visualize the scattering of a data set. The data set is divided into quartiles.

The whiskers represent the data variability outside the upper and the lower quartile. The box indicates the variability of the data around the median. A small box and whiskers represent data, which are close to the median. A large box and whiskers indicate a high scattering of the data. The boxplot can not represent the number of signals (Figure 39). The number of signals was not incorporated in the analysis, since there was a large variability in the individual ROIs and animals (Figure 18B). Overall, no difference in signal quantities could be found between cKO and control (Figure 18B). Therefore, it was not analyzed further. For comparison of the signal composition only ratios of the different signal groups were included. Ratios differing over 5% counted as significantly different. The statistical parameters can be found in 8.6.

4.5.1 Baclofen application leads to smaller but longer Ca^{2+} signals

To investigate how of Ca^{2+} signals were modulated by astrocytic GABA$_B$ receptors acutely isolated brain slices were treated with the GABA$_B$ agonist baclofen (Perea *et al.*, 2016). Animals were treated with tamoxifen on five consecutive days at an age of 4 weeks and slices were prepared at an age of eight weeks (Figure 19A). Ca^{2+} signals were recorded before (baseline, gray) and during baclofen application (baclofen, green) in control and cKO animals (Figure 19 and Figure 20).

Neither amplitude nor duration of somatic Ca^{2+} signals were changed after baclofen application (Figure 19B, C). In the gliapil the amplitude of small signals was only reduced by 5% in the presence of baclofen (Figure 19B). Small (1SD) and medium (2SD) signals were longer and display a higher data scattering (Figure 19C). Large signals were not affected by baclofen (Figure 19C).The signal composition represents the percentage of signals in all three different groups (Figure 19D, small (1SD), medium (2SD), large (3SD)). Application of baclofen led to an increase in the proportion of small signals, whereas the large signal proportion (3SD) in gliapil and cell somata was decreased (Figure 19D). The percentage of medium signals was almost doubled after baclofen application in somatic Ca^{2+} signals, while they remained constant in the gliapil.

Taken together the application of baclofen leads to longer signals in the gliapil of control animals. Furthermore, the percentage of small signals was increased, whereas the number of large signal was decreased in gliapil and cell somata.
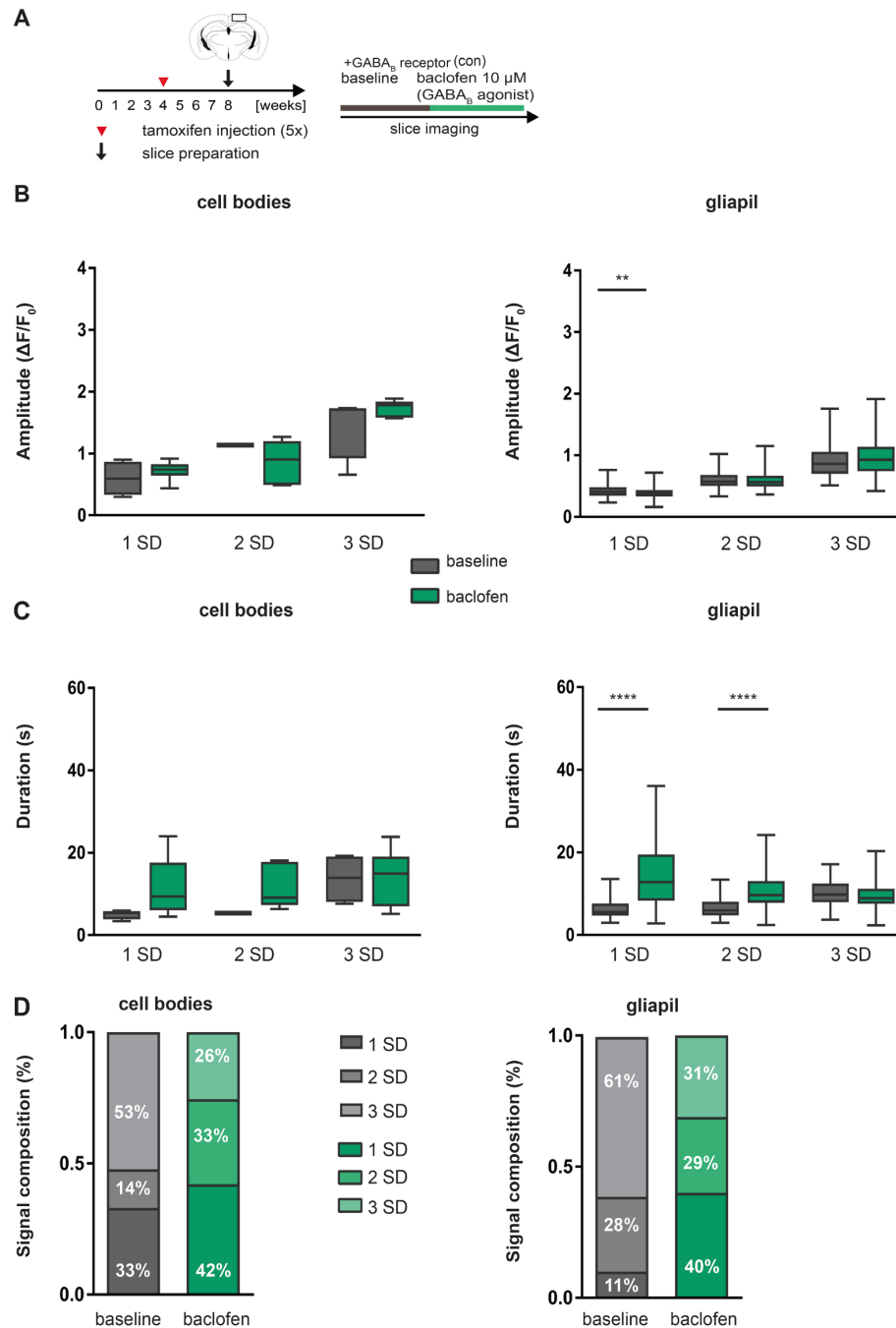
Figure 19: Baclofen application leads to longer signals in control animals

A: Tamoxifen with four weeks and analysis in acutely isolated slices with eight weeks. B: No change in signal amplitude of somatic Ca^{2+} peaks after baclofen application. Small signals (1SD) were smaller after baclofen, whereas medium (2SD) and large (3SD) signals were not altered in the gliapil. C: No change in duration of somatic Ca^{2+} peaks, whereas small and medium signals were longer during baclofen application in the gliapil. D: After baclofen more small signals and less large signals were detected in soma and gliapil. The percentage of medium signals was not altered in the gliapil but doubled in cell bodies after baclofen treatment (n= 1 animal and 3 slices).
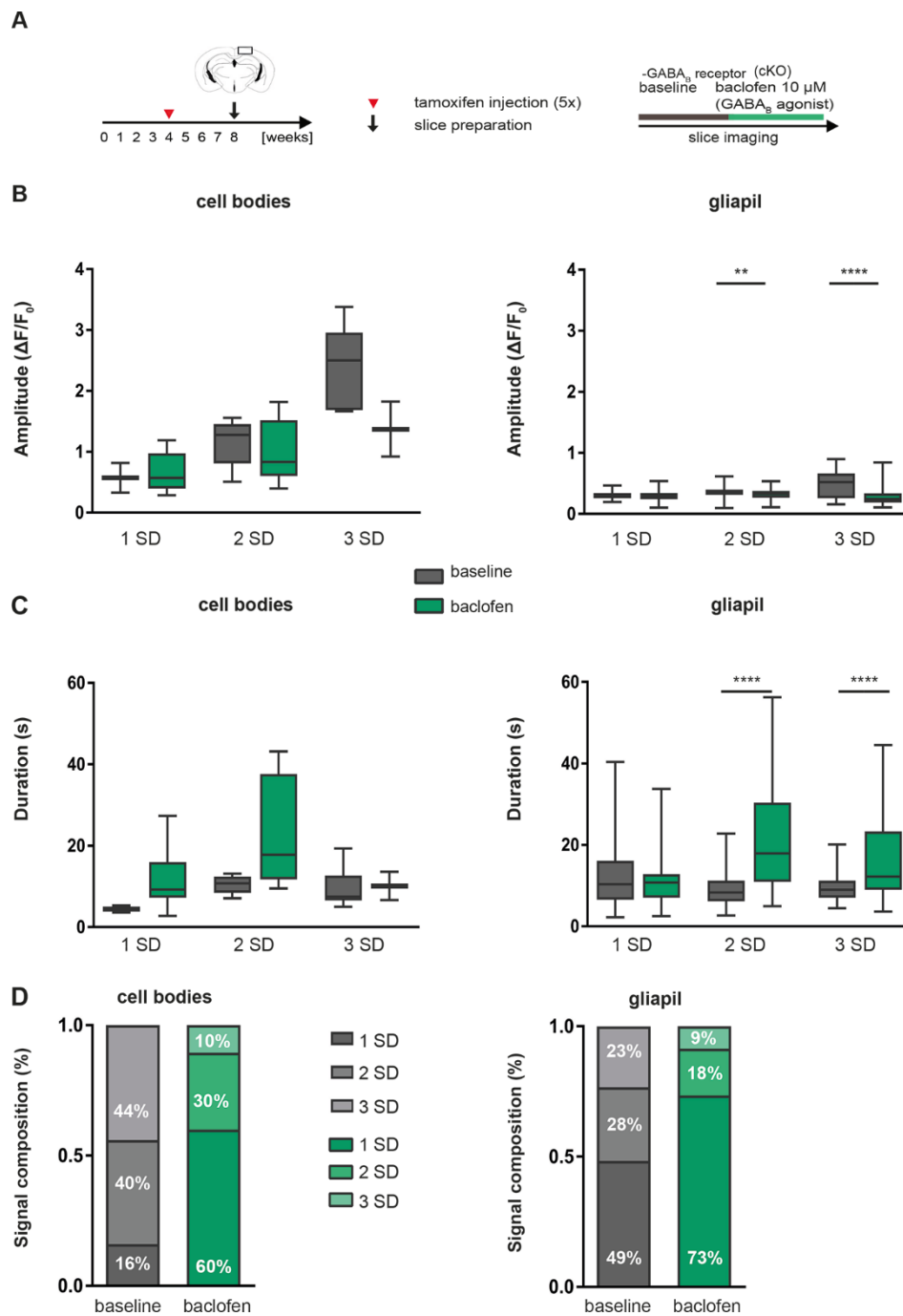
Figure 20: Application of baclofen leads to smaller and longer signal in cKO mice

A: Tamoxifen with four weeks and analysis in acutely isolated slices with eight weeks. Baseline (gray) and the signals during baclofen application (green). B: No change in somatic Ca^{2+} peaks after baclofen application. Medium and large signals were smaller C: In the gliapil medium and large Ca^{2+} signals were longer and no changes in somatic signals comparing baseline to baclofen treatment. D: Baclofen application led to an increase in the proportion of small signals and to a decrease in medium and large signals (n= 2 animals and 4 slices).

Next, baclofen was applied to animals lacking the astrocytic GABA$_B$ receptors (cKO). As observed in control animals, the amplitude and duration of somatic Ca^{2+} signals were not altered after baclofen application (

Figure 20B, C). In the gliapil cKO medium (2SD) and large (3SD) signals were smaller and longer after baclofen treatment, while small signals were not affected (

Figure 20B, C). In the presence of baclofen medium and large signals displayed a higher scattering of the signal duration. As shown in control animals, baclofen administration resulted in an increase in the proportion of small signals, subsequently medium and large signals in gliapil and cell somata were decreased (

Figure 20D).

In summary:

- Application of baclofen leads to an 1.6-2 fold increase in the signal duration in control animals

- In cKO the signal amplitude of medium and large signal were smaller (2SD 8%; 3SD 54%)

- In cKO the signal duration was doubled in medium and large signals

- In control as well as in cKO baclofen leads to an increase the proportion of small and to a decrease of large signals

- Somatic Ca^{2+} signals were not affected by application of baclofen in cKO and control mice

4.5.2 cKO mice show signals with reduced amplitude

Ca^{2+} changes of cKO (turquoise) and control animals (gray) in the presence of baclofen (green line) and during baseline (gray line) were compared with each other (Figure 21). Baclofen did not affect somatic Ca^{2+} signals in cKO and control (Figure 19 and

Figure 20). By comparing cKO to control, no difference in signal amplitude and duration of somatic Ca^{2+} peaks could be observed (Figure 21B, C, gray and green line). But, these signals showed a high data scattering indicated by the large size of the boxplot and the whiskers.

In the gliapil, application of baclofen evoked smaller and longer signals in cKO and control animals (Figure 19 and

Figure 20). By compared cKO to control, the signal amplitude in cKO was reduced in the baseline and in the presence of baclofen (Figure 21B). By comparing the signal duration, small (1SD) and medium (2SD) signals were elongated in cKO during baseline (Figure 21C). By application of baclofen, cKO medium and large signals were
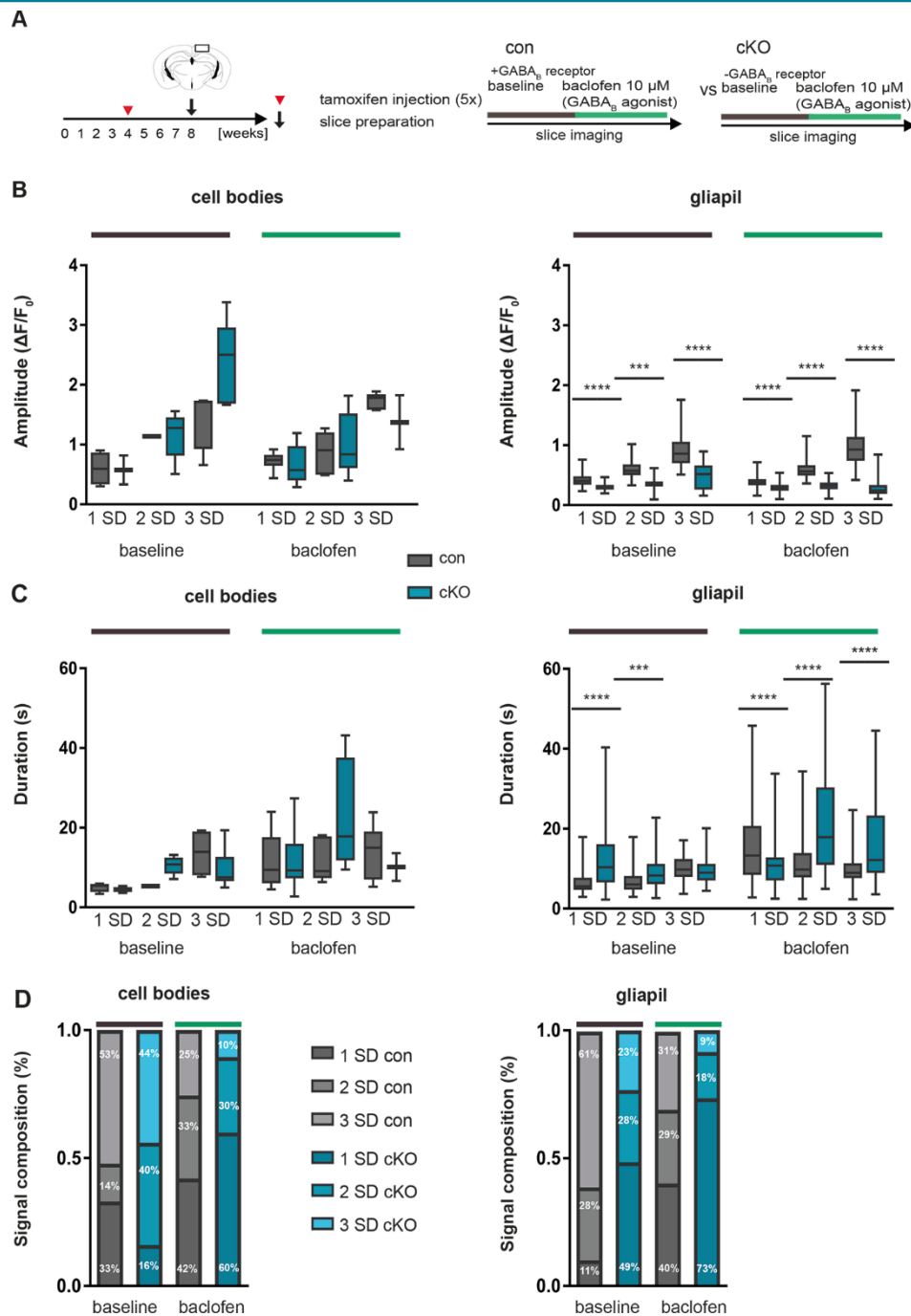
longer, but small signals shorten compared to control (Figure 21C). Overall cKO displayed a higher variability in the duration of Ca^{2+} signals compared to control.

Figure 21: Smaller signals in cKO before and after baclofen administration

A: Experimental design B: No difference in the signal amplitude of somatic Ca^{2+} signals. In the gliapil cKO Ca^{2+} signals were smaller compared to con (baseline and baclofen). C: In the gliapil small and medium signals were longer in cKO. After baclofen application signal duration of medium and large signals increased and small signals were shorten in cKO compared to con. No change in the signal duration of somatic Ca^{2+} signals. D: During baseline the proportion of small small and large somatic Ca^{2+} signals was reduced in cKO. After baclofen application the proportion of small signals was increased and the proportion of large signals

was decreased compared cKO to con. In the gliapil cKO showed always a higher proportion of small and lower proportion of large signals compared cKO to con (n= 3 animals and 7 slices)

The proportion of small signals was increased and large signals was reduced in the gliapil and cell somata during baclofen application (Figure 19 and

Figure 20). By comparing the signal composition of somatic Ca^{2+} signals, the cKO showed a lower proportion of small (1SD) and large (3SD) signals with a higher proportion of medium signals in the baseline. In the presence of baclofen, the proportion of small signals was increased and the percentage of large signals was decreased in cKO (Figure 21D). In the gliapil cKO displayed always a higher proportion of small and a lower proportion of large signals despite baseline or baclofen (Figure 21D).

In summary:

- Somatic Ca^{2+} signals were not changed in cKO compared to control

- In cKO the signal amplitude was reduced by 40% in the baseline and during baclofen application

- The signal duration was doubled in cKO

- In the presence of baclofen, cKO mice displayed a higher percentage of small and a lower percentage of large signals in the gliapil and cell somata

4.5.3 Baclofen and CGP34358 modulate astroglial Ca^{2+} signals

Next, Ca^{2+} signals were investigated in the presence of baclofen and the $GABA_B$ antagonist CGP34358 (Perea *et al.*, 2016). Furthermore, the slices were treated with TTX (Tetrodotoxin, fast sodium channel blocker (Chen & Chung, 2014)) to inhibit neuronal influence. Ca^{2+} signals were recorded before (baseline, dark gray) as well as during CGP34358 and baclofen application (CGP light gray, baclofen green) in control animals (Figure 22 and Figure 23).

Overall signal amplitude and duration of somatic Ca^{2+} signals were not affected by the application of CGP34358 (CGP, light gray) and baclofen (baclofen, green) in control animals (Figure 22B, C). The indicated statistical difference resulted from high data scattering, displayed by a large boxplot and large whiskers. In the gliapil, small and medium signals were smaller after application of CGP. In the presence of baclofen the signal amplitude was increased again (Figure 22B). The signal amplitude of large signals was increased in the presence of CGP or baclofen compared to baseline. All classes of signals (1,2,3SD) were shorter after baclofen application compared to baseline and CGP application (Figure 22C). The signal duration of medium and large
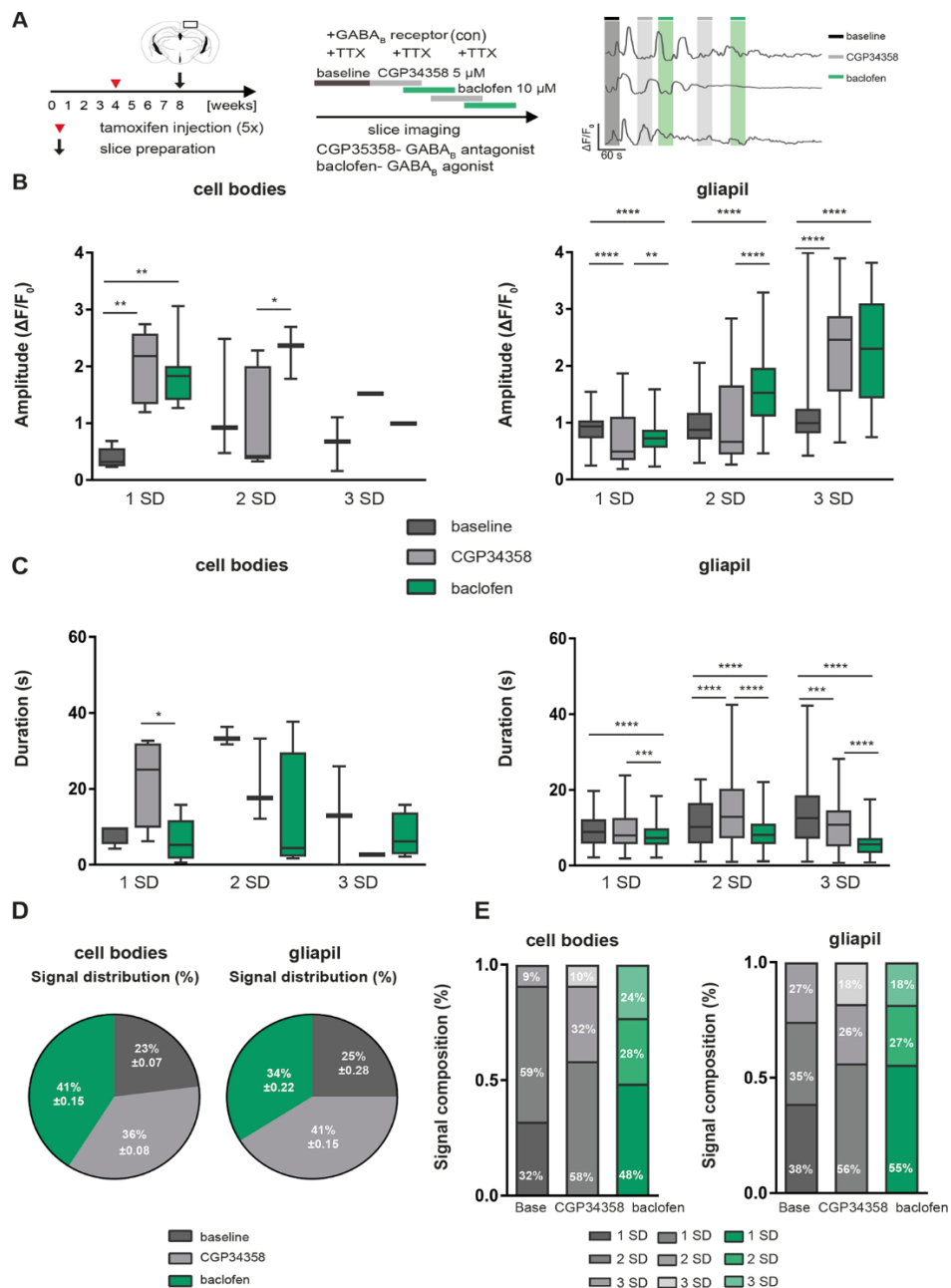
signals was affected by CGP application, whereas small signals were not altered (Figure 22C).

Figure 22: Smaller signals by CGP34358 application, rescued by baclofen application in control animals

A: Tamoxifen with four weeks and analysis with acutely isolated slices with eight weeks. Baseline (dark gray) and the signals during CGP34358 (light gray) and baclofen application (green). B: Increased signal amplitude of somatic small and medium Ca^{2+} signals after CGP and baclofen application. In the gliapil signal amplitude of small and medium signals was reduced after CGP application and larger after baclofen application. Amplitude of large signals was increased

between baseline and baclofen and between CGP and baseline. C: In the gliapil small signals were shorter compared baseline to baclofen and CGP to baclofen. Medium signals were longer after CGP application and shorter after baclofen application. Large signals were shorter after application of CGP and baclofen. No change in duration of somatic Ca^{2+} signals could be found, except signal duration of small signals was shorter compared CGP to baclofen.

D: Signal distribution was not changed compared gliapil to cell somata. The proportion of signals was increased after baclofen and CGP application. E: Higher proportion of small signals after application of CPG and baclofen compared to baseline in gliapil and cell somata. In cell somata the proportion of large signals was higher after application of CGP and baclofen and the proportion of medium signals lowered. In the gliapil the proportion of medium and large signals was decreased after application of CPG and baclofen (n= 1 animal and 3 slices).

The signal distribution, representing the proportion of signals encountered in baseline, CGP and baclofen application, was not altered between gliapil and cell somata (Figure 22D, pie chart). But somatic signals showed a higher variability indicated by higher standard deviation. After application of CGP, the proportion of small signals was higher in gliapil and cell somata (Figure 22E). By baclofen application, the proportion of small signal was slightly decreased or equal compared to CGP but still higher than the baseline. In cell somata the proportion of large signals was increased, while the proportion of medium signals lowered compared CGP and baclofen to baseline. In the gliapil the proportion of large and medium signals decreased after application of CGP or baclofen compared to baseline.

Taken together, CGP led to smaller signals in the gliapil of control mice. In the presence of baclofen the amplitude of the signals was increased. Somatic Ca^{2+} signals were not altered by the $GABA_B$ antagonist and agonist. Application of CGP and baclofen increased the proportion of small signals in gliapil and cell somata compared to baseline.

As shown in the control, also cKO somatic Ca^{2+} signals were not changed after of CGP34358 and baclofen application (Figure 23B, C). In the gliapil only the signal amplitude of medium signals was reduced in the presence of CGP application, whereas the amplitude of small and large signals was larger or not altered (Figure 23B). In the same line with the control, also the application of baclofen led to an increase in signal amplitude in cKO. In the presence of CGP all cKO signals were longer (Figure 23C). Small signals were as in control, longer compared baseline to baclofen, whereas large signals were shortened (Figure 23C).
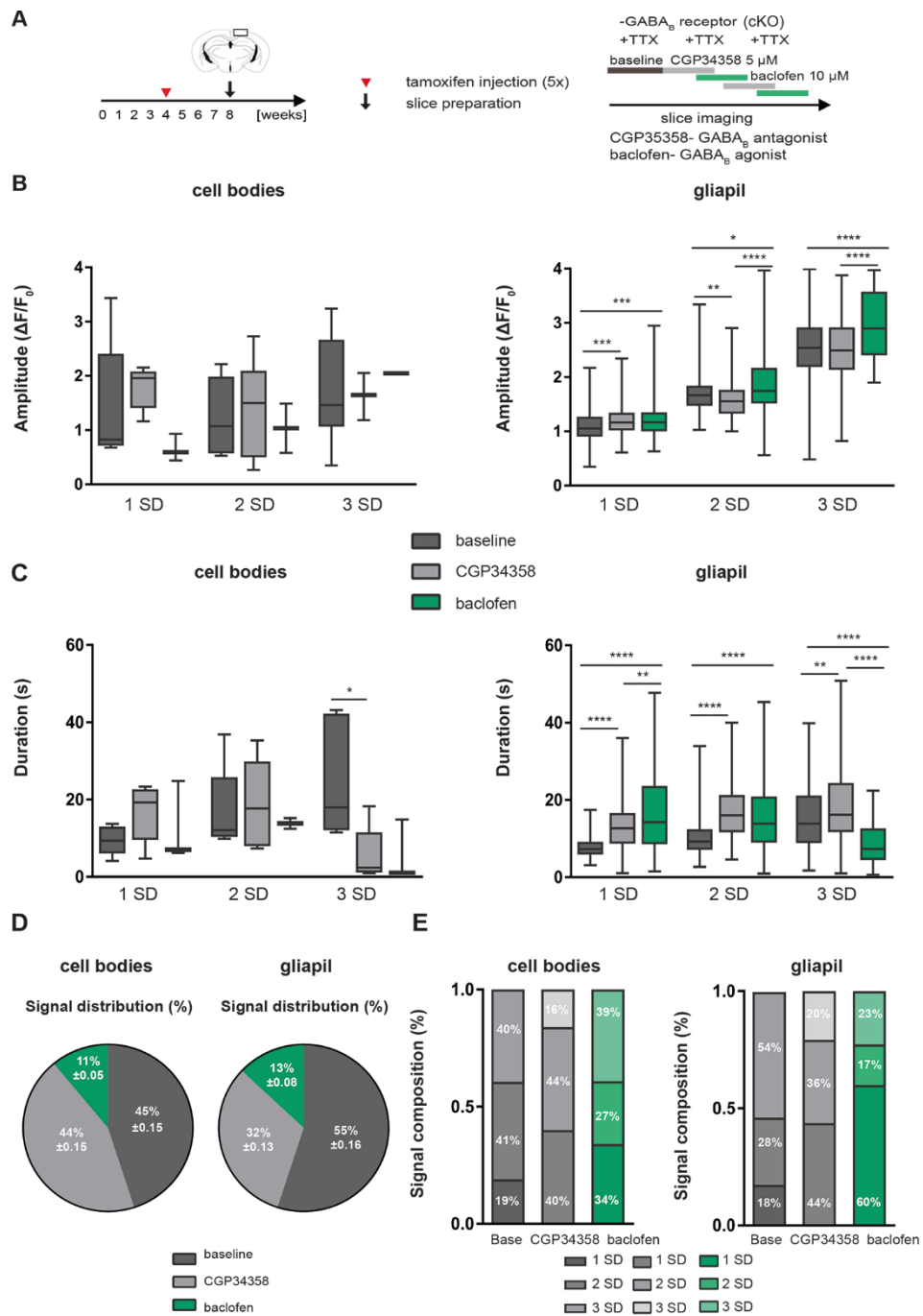
Figure 23: Changes in Ca^{2+} properties after CGP34358 and baclofen application in cKO

A: Tamoxifen with four weeks and analysis with acutely isolated slices with eight weeks. Baseline (dark gray) and the signals during CGP34358 (light gray) and

baclofen application (green). B: Amplitude of somatic Ca^{2+} signals was not altered. In the gliapil increased signal amplitude after baclofen application compared to baseline and to CGP. After CGP application amplitude of large signals was not altered, but medium signals were smaller and small signals larger. C: In the gliapil Ca^{2+} signals were longer after application of CGP, while after baclofen application arge signals were shorter and small signals longer. The duration of somatic Ca^{2+} signals was not altered, except large signals were shorter after application of CGP.

D: The proportion of signals, encountered in baseline, was increased compared to CGP and baclofen in gliapil and cell somata. E: The proportion of small signals was increased after application of CGP and baclofen. The proportion of large signals was smaller or equal compared baseline to CGP and baclofen application in cell somata and less in gliapil. The proportion of medium signals was smallest during baclofen application (n= 1 animal and 3 slices).

No changes in the signal distribution between gliapil and cell somata could be observed (Figure 23D, pie chart). Interestingly, compared to control, the proportion of signals in the baseline was higher in cKO, concurrently the proportion of signals during baclofen application was lower (Figure 23D). As indicated in the control, also in cKO the application of CGP and baclofen increased the proportion of small signals in cell somata and gliapil (Figure 23E). The proportion of medium signals was higher after CGP application but then reduced in the presence of baclofen. In the cKO the proportion of large signals was decreased in the presence of $GABA_B$ antagonist and agonist.

In summary:

- The signal duration and amplitude of somatic Ca^{2+} signals were not altered in cKO and control by application of CGP34358 and baclofen

- In the gliapil, the amplitude of signals was reduced by 40%, whereas in the cKO only the amplitude of medium signals was reduced by 11% in the presence of CGP34358

- The application of baclofen increased the signal amplitude in cKO by 10%, whereas in control by 70%.

- In cKO the signals were longer by 70% in the presecence of CGP34358

- In the proportion encountered in the baseline was increased in cKO

- In cKO and control mice the proportion of small signals was increased by application of CGP34358 and baclofen

4.5.4 Larger and longer Ca^{2+} signals in cKO compared to control

By comparing cKO (turquoise) to control (gray) overall no change in the somatic signal duration or amplitude could be detected (Figure 24B, C). In the gliapil the amplitude and duration of the Ca^{2+} signals in the cKO were increased compared to control during CGP34358 (gray line) and baclofen application (green line) (Figure 24B, C). Overall, all signals showed a high data scattering indicated by a large boxplot and long whiskers.

Application of CGP and baclofen increased the proportion of small signals. The cKO showed a lower proportion of small signals compared to control in gliapil and cell somata (Figure 24D). In contrast, the proportion of large signals was higher in cKO compared to control (Figure 24D). The proportion of cKO medium signals was reduced during baseline in gliapil and cell somata. By CPG application the proportion of medium signals was higher.
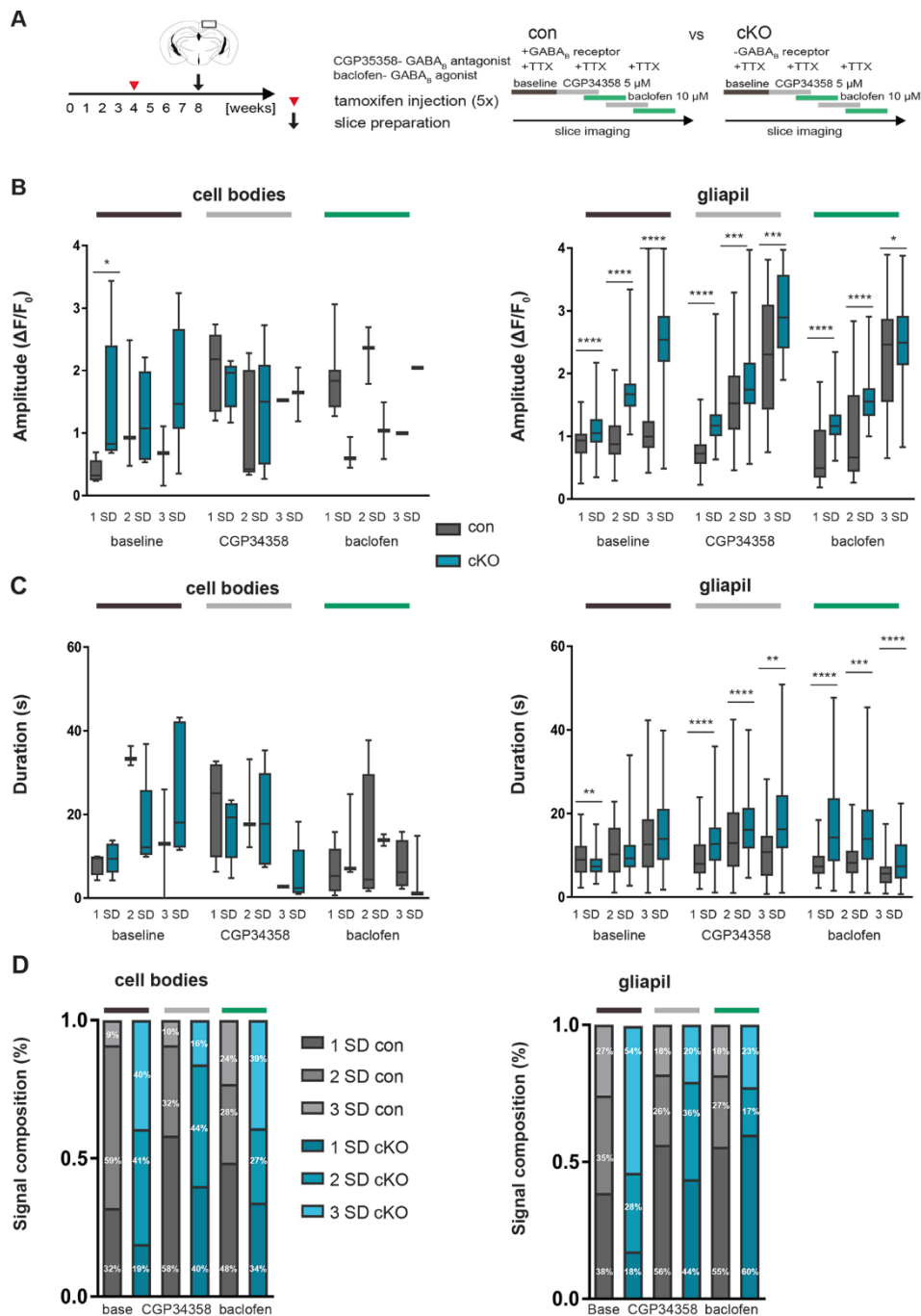
Figure 24: Larger and longer Ca^{2+} signals in cKO compared to control after application of CGP34358 and baclofen

A: Experimental design. B: The amplitude of somatic Ca^{2+} signals was not altered compared cKO to con. In the gliapil, the signal amplitude was increased in cKO. C: cKO mice with longer signals in the gliapil, whereas somatic Ca^{2+} signals were not altered. D: Lower proportion of small signals in cKO during baseline, CGP and baclofen application in cell somata and gliapil. The proportion of large signals was higher in cKO. The percentage of medium signals was increased under CGP influence but decreased in the cKO during baseline and baclofen (n= 2 animals and 6 slices).

In summary:

- The amplitude and duration of somatic Ca^{2+} signals was not changed

- A 1.5-2 fold increase in the signal amplitude in the cKO

- The signal duration was increased by 50% compared to control

From all data, generated in acutely isolated slices, we conclude:

- Somatic Ca^{2+} signals were not affected by application of CGP or baclofen with or without TTX.

- The signal properties of somatic Ca^{2+} signals were not altered by the deletion of astrocytic $GABA_B$ receptors.

- In the cKO signals were smaller in the gliapil without TTX

Therefore, we conclude that astrocytic $GABA_B$ receptors are mainly expressed on the processes.

4.6 Analysis of Ca^{2+} properties *in vivo*

After the analysis of Ca^{2+} signals in acutely isolated brain slices, the signal properties were investigated *in vivo*. The animals were either injected with tamoxifen at 4 or 7 weeks and always at an age 15-20 weeks the cranial window was implanted. After recovery from the surgery, repetitive image sessions were started. Data, which were recorded in the first ten days after the surgery, were grouped together. Since we conclude, that during this time period the Ca^{2+} signal properties were not changed between the individual imaging sessions. Changes in the Ca^{2+} properties were recorded in anesthetized (2% isoflurane) and awake animals, since anesthesia influences Ca^{2+} signals, by masking large signals and reduced signal number (Thrane *et al.*, 2012). The imaging process with 2P-LSM can induce auto-activation of astrocytic Ca^{2+} signals *in vivo* (Schmidt *et al.*, 2018). We could not detect an auto-activation of signals; the displayed heat maps did not show more signals or an increase in signal amplitude or duration signals with increasing imaging time (Apendix I). Therefore we conclude, that the following data were spontaneous Ca^{2+} signals. Futhermore, by comparing heat maps of cKO and control animals, on specific signal pattern or difference could be detected (Apendix I, Figure 40-43). The heat maps displayed spontaneous, but also synchronized large signals, which included several ROIs. But a detailed analysis of signal amplitude and duration has to be done.

4.6.1 Reduced signal amplitude and duration in cKO animals

Animals were injected five times with tamoxifen at age of 4 weeks and the Ca^{2+} signals were recorded in anesthetized and awake mice (Figure 25A and Figure 25A, black arrows). After deletion of astrocytic $GABA_B$ receptors, small (1SD) and medium (2SD) somatic Ca^{2+} signals were smaller but the duration was not altered (Figure 25B,C). Large signals (3SD) were shorter in anesthetized animals. In gliapil the amplitude of all signals was reduced compared cKO to control (Figure 25B). In addition, the duration of small and medium signals was decreased (Figure 25C).

The signal composition, representing the proportion of signals in the three different groups (small (1SD), medium (2SD), large (3SD)), displayed a higher proportion of small signals (1SD) in gliapil and cell somata in cKO compared to control (Figure 25D). The proportions of medium (2SD) and large signals were not altered in the gliapil, whereas the proportion of medium signals was higher in cKO cell somata.

In awake animals, the signal amplitude and duration of somatic Ca^{2+} signals and signals in gliapil were reduced compared cKO to control (Figure 26B, C). Interestingly, compared to acutely isolated brain slices, control animals exposed a higher data scattering, whereas the data in the cKO was more concentrated. In the absence of astrocytic $GABA_B$ receptors the proportion of small signals was lower, whereas the proportion of large signals was increased comparing cKO to control (Figure 26D).

In summary:

- In anesthetized cKO animals the signal amplitude was reduced by 60% and the duration by 70% in the gliapil

- In cell somata only the signal amplitude was reduced by 20%

- In awake animals the signal amplitude was reduced by 75% in gliapil and by 20% in cell somata

- The duration was reduced by 30% in cell somata and gliapil

- In anesthetized cKO animals, the proportion of small signals was increased, whereas in awake animals the proportion of large signals was increased

Figure 25: Smaller amplitude and shorter duration in anesthetized cKO mice

A: Tamoxifen with four weeks; cranial window between 15-20 weeks, imaging session 3, 4, 5, 8 days after recovery time. Animals were anesthetized with 2% isoflurane (mouse with closed eye). B: Somatic small and medium Ca^{2+} signals were smaller in cKO. In gliapil all signal groups displayed a reduced amplitude compared cKO to control. C: The duration of small and medium signals in the gliapil and of somatic large signals was reduced. D: A higher proportion of small signals in cKO gliapil and cell somata. Proportion of medium and large signals remained unchanged in gliapil, with less medium signals in cKO cell somata (n= 3 animals and 5 FOVs).
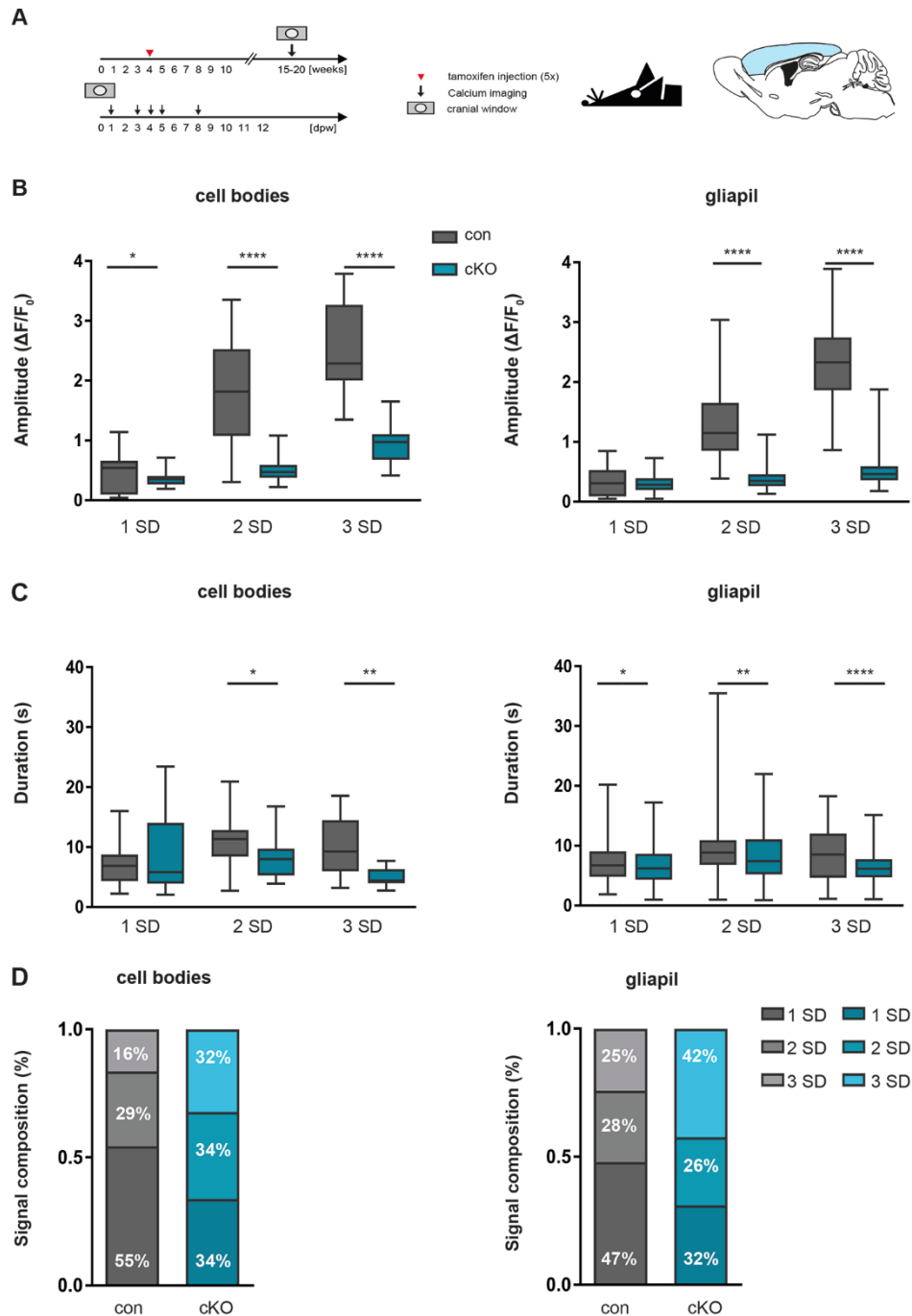
Figure 26: Reduced signal amplitude and duration in awake cKO animals

A: Tamoxifen with four weeks; cranial window between 15-20 weeks, imaging session 1, 3, 4, 5, 8 days after recovery time. Animals were awake during the imaging session (mouse with open eye). B: Smaler somatic Ca^{2+} signals in cKO. In the gliapil reduced signal amplitude of medium and large cKO signals compared to con. C: Shorter signals in cKO cell somata and gliapil. D: Proportion of small signals was decreased in cKO, whereas the proportion of large signals was increased in cell somata and gliapil. Proportion of medium signals remained unchanged (n= 4 animals and 7 FOVs).

4.6.2 Reduced proportion of small and increased proportion of large signals in awake animals

Ca^{2+} signals from awake (light gray and light turquoise) and anesthetized (dark gray and turquoise) animals were compared with each other to investigate, if anesthesia influences the modulation of astrocytic $GABA_B$ receptors in the Ca^{2+} signals (Figure 27A).

The proportion of small signals was increased and the proportion of large signals reduced compared anesthetized to awake control mice (gray pie charts, Figure 27B). In cKO the percentage of small signals was reduced and the percentage of large signals was increased compared anesthetized to awake animals (turquoise pie charts, Figure 27B).

Figure 27: Increased proportion of large signals in awake animals

A: Experimental design: B: In control awake animals the proportion of small signals increased whereas the proportion of large signals was lower in cell somata compared to anesthetized mice. Awake cKO animals displayed a higher proportion of large and a lower proportion of small signals. C: In cKO and control the proportion of small signals was lower, whereas the percentage of large signals was increased without isoflurane (n= 7 animals and 12 FOVs).

In the gliapil of awake cKO and control animals the proportion of small signals was reduced, whereas the proportion of large signals was increased (Figure 27C). The signal composition itself was not altered between anesthetized and awake control mice (gray pie charts, Figure 27C). In the cKO the proportion of small signals was halved in awake animals, whereas the proportion of large signals was more than doubled (turquoise pie charts, Figure 27C).

Without influence of isoflurane, the signal amplitude and duration was increased in the gliapil in cKO and control mice (Figure 44B, C). Somatic Ca^{2+} signals were larger in cKO and control without isoflurane (Figure 44B). In control animals signals were longer without isoflurane (Figure 44C).

In summary:

- The signal duration was 1.5-2 fold increased in awake animals

- The signals were longer by 30% in awake animals

- The proportion of large signals was increased, whereas the proportion of small signals was decreased

4.6.3 Reduced signal duration and amplitude in cKO mice injected at an age of 7 weeks

To investigate if there was a time-related change in the potential pheotype *in vivo* the animals were injected with seven weeks (3x) and the cranial window was implanted at an age between 15-20 weeks (Figure 28A).

In anesthetized mice, the amplitude of somatic Ca^{2+} signals was reduced, whereas the duration was not altered compared cKO to control (Figure 28B, C). In the gliapil all signals were smaller and shorter (Figure 28B, C). Control animals showed, compared to cKO, a higher data scattering, indicated by larger boxplots and longer whiskers. The proportion of small signals was higher, whereas the proportion of medium and large signals was decreased in the cKO in both locations (Figure 28D).

In cKO awake mice, the signal amplitude and duration was reduced in cell somata and gliapil (Figure 29B, C). As indicated in the anesthetized cKO animals, here also the proportion of large signals was increased comparing cKO to control (Figure 29D). In contrast to the anesthetized animals, the proportion of small signals was not changed or slightly reduced (Figure 29D).
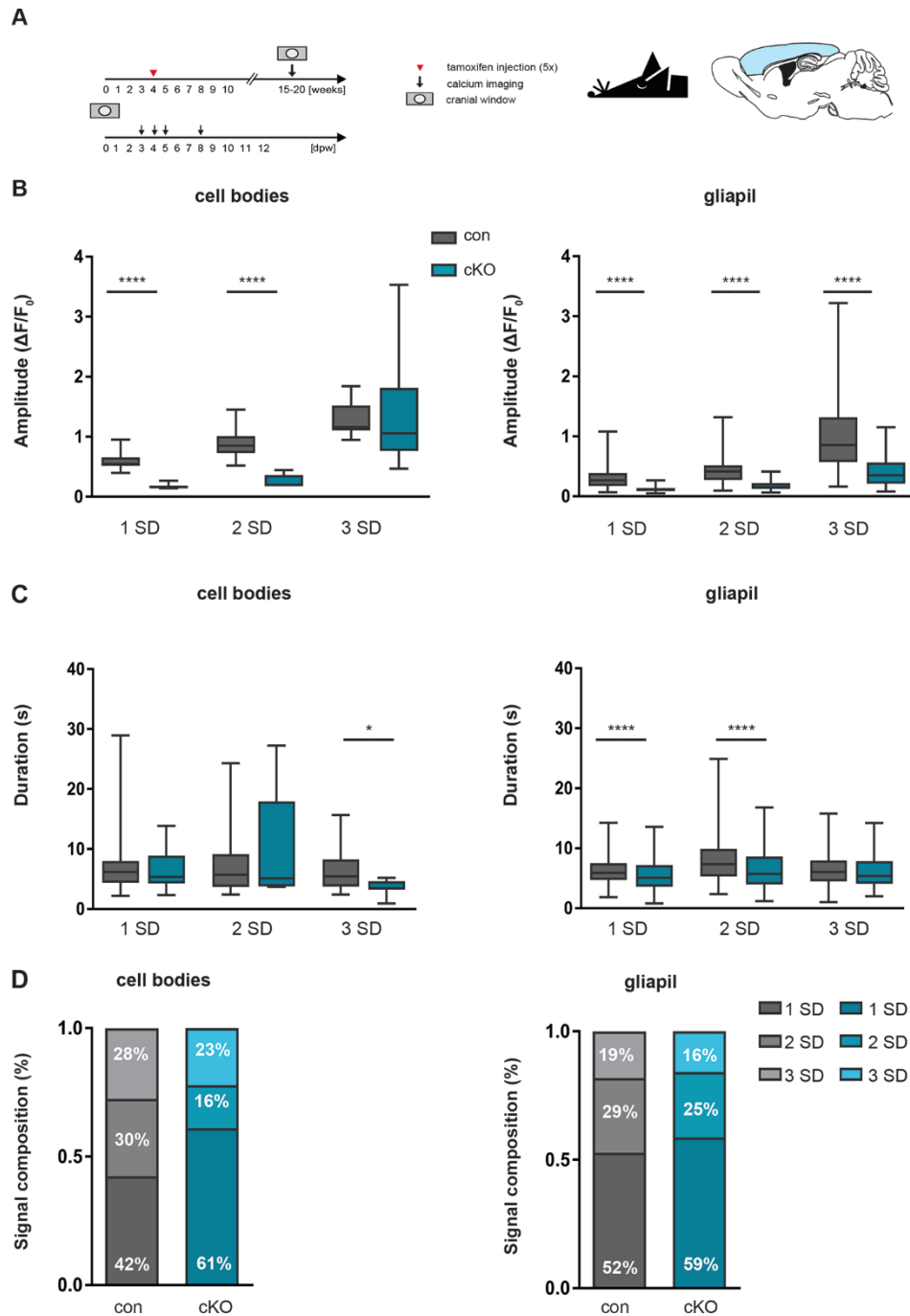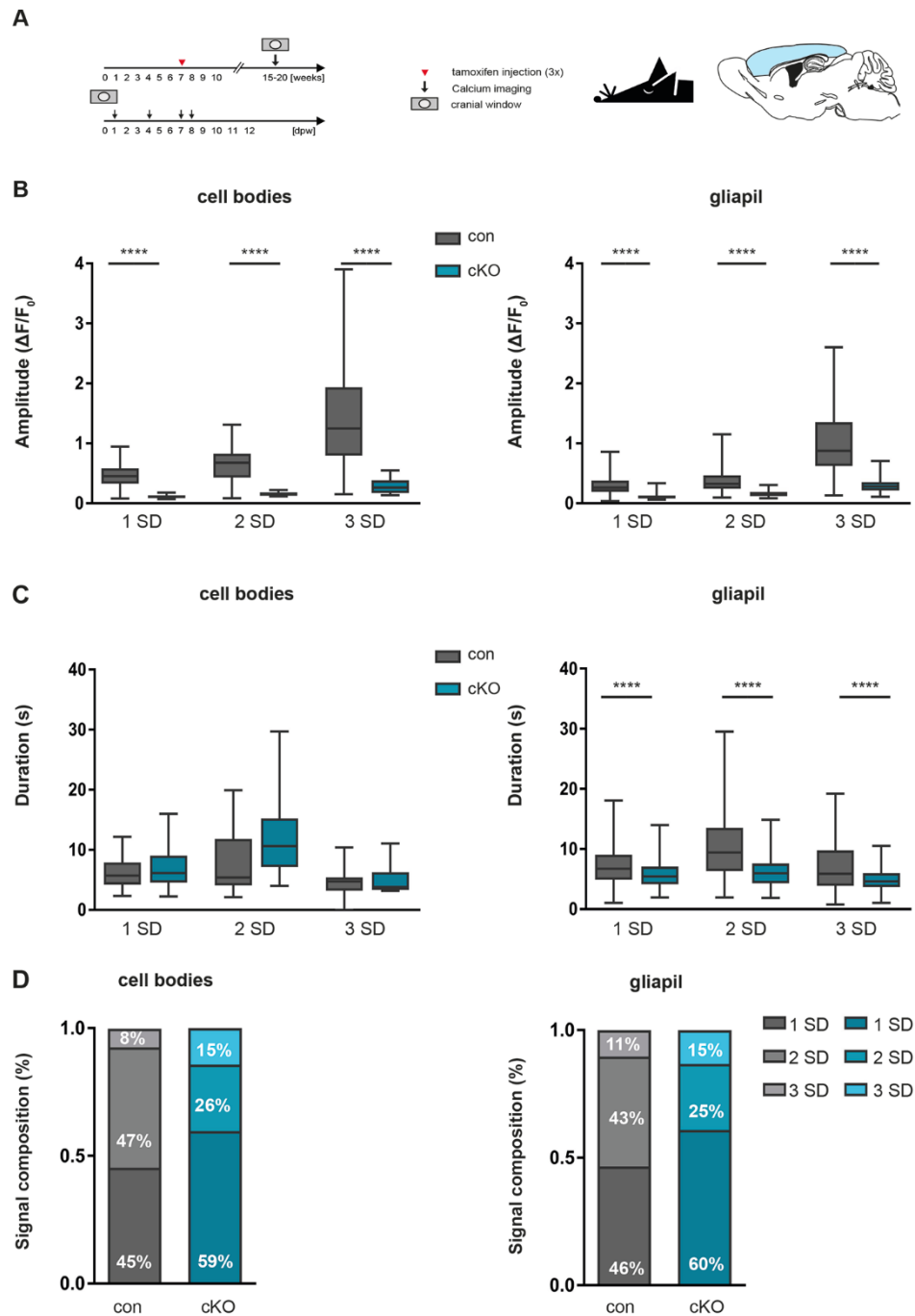
Figure 28: Smaller and shorter Ca^{2+} signals in anesthetized cKO mice

A: Tamoxifen with seven weeks; cranial window between 15-20 weeks, imaging session 1, 4, 7 8 days after recovery time. Animals were anesthetized with 2% isoflurane. B: Smaller Ca^{2+} signals in cell somata and gliapil C: In gliapil the signal duration was decreaed,whereas somatic Ca^{2+} signals were not altered. D: The proportion of small signals was higher, whereas the proportion of medium and large signals was lower comparing cKO to con (n= 2 animals and 4 FOVs).
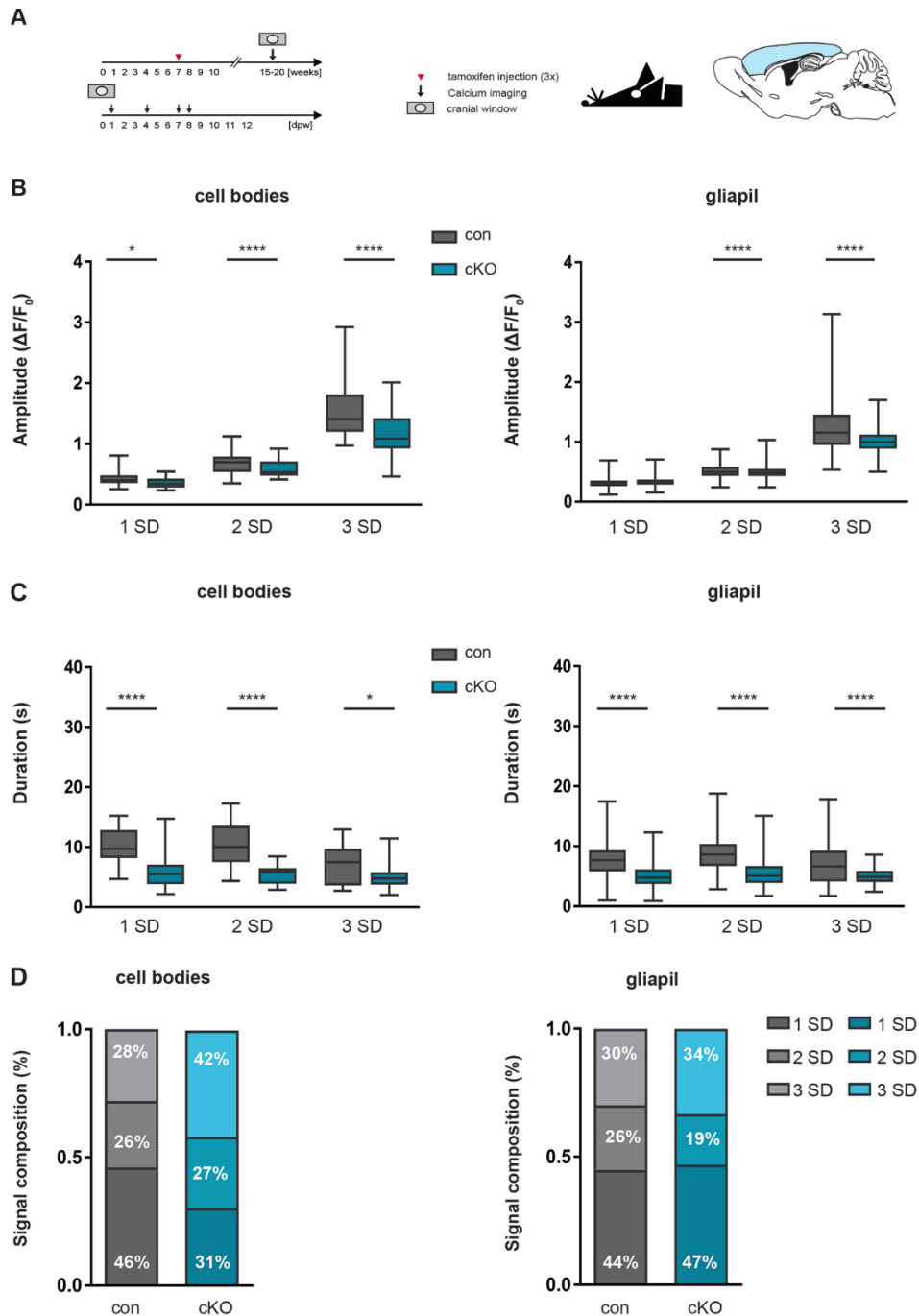
Figure 29: Smaller and longer Ca^{2+} signals in the absence of GABA$_B$ receptors

A: Tamoxifen with seven weeks; cranial window between 15-20 weeks, imaging session 1, 4, 7, 8 days after recovery time in awake animals. B: All signals were smaller compared cKO to con. C: The duration was reduced in cell somata and gliapil. D: Increase in the proportion of large signals in cKO, but the proportion of small signals was not changed or slightly reduced depending on the location. Percentage of medium signals remained unchanged in cell somata and gliapil (n= 4 animals and 10 FOVs).

In summary:

- In anesthetized cKO animals the signal amplitude was reduced by 60% and the duration by 80% in the gliapil

- In cell somata of cKO mice only the signal amplitude was reduced by 30%

- In awake animals the signal amplitude was reduced by 75% in gliapil and by 25% in cell somata

- The signals were shorter by 40% in cell somata and gliapil

4.6.4 Increase of the proportion of large signals in awake animals

Ca^{2+} signals from awake (light gray and light turquoise) and anesthetized (dark gray and turquoise) animals were compared to investigate if anesthesia influences astrocytic $GABA_B$ receptor activity (Figure 27A).

Overall, the proportion of large signals was increased in awake animals, regardless of location or genotype (Figure 30B, C). This increase led to an altered proportion change in small and medium signals depending on location and genotype. In control animals the proportion of medium Ca^{2+} signals was lower in awake mice, whereas the proportion of small signals was not changed (gray pie chart, Figure 30B, C). In cKO the proportion of small signals was decreased in gliapil and cell somata (turquoise pie chart, Figure 30B, C).

Furthermore, the signal composition was not changed in awake animals compared cKO to control (light turquoise and gray pie chart, Figure 30B, C). In anesthetized animals, cKO displayed an increase in small and large signal proportion (turquoise and gray pie chart, Figure 30B, C).

In the gliapil the amplitude of Ca^{2+} signals was increased in awake animals (Figure 45B). The duration of the signals was also altered (Figure 45C). Control somatic Ca^{2+} signals were longer but the signal amplitude was not changed (Figure 45B, C). cKO somatic Ca^{2+} signals on the other hand, showed only larger signals in awake animals (Figure 45B, C).

In summary:

- The signal amplitude was increased by 20% in control and by an 3-fold increase in cKO awake animals

- The signals were longer by 70% in awake control animals

- The proportion of large signals was increased without anesthesia
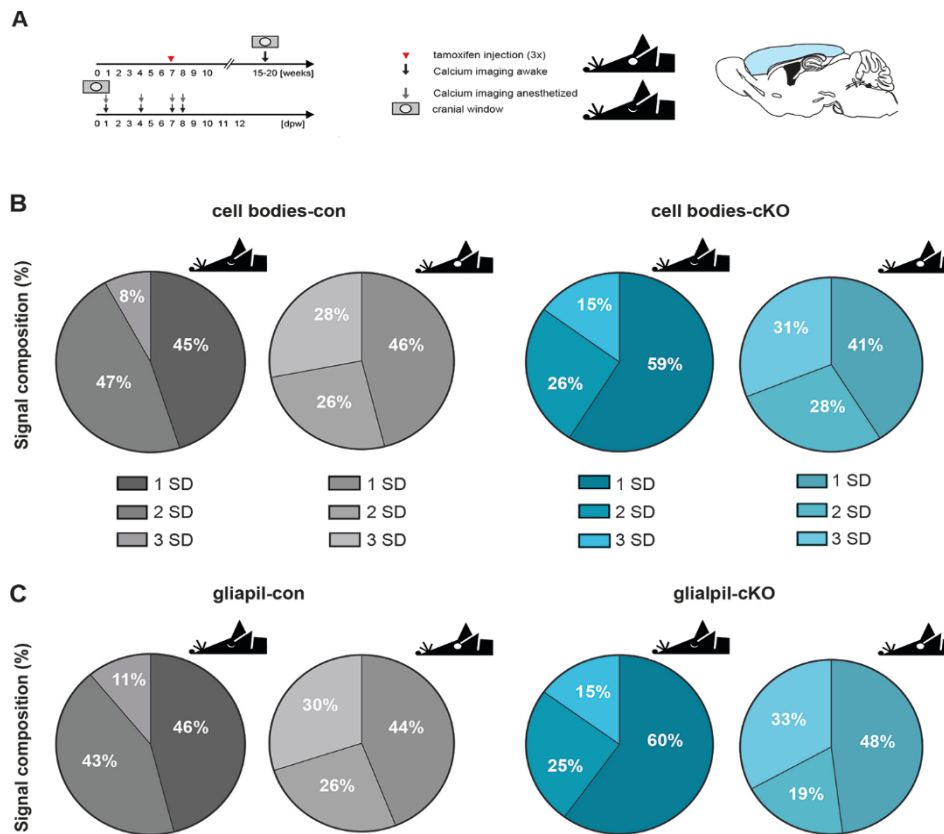
Figure 30: Reduced proportion of small signals and increased proportion of large signals
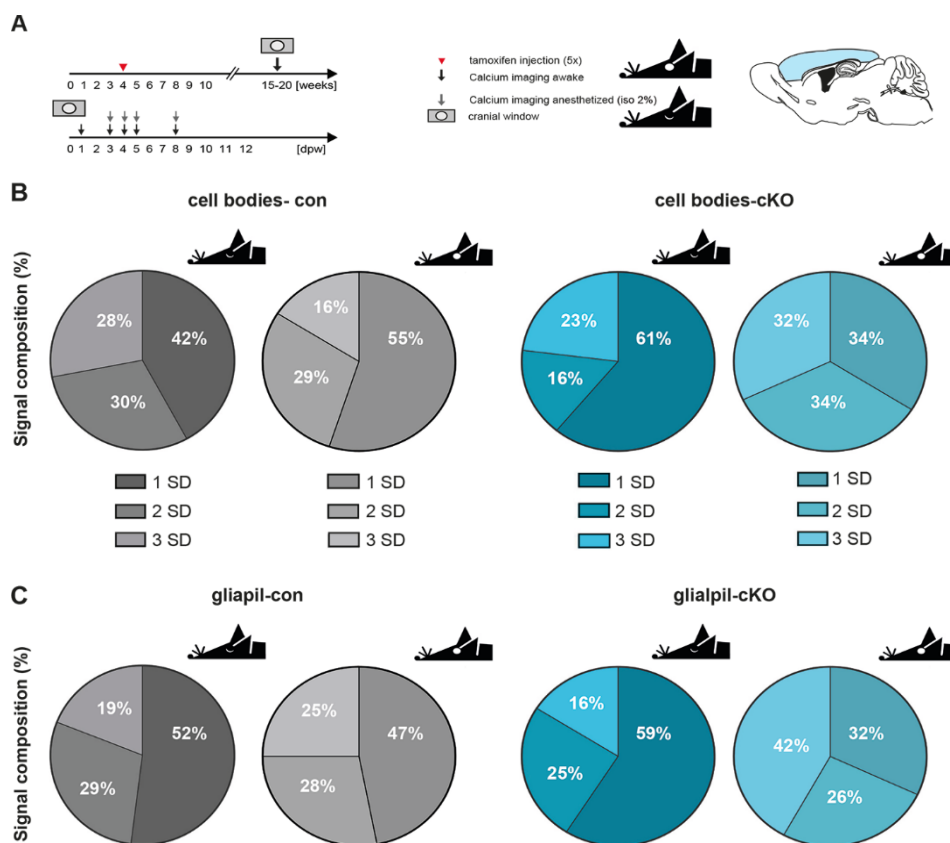
A: Experimental design. B: In control awake animals the proportion of large signals was increased and the proportion of medium signals was decreased. cKO awake animals displayed an increase of large signals while the proportion of small signals was decreased. C: In awake cKO and control animals the proportion of large signals was higher, whereas in the cKO the proportion of small signals and in the control the proportion of medium signals was lower (n= 7 animals and 12 FOVs).

4.6.5 Comparison of Ca^{2+} changes in cKO using different tamoxifen protocols

The deletion of the astrocytic GABA$_B$ receptors was induced with either at an age of 4 weeks or at an age of 7 weeks and analysis was always done between 15-20 weeks. Both tamoxifen protocols were compared to investigate whether the time point of injection influences a potential phenotype of the cKO. cKO animals injected with different tamoxifen protocols (4 weeks (5x) and 7 weeks (3x)) displayed the same changes in Ca^{2+} signals. In both cases, Ca^{2+} signals of cKO animals displayed a reduced signal amplitude and duration. Anesthetized and awake animals were compared separately.

Anesthetized cKO animals, injected at an age of 7 weeks, displayed smaller and also shorter signals in the gliapil, compared to cKO animals, injected at an age of 4 weeks (Figure 31B, C; 4 weeks (turquoise) 7 weeks (turquoise with dots)). However, Ca^{2+} signals in control animals were also altered in signal amplitude and duration (Figure 31B, C; 4weeks (gray) 7 weeks (gray with dots)).

Futhermore, somatic Ca^{2+} signals in cKO animals, injected at an age of 7 weeks, displayed a reduced signal amplitude compared to cKO animals, injected at an age of 4 weeks, as well as control animals for both protocols. Signal durations on the other hand, displayed no difference among those groups (Figure 31B, C).

Comparing the signal composition of anesthetized control animals, injected at an age of 7 weeks to control animals, injected at an age of 4 weeks, the former group displayed a higher proportion of medium signals but a lower proportion of large signals (Figure 31D). In cKO animals, the signal composition revealed no difference, comparing both tamoxifen protocols (Figure 31D).
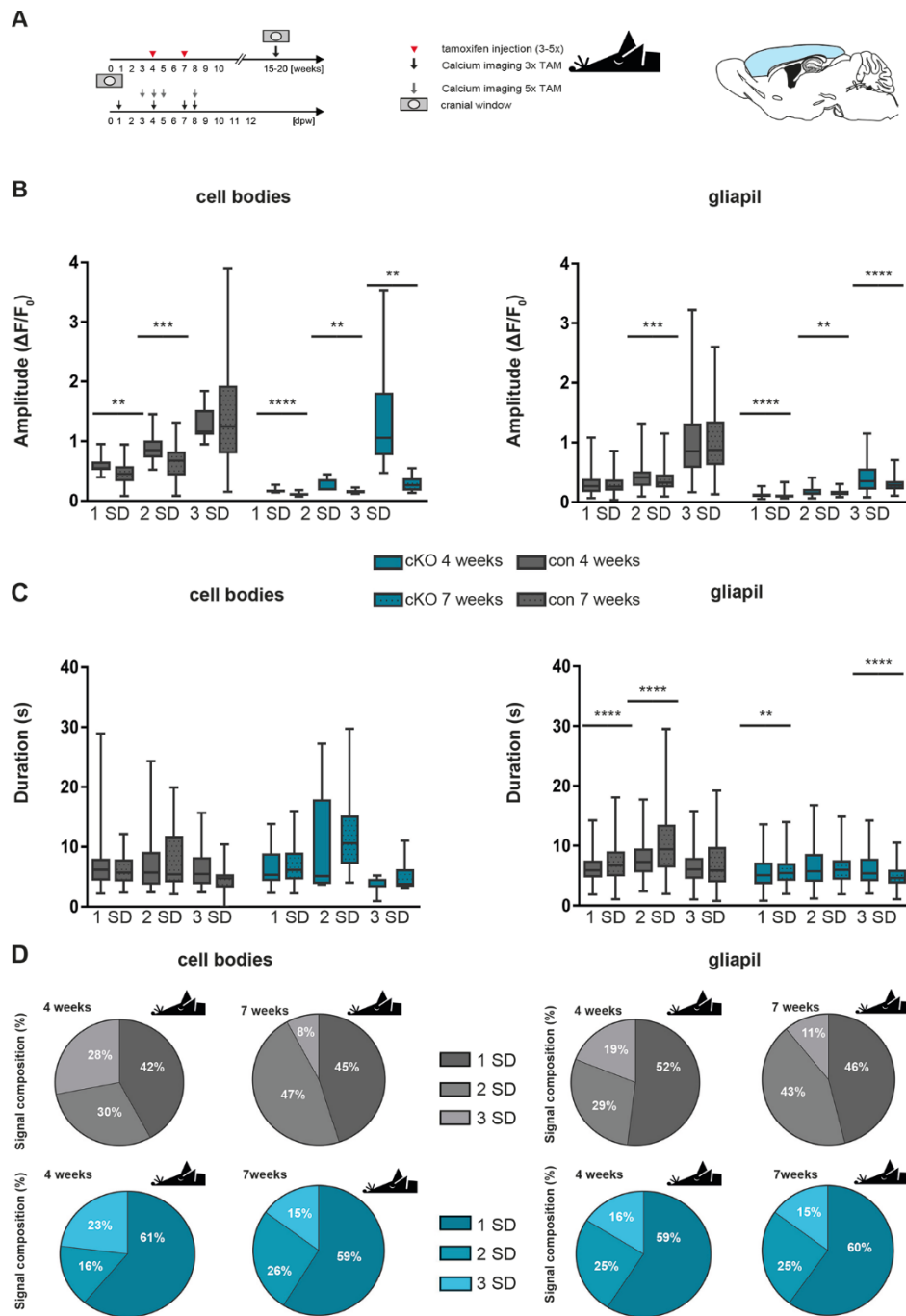
Figure 31: Smaller and shorter Ca^{2+} signals in cKO animals injected an an age of 7 weeks

A: Experimental design B: Signal amplitude was reduced in mice injected at an age of 7 weeks. C: Signal duration was not changed in somatic signals. In the gliapil signals were longer in control and in cKO shorter compared both tamoxifen protocols. D: Control animals (injected at an age of 7 weeks) displayed a higher proportion in medium signals but a lower proportion in large signals in cell somata and gliapil. No difference in signal composition of cKO animals with both tamoxifen protocols. (n= 5 animals and 9 FOVs).

Next, both tamoxifen protocols were compared in awake animals. The signal amplitude was increased and the duration decreased in the gliapil compared cKO animals, injected at an age of 7 weeks to cKO animals, injected at an age of 4 weeks (Figure 31B, C; 4 weeks (turquoise) 7 weeks (turquoise with dots)). Signal amplitude and duration were also changed in control animals in both tamoxifen protocols (Figure 31B, C; 4weeks (gray) 7 weeks (gray with dots)). The control mice, injected at an age of 7 weeks, displayed smaller and shorter somatic Ca^{2+} signals compared to animals, injected an age of 4 weeks (Figure 31B, C; 4weeks (gray) 7 weeks (gray with dots)). Comparing both tamoxifen protocols in cKO animals revealed no changes in somatic Ca^{2+} signals (Figure 31B, C). Comparing the signal composition in awake mice, the later injected group (7 weeks) displayed a higher proportion of large signals (Figure 31D). In the absence of $GABA_B$ receptors, animals injected an age of 7 weeks showed a higher proportion of small signals, whereas the proportion of large or medium signals were altered depending on the location (Figure 31D).

By evaluating both tamoxifen protocols, the phenotype of the cKO was stronger in cKO animals injected at an age of 7 weeks. However, also the control groups displayed changes in their Ca^{2+} signals, which might be due to biological variance.

In summary:

- The signal amplitude was reduced by 20% in anesthetized cKO injected at an age of 7 weeks

- The duration was reduced by 30% in awake cKO injected at an age of 7 weeks

- Ca^{2+} properties were also changed in control animals with both tamoxifen protocols
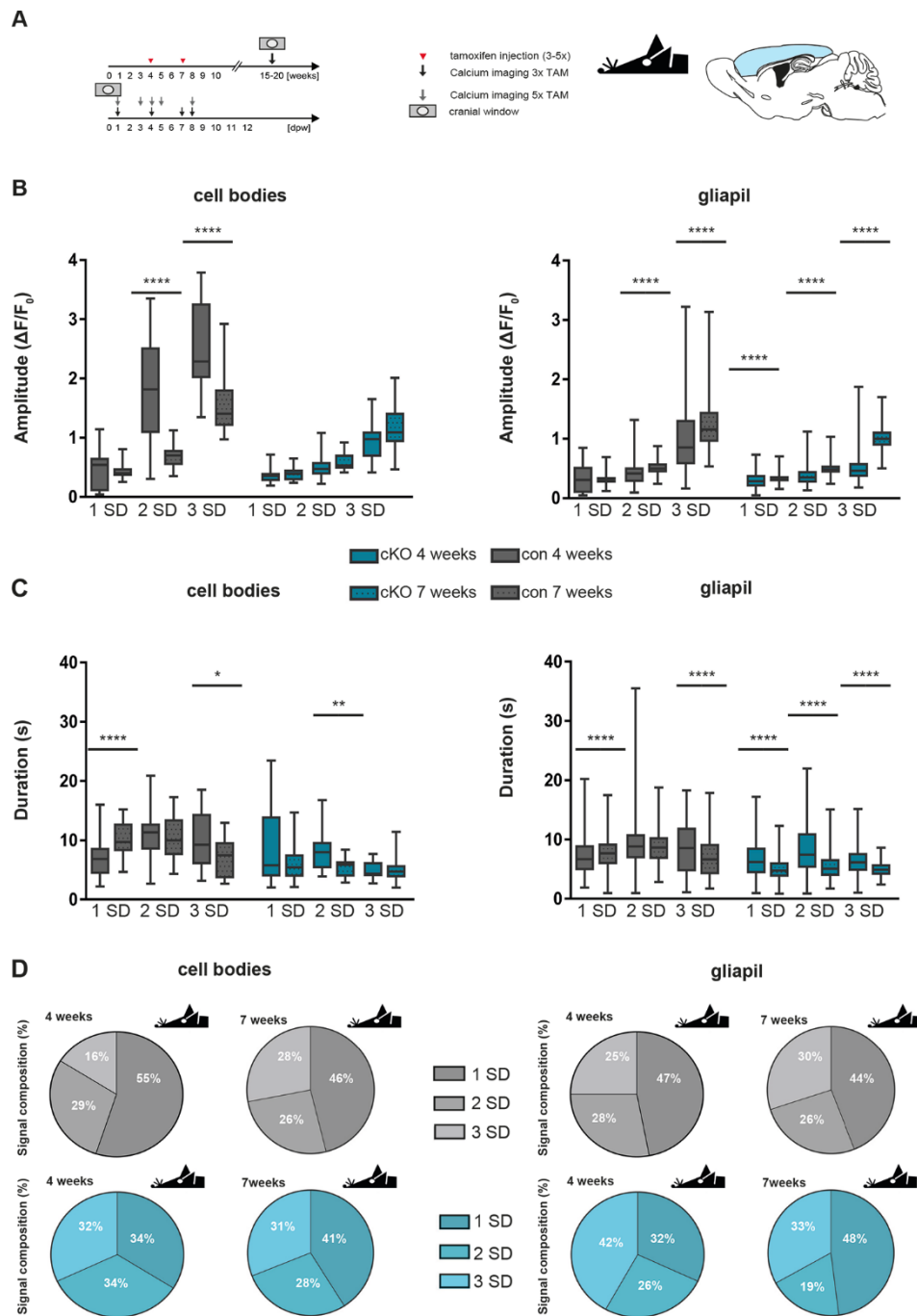
Figure 32: Smaller signals in awake mice injeceted an age of 7 weeks

A: Experimental design B: Somatic Ca^{2+} peaks were smaller in control animals injeceted an age of 7 weeks. In the gliapil signals were larger comapred both tamoxifen protocols. C: Signal duration was altered in the control groups. In cKO injeceted an age of 7 weeks. signals were shorter in gliapil and cell somata. D: The proportion of large signals was increased in later injected control animals In the cKO the proportion of small signals was increased and the amount of large signals was reduced in cell somata and gliapil. The amount of medium signals was not altered. (n= 8 animals and 17 FOVs).

4.6.7. Increased signal amplitude evoked by GHB *in vivo*

Taken together, the loss of astrocytic $GABA_B$ receptors leads to smaller and shorter signals mainly in the gliapil *in vivo*. Therefore, the activation of $GABA_B$ receptors should lead to larger and longer signals in control. Therefore, GHB (ɣ-hydroxybutric acid) was injected in the tail vein of slight anesthetized animals ((0.5% isoflurane) (Maitre *et al.*, 2005)). Ca^{2+} signals were recorded before and during the injection in the field of view (Figure 33) Laura C. Caudal (Molecular Physiology) kindly provided data and statistical analysis. Only control somatic Ca^{2+} signals were larger after application of GHB, whereas cKO did not changed. In the gliapil cKO signal amplitude was altered compared before and after the GHB injection (Figure 33B). The signal duration was overall not affected (Figure 33C). Furthermore, cKO displayed smaller Ca^{2+} signals compared to control.
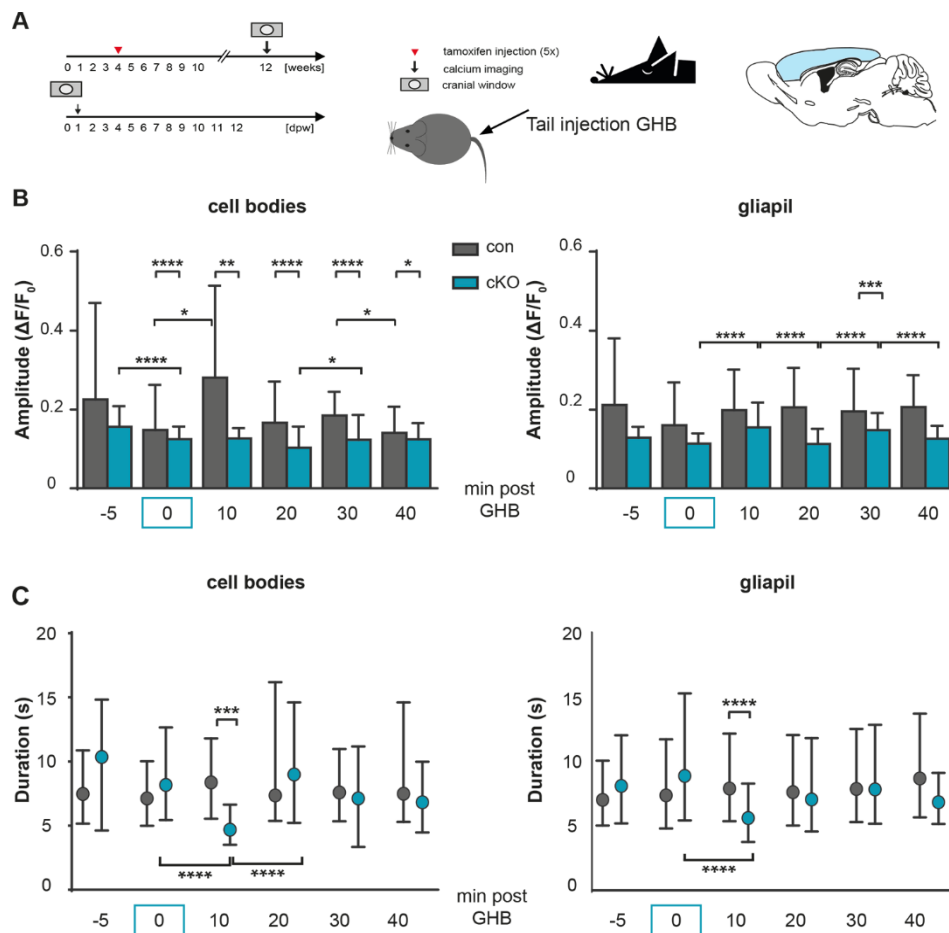
Figure 33: GHB evokes stronger Ca^{2+} signals in cell somata

A: Tamoxifen with seven weeks; cranial window at 12 weeks B: Control somatic signal amplitude was increased in the presence of GHB whereas cKO was not changed. cKO showed always smaller signals compared to control. In the gliapil cKO showed a change to GHB, whereas control not. C: Signal duration was not changed overall (n= 1 animal and 1 FOV).

Overall, the results *in vivo* can be summarized in the following:

- cKO displayed a reduced signal amplitude and duration

- In anesthetized animals only signals in the gliapil are affected

- In awake animals gliapil and somata are affected equally

- cKO injected at an age of 7 weeks, displayed a stronger phenotype than cKO injected at an age 4 weeks

4.7 Comparison of cKO and control mice using NGS

Using next generation sequencing (NGS) of MACS isolated cortical astrocytes, changes after astrocytic deletion of GABA$_B$ can be visualized for more than one gene. A Volcano Plot comparing next generation data of control and cKO mice revealed mainly changes in the mRNA expression after the loss of astrocytic GABA$_B$ receptors (Figure 34A). Additionally, genes of other pathways were investigated to see if they reveal changes in the downstream mechanism. Besides the GABA$_{B1}$ subunit, also the GABA$_{B2}$ subunit was significantly reduced. Furthermore, GABA$_A$ receptor expression is reduced, indicated by GABA$_A$β subunit (gabaa β) and GABA$_A$ receptor associated protein (gabaarap), whereas synthesis (gad2) and uptake of GABA (slc6a1) was not altered in cKO (Figure 34B).

The expression of other receptors on astrocytes like; Glycine (glrb), AMPA (gria4), NMDA (grin1) and P2Y1 (p2y1r) receptors was not changed in cKO (Figure 34C). The loss of astrocytic GABA$_B$ receptors led to upregulation of G protein coupled potassium channels (kcnj2) and an altered expression of vesicle release associated proteins (syt10, syt14, vti1b and snapin) (Figure 34B,E). No change in the expression of G protein coupled sodium channel (scn1a). Furthermore, the calcium binding protein S100B was upregulated, while GFAP mRNA was down regulated in the cKO, which was shown before with immunohistochemistry and western blot.
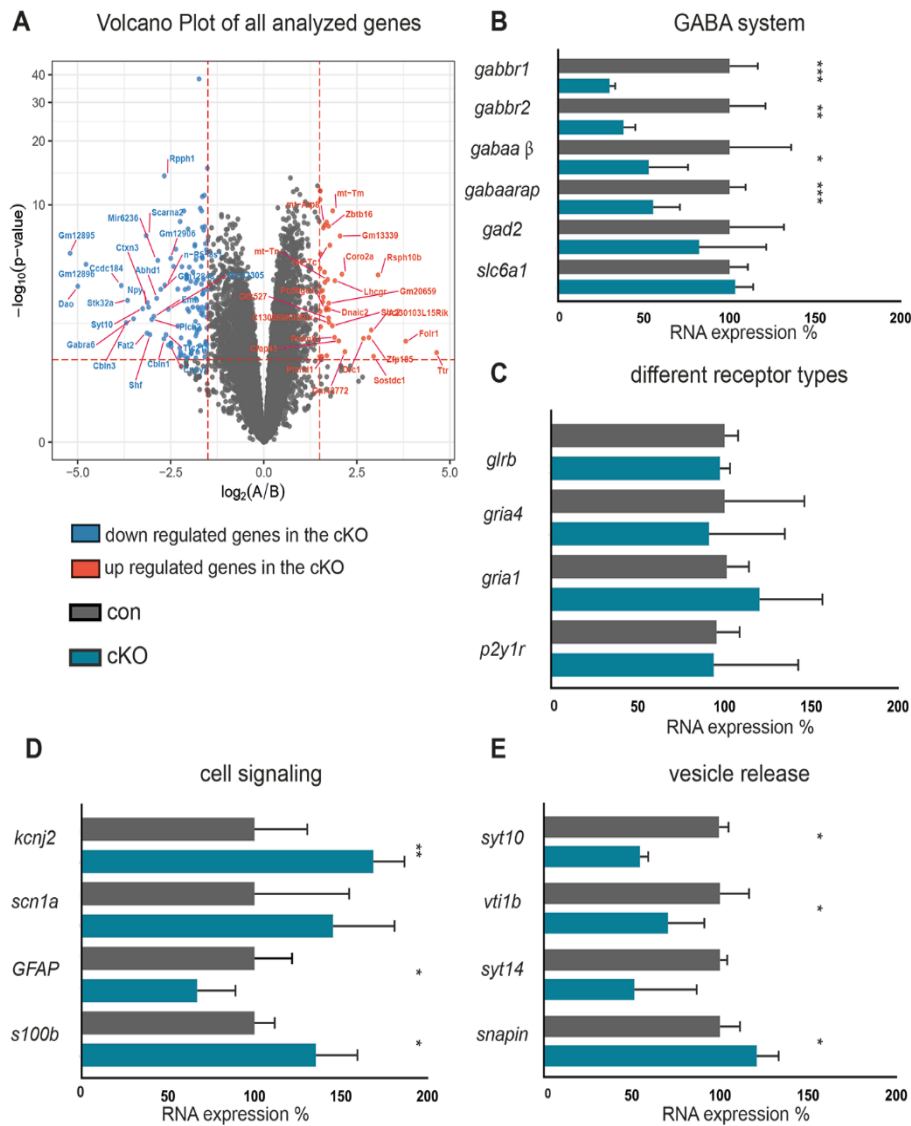
Figure 34: NGS analysis reveals changes of different mRNAs in cKO

A: Volcano plot displaying up and down regulated genes in cKO. B: Reduced mRNA expression of the GABA$_B$ (gabbr1 and gabbr2), GABA$_A$ receptor (gabaa β) and GABA$_A$ receptor associated protein (gabaarap). Glutamate decarboxylase (gad2) and GABA transporter (slc6a1) were not altered. C: No change in the mRNA expression of glycine (glrb), NMDA (grin1), AMPA (gria4) and P2Y1 (p2y1r) receptors. D: Upregulation of S100B (s100b) and G protein coupled potassium channels (kcnj2) and down regulation of GFAP (gfap). The expression of sodium channels (scn1a) was not changed. E: Altered expression of genes responsible for vesicle release in cKO compared control (syt10, syt14 = synaptotagmin, vti1b= vesicle transport, snapin= SNARE associated protein) (n=5 animals).

5. DISCUSSION

The aim of this thesis is to investigate the modulation of Ca^{2+} signals by astrocytic $GABA_B$ receptors.

By using the tamoxifen inducible Cre-LoxP system this receptor was deleted in a temporal and spatial manner. The TgH (GLAST-CreERT2) mouse line was crossbred to TgH ($GABA_{B1}{}^{fl/fl}$) mice, allowing the deletion of the $GABA_{B1}$ subunit specifically in astrocytes, preventing the formation of the functional receptor (Haller *et al.*, 2004; Mori *et al.*, 2006). Furthermore, two different reporter lines TgH (Rosa 26-CAG-lsl-GCaMP3) and TgH (Rosa 26-CAG-lsl-tdTomato) were used to visualize recombined cells (Madisen *et al.*, 2010; Paukert *et al.*, 2014). The genetically encoded Ca^{2+} indicator GCaMP3 was used for Ca^{2+} imaging.

For the molecular analysis, tamoxifen was administered at an age of four weeks for three to five consequective days. At an age of four weeks, a high expression of $GABA_B$ receptors was found in isolated astrocytes (Figure 1;(Zhang *et al.*, 2014)) and three to five doses of tamoxifen resulted in the highest recombination efficiency in the cortex and being less stressful for the animals at the same time (Jahn *et al.*, 2018).

The following summary presents the results (Figure 35):

- Significant reduction of $GABA_{B1}$ alleles after tamoxifen administration in homogenates of different brain regions and in MACS isolated cortical astrocytes

- Reduced $GABA_{B1}$ mRNA expression by 50% in MACS isolated astrocytes

- Loss of $GABA_{B1}$ mRNA visualized by FISH in different brain regions

- Loss of the $GABA_{B1}$ and $GABA_{B2}$ subunits in cerebellum and cortex using IHC and NGS

- Reduced GFAP expression in cKO in healthy and injured brain (IHC and NGS)

- Reduced Ca^{2+} signal amplitude and duration in cKO *in vivo* and in acutely isolated brain slices

- cKO animals displayed a higher proportion of small signals

- Activation of astrocytic $GABA_B$ receptors with baclofen leads to longer and larger signals in acutely isolated slices
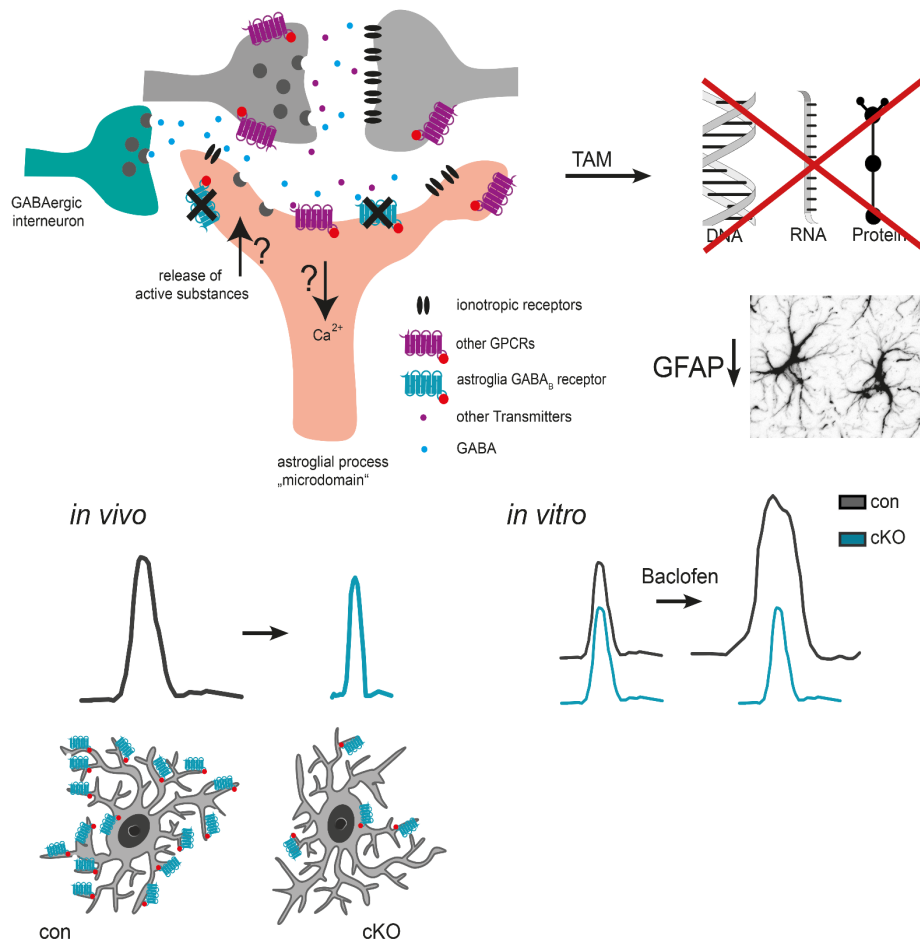
Figure 35: Potential roles of astrocytic GABA_B receptors

Deletion of astrocytic GABA_B receptors lead to: (1) Reduction of GFAP expression, (2) Reduced signal amplitude and duration in cKO, (3) Application of baclofen resulted in an increase of signal amplitude and duration.

5.1 Successful deletion of GABA$_B$ receptor DNA, mRNA and protein

5.1.1 Deletion of GABA$_{B1}$ alleles after tamoxifen administration

Recombination of GABA$_{B1}$ alleles was investigated in homogenates of different brain regions with qRT-PCR. In all brain region a loss of the GABA$_{B1}$ alleles could be detected; 20% in brainstem, cortex and hippocampus, optic nerve 38% and cerebellum 15%. Neurons and other glial cells, not targeted by GLAST-CreERT2, still had GABA$_{B1}$ alleles, therefore the reduction displayed the proportion of astrocytes in a given brain region (Bettler *et al.*, 2004; Jahn *et al.*, 2018). The percentage of cortical astrocytes was estimated to be by 20% (Ren *et al.*, 1992; Han *et al.*, 2012; Jahn *et al.*, 2018). For astroglia-specific recombination, cortical astrocytes were isolated by MACS (magnetic activated cell sorting) and revealed a reduction about 50% in GABA$_{B1}$ allele expression in cortical astrocytes. This probably does not reflect the total reduction due to contamination of about 20% with microglia, OPC and neurons still expressing GABA$_B$ receptors in these probes (Benke *et al.*, 1999; Calver *et al.*, 2000; personal communication with Carmen V. Kasakow). Therefore, the experiment has to be repeated and the MACS protocol improved to reduce contamination to confirm the quantity of recombined alleles in astrocytes.

5.1.2 Reduction of the GABA$_{B1}$ mRNA in different brain regions

In total, in cell homogenates no reduction of GABA$_{B1}$ mRNA could be detected in the different brain regions. Since GABA$_{B1}$ is highly expressed in interneurons, Purkinje cells and microglia, it is difficult to visualize an astroglial loss (Calver *et al.*, 2000; Princivalle *et al.*, 2000; Lee *et al.*, 2011b). NGS analysis of MACS isolated cortical and cerebellar astrocytes revealed a reduction by 50-70% of GABA$_{B1}$ mRNA. A contamination of about 30% with oligodendrocytes and other cell types expressing GABA$_{B1}$ (see Figure 37) , might prevent a further reduction .

Fluorescence in situ hybridization (FISH) allows a visualization of GABA$_{B1}$ mRNA expression. Astrocytes, positive for GFAP/S100B or S100B/GCaMP3, expressed GABA$_{B1}$ mRNA. In cKO GABA$_{B1}$ mRNA was lacking in the investigated brain regions. In cKO mice, GABA$_{B1}$ mRNA was still expressed in cerebellar Purkinje cells and cortical neurons.

5.1.3 Reduction of GABA$_B$ protein in different brain regions

The expression of astrocytic GABA$_B$ receptors in cell culture has already been proven (Calver *et al.*, 2000). Here, we could show the expression of the GABA$_{B1}$ protein in different brain regions. 21 days after tamoxifen injection, fine astrocytic processes were lacking the GABA$_{B1}$ subunit in the brain investigated regions, indicating the degradation of the GABA$_{B1}$ protein after successful deletion of floxed alleles.

Due to the heterogeneous nature of astrocytes, it is not yet known how many of these cells express GABA$_B$ receptors. It is also not known, if there is a difference of expression in specific brain regions or in a specific layer. The expression of neuronal GABA$_B$ receptors is higher in cerebellum than in cortex (Calver *et al.*, 2000). Rat cortical layer V showed the highest expression of neuronal GABA$_B$ receptors, whereas in layer I-III the expression was in a medium range (Margeta-Mitrovic *et al.*, 1999; Princivalle *et al.*, 2000). The expression of astrocytic GABA$_B$ receptors was analyzed on mRNA and protein level. About 60-70% of all cortical astrocytes through all layers were positive for GABA$_{B1}$ mRNA and protein. Three weeks after the first tamoxifen injection only 30% of astrocytes were positive for GABA$_{B1}$ protein and mRNA. Using four additional tamoxifen protocols, in which the time between induction and analysis was prolonged, or required additional tamoxifen injections, did not lead to further reduction. This was not region specific, since 50% of total hippocampal astrocytes expressing GABA$_{B1}$ in control and in cKO 30% remained positive.

This remaining number can be explained by either unspecific binding of the antibody or a long lifespan of metabotropic receptors, while the loss of ionotropic AMPA receptors is detectable already after three days (Saab *et al.*, 2012). However, our data indicates a longer lifespan for GABA$_B$ receptors. In addition, the majority of GABA$_B$ receptors is often recycled and stored in vesicles until they are activated (Grampp *et al.*, 2008). The deletion of astrocytic GABA$_B$ receptors was induced at an age four weeks, therefore we were not able to delete GABA$_B$ receptors, which were already produced and stored in vesicles.

The GABA$_B$ receptor consists of two essential subunits (GABA$_{B1}$ and GABA$_{B2}$) (Bettler *et al.*, 2004; Haller *et al.*, 2004). We could show the expression of both subunits in astrocytes in different brain regions. In cKO both subunits were deleted in cerebellum and cortex. This could indicate, that the GABA$_{B2}$ subunit is not transported to the cell membrane without the GABA$_{B1}$ subunit (Bettler *et al.*, 2004).

Taken together, the loss of the astrocytic GABA$_{B1}$ subunit was shown on DNA, mRNA and protein level in different brain regions. Furthermore, no functional receptor was formed, since no GABA$_{B2}$ subunit was expressed in cKO. Only 60% of cortical astrocytes expressed GABA$_B$ receptors, which was reduced by 50% in cKO.

5.2 Changes of GFAP expression in cKO under physiological and pathological conditions

The glial fibrillary acid protein (GFAP) is the major intermediate filament in astrocytes (Eng *et al.*, 1971; Bignami *et al.*, 1972). In the cortex, under physiological conditions GFAP is weakly expressed in young adult mice, but highly upregulated in the developing and aging brain (Middeldorp & Hol, 2011). Under pathological conditions GFAP is also upregulated and involved in the glial scar formation (Burda *et al.*, 2016). The expression of GFAP can be further influenced by the transmitter GABA. Activation of the GABAergic system in rat forebrains increased GFAP expression mediated through $GABA_A$ receptors (Runquist & Alonso, 2003). However, the influence of the $GABA_B$ receptors on the expression of GFAP has not yet been shown. In this study, a reduction of GFAP mRNA and protein expression was observed, hinting to a potential role of $GABA_B$ receptors in regulating GFAP expression. The exact mechanism has to be evaluated in further experiments.

The expression of GFAP is increased under pathological conditions (Burda *et al.*, 2016). Therefore, we investigated the expression of GFAP in cKO and control animals after stab wound injury (SWI). In cKO and control with tdTomato as reporter, GFAP was upregulated in the injury site. The expression level in cKO was reduced compared to control, whereas contralateral GFAP expression was not altered between cKO and control. The reduced GFAP expression at the injury side might result in a thinned scar, influencing the regeneration of the surrounding tissue.

Taken together, astrocytic $GABA_B$ receptors play a role in the regulation of GFAP under physiological and pathological conditions. But more experiments have to confirm these findings and evaluate the mechanism.

5.3 The influence of GABA$_B$ receptors on astrocytic Ca^{2+} signals

Astrocytes communicate via Ca^{2+} signals, but the language of these signals is not well understood. There are several approaches to translate the Ca^{2+} code of astrocytes and with new techniques, the understanding of the astrocytic language will be improved. At the tripartite synapse astrocytes sense the activity of neurons, trigger Ca^{2+} signals and influence neuronal activity by gliotransmitter release (Araque *et al.*, 2014). Intrinsic Ca^{2+} fluctuation without external influences, regulate intrinsic processes or signal transduction in other cells (Nett *et al.*, 2002; Berridge *et al.*, 2003). Ca^{2+} signals can be classified by their signal properties (1) as well as their locations (2).

Bergmann glia Ca^{2+} signals were categorized into sparkles, bursts and flares (1). Sparkles are small signals, occurring on individual cells. Bursts are spontaneous, larger signals, covering a radius of about 55 µm. Flares are large signals, connected to movement and incorporated into network activity of the astrocytic syncytium (Nimmerjahn *et al.*, 2009). Flares are very sensitive to anesthesia and only accrue in awake moving animals (Nimmerjahn *et al.*, 2009).

Furthermore, Ca^{2+} signals can be classified by their location (2) in the astrocytes; in microdomains or in soma, processes or endfeet (Bindocci *et al.*, 2017b).

This study, signals were divided into cell somata and gliapil, containing processes and end feet. Ca^{2+} signals were divided into small (1SD), medium (2SD) and large (3SD) signals depending on signal amplitude. In addition, signal duration was analyzed. The spatial extent of the signals was not yet investigated. Furthermore, the proportion of signals occurring during an imaging session were examined (signal composition). Activation of neuronal GABA$_B$ receptors inhibit Ca^{2+} channels through the coupled G protein (Bowery *et al.*, 1980; Benarroch, 2012). Activation of astrocytic GABA$_B$ receptors resulted in a change of intracellular Ca^{2+}, displaying an increase or a decrease (Albrecht *et al.*, 1986; Kang *et al.*, 1998; Mariotti *et al.*, 2016).

The changes in Ca^{2+} signal properties were investigated *in vivo* and in acutely isolated brain slices using 2-Photon microscopy (2P-LSM). For the analysis *in vivo*, two different tamoxifen protocols were used: injection at an age of 4 weeks or at an age of 7 weeks. This was done to investigate the influence of the protocol itself on the properties of the Ca^{2+} signals. Furthermore, the animals were imaged awake as well as under the influence of isoflurane. Anesthesia reduced Ca^{2+} signals and synchronous network activity was suppressed, which was already shown in (Nimmerjahn *et al.*, 2009). Overall, an increase in signal amplitude and duration were observed in awake mice. Also the proportion of large signals was increased. Both findings support the diminishing effect of anesthesia on Ca^{2+} signals.

5.3.1 Reduced Ca²⁺ signal amplitude and duration in astrocytic GABA$_{B1}$ receptor knockout *in vivo*

In anesthetized animals, the signal amplitude was reduced by 60% and the duration by 20% in the gliapil after deletion of astrocytic GABA$_B$ receptors. In awake cKO animals, signals were smaller by 80% and shorter by 44% compared to control in gliapil. Furthermore, somatic cKO Ca²⁺ signals were smaller by 20% and shorter by 30% in awake animals. This indicates that GABA$_B$ receptors are mainly expressed on astrocytic processes, which is line with a recent publication, showing baclofen evoking Ca²⁺ signals *in vivo* mainly in the processes (Mariotti *et al.*, 2016). Changes in somatic Ca²⁺ signals only occur in awake animals, hinting to a downstream mechanism involving other signal pathways. The proportion of small signals was increased in anesthetized cKO animals. Since the signals were smaller and shorter, the number of signals must increase to compensate this change and to ensure the signal transmission. Contrary, in awake cKO animals, the proportion of large signals was increased, which might compensate for the reduced signal duration and amplitude. This difference between awake and anesthetized cKO animals might be a consequence of the anesthesia, which is known to suppress large signals.

In cKO mice, signal amplitude and duration were reduced with both tamoxifen protocols. However, anesthetized animals injected an age of 7 weeks expressed a stronger reduction in signal amplitude and duration, compared to animals injected at an age of 4 weeks. Form this point of view, it seems that a longer time-period between tamoxifen injection and analysis obfuscates the phenotype. Compensatory mechanisms and upregulation of other metabotropic or ionotropic receptors could influence signal properties. GABA$_A$ receptors could play a secondary role with their reduced expression in cKO. Furthermore, control animals displayed a difference in signal amplitude and duration comparing both tamoxifen protocols.

Therefore, to investigate the changes in the Ca²⁺ properties after deletion of astrocytic GABA$_B$ receptors, the experimental design has to be re-evaluated. One possibility is to reduce time between induction and analysis or incorporate additional imaging sessions between the induction time point and final analysis to more accurately follow the changes in Ca²⁺ signals.

Summing up, the loss of astrocytic GABA$_B$ receptors leads to smaller and shorter signals mainly in the gliapil *in vivo.* GABA$_B$ receptors are expressed at the processes, proven with immunohistochemistry. Somatic Ca²⁺ signals were smaller and shorter only in awake animals. Therefore, the activation of GABA$_B$ receptors should lead to larger and longer signals in control, while in cKO, due to the loss of astrocytic GABA$_B$ receptors, no change in signal properties is expected.

This could be partially confirmed by injection of GHB (ɣ-hydroxybutric acid) in the tail vein in slightly anesthetized animals (0.5% isoflurane, data were done by Laura C. Caudal)). In control animals, the signal amplitude of somatic Ca^{2+} was increased after application of GHB, whereas cKO did not change. In the gliapil, cKO signal amplitude was altered compared before and after the GHB injection. Furthermore, cKO displayed also a reduced signal amplitude and duration in line with our data. Only in awake animals, somatic Ca^{2+} signals were affected. This might be due to different concentration of isoflurane or that GHB is only a weak agonist for $GABA_B$ receptors and the changes of somatic Ca^{2+} signals are a secondary response (Maitre *et al.*, 2005). Furthermore, the signals were not divided into small, medium and large signals, this might mask for potential response to GHB in the glia.

5.3.2 Pharmacokinetic analysis in acutely isolated slices revealed larger and longer signals in the presence of baclofen

Deletion of astrocytic $GABA_B$ receptors leads to a reduced signal amplitude and duration *in vivo*. Therefore, the activation of astrocytic $GABA_B$ receptors should then result in an increase in signal amplitude and duration. To confirm this finding, acutely isolated brain slices were treated with the $GABA_B$ agonist baclofen and the $GABA_B$ antagonist CGP34358 (Perea *et al.*, 2016). Furthermore, some slices were treated with TTX to inhibit neuronal activation.

Application of baclofen in control slices led to prolonged Ca^{2+} signals in the gliapil. In absence of astrocytic $GABA_B$ receptors baclofen application led to a reduced signal amplitude but also longer Ca^{2+} signals. Changes in Ca^{2+} signals in cKO mice in the presence of baclofen could be mediated over neuronal input. Activation of neuronal $GABA_B$ receptors by baclofen could influence astrocytes (Nilsson *et al.*, 1993). This neuronally triggered elevation could result in longer signals. Furthermore, some $GABA_B$ receptors were still present in the cKO as indicated with the immunohistochemistry data.

Somatic Ca^{2+} signals were not altered. This supports the expression of $GABA_B$ receptors mainly on the fine processes as already indicated by *in vivo* Ca^{2+} imaging and by immunohistochemistry. Comparing cKO to control during the baseline recording, cKO Ca^{2+} signals displayed a reduced signal amplitude but longer signal duration, which is partially in line with the *in vivo* data. The increase in the signal duration could be a technique issue, since Ca^{2+} signals were recorded in slices and not *in vivo.* Application of baclofen in cKO and control resulted in an increase in the percentage of small signals.

Comparing cKO to control we still have an increase in percentage of small signals and decrease in large signals, this is in line with the *in* vivo data. This could mean that astrocytic GABA$_B$ receptors are mainly responsible for small and long signals.

Neuronal input was prevented using the fast sodium channel blocker TTX and slices were treated alternating with GABA$_B$ antagonist CGP34358 (CGP) and GABA$_B$ agonist baclofen. Overall somatic Ca^{2+} signals were not changed by application of baclofen and CGP34358, comparing cKO to control, which is in line with results *in vivo* and the results of the baclofen application. The indicated differences in the somatic Ca^{2+} signal properties were results of high data scattering.

In the gliapil of control animals, blocking of GABA$_B$ receptors with CGP34385 led to a reduced signal amplitude and application of baclofen could rescue the reduction of signal amplitude. In cKO, small and medium signals were indeed larger after application of CGP and baclofen, but only by 10% with a high biological variance. Therefore, we conclude, that activation of GABA$_B$ receptors leads to an increase of signal amplitude.

In the control slices, Ca^{2+} signals were longer in the presence of CGP34358 and shorter in presence of baclofen. In cKO the signals were longer in presence of CGP34358 and baclofen. These results are counterintuitive. However, the number of animals was small and the data displayed a high scattering, indicated by a large boxplot and long whiskers. Therefore, more experiments have to be done. Furthermore, we did not block vesicular release, which also influences astrocytic Ca^{2+} signals.

Comparing signal distribution (baseline, CGP, baclofen) of cKO to control, the majority of the signals occurred during baseline recording in the cKO and were no longer triggered by application of baclofen and CGP. This indicates a missing target for agonist and antagonist. Since signals were still evoked by antagonist and agonist, this might be due to remaining GABA$_B$ receptors on cKO astrocytes, as already indicated on mRNA and protein analysis. In the presence of CGP34358 and baclofen, cKO displayed larger and longer Ca^{2+} signals compared to control, contradictive to the previous findings. *In vivo* and in acutely isolated slices without TTX the conditional knockout displayed always a reduced signal amplitude and duration. But the dataset displayed a high data scattering, indicating quality variations of the brain slices. The number of animals has to be increased and the experiments repeated.

In summary, activation of astrocytic GABA$_B$ receptors resulted in an increase of signal amplitude and duration. In line with these results is the recent publication: Baclofen evokes long-lasting Ca^{2+} oscillation and increases in Ca^{2+} signals *in vivo* (Mariotti et al., 2016). We could show, that GABA$_B$ receptors change the Ca^{2+} properties by evoking larger and longer signals. However, there are still open questions, which have to be study in further experiments.

5.4 Changes in mRNA expression in cKO animals

Using next generation sequencing (NGS) of MACS isolated cortical astrocytes allows visualizing changes in mRNA expression for multiple genes.

Besides the $GABA_{B1}$ subunit, also the $GABA_{B2}$ subunit was significantly reduced, supporting the results obtained by immunohistochemistry. Furthermore, $GABA_A$ receptor expression was reduced but the GABA synthesis and uptake of GABA was not affected by the deletion of $GABA_B$ receptors. However, investigating the loss of $GABA_B$ receptors revealed no influence on the expression of other receptors like; glycine, AMPA, NMDA and P2Y1. The loss of astrocytic $GABA_B$ receptors led to an altered expression of vesicle release associated proteins, which has not yet been linked to each other. Moreover, the calcium binding protein S100B was upregulated, while GFAP mRNA was down-regulated in the cKO. The down-regulation of GFAP was already shown by Western blot and RT-PCR.

The NGS analysis supports of our data. However, it also reveals changes in other pathways, which were not yet associated with astrocytic $GABA_B$ receptors. For this reason, a more detailed analysis has to be conducted.

6. OUTLOOK AND CONCLUSION

By using RT-PCR, FISH and immunohistochemistry the reduction of the $GABA_B$ receptors in different brain regions was visualized.

Nevertheless, the consequence of the loss of GABAergic input via astrocytic $GABA_B$ receptors remains unclear. Futhermore, we could show that the loss of astrocytic $GABA_B$ receptors reduced GFAP expression. NGS analysis revealed a large number of genes which were altered in the absence of astrocytic $GABA_B$ receptors. In next step a pathway analysis has to be conducted.

In vivo Ca^{2+} imaging in awake and anesthetized cKO mice revealed a reduced signal amplitude and duration. Therefore, activation of astrocytic $GABA_B$ receptors is expected to result in larger and longer signals, which was partially confirmed in acutely isolated brain slices experiments with the $GABA_B$ agonist baclofen. Furthermore, the spatial extent of Ca^{2+} signals and also the signal transduction in glial syncytium has to be evaluated, since it is not yet clear, what the role of astrocytic $GABA_B$ receptors is.

7. REFERENCE

Alberdi E, Sánchez-Gómez MV & Matute C. (2005). Calcium and glial cell death. *Cell Calcium* **38,** 417-425.

Albrecht J, Pearce B & Murphy S. (1986). Evidence for an interaction between GABAB and glutamate receptors in astrocytes as revealed by changes in Ca2+ flux. *Eur J Pharmacol* **125,** 463-464.

Araque A, Carmignoto G, Haydon PG, Oliet SHR, Robitaille R & Volterra A. (2014). Gliotransmitters Travel in Time and Space. *Neuron* **81,** 728-739.

Araque A, Parpura V, Sanzgiri RP & Haydon PG. (1999). Tripartite synapses: glia, the unacknowledged partner. *Trends Neurosci* **22,** 208-215.

Benarroch EE. (2012). GABAB receptors: structure, functions, and clinical implications. *Neurology* **78,** 578-584.

Benes FM & Berretta S. (2001). GABAergic interneurons: implications for understanding schizophrenia and bipolar disorder. *Neuropsychopharmacology* **25,** 1-27.

Benke D, Honer M, Michel C, Bettler B & Mohler H. (1999). gamma-aminobutyric acid type B receptor splice variant proteins GBR1a and GBR1b are both associated with GBR2 in situ and display differential regional and subcellular distribution. *J Biol Chem* **274,** 27323-27330.

Berridge MJ, Bootman MD & Roderick HL. (2003). Calcium signalling: dynamics, homeostasis and remodelling. *Nat Rev Mol Cell Biol* **4,** 517-529.

Bettler B, Kaupmann K, Mosbacher J & Gassmann M. (2004). Molecular structure and physiological functions of GABA(B) receptors. *Physiol Rev* **84,** 835-867.

Bignami A, Eng LF, Dahl D & Uyeda CT. (1972). Localization of the glial fibrillary acidic protein in astrocytes by immunofluorescence. *Brain Res* **43,** 429-435.

Bindocci E, Savtchouk I, Liaudet N, Becker D, Carriero G & Volterra A. (2017). Three-dimensional Ca(2+) imaging advances understanding of astrocyte biology. *Science* **356**.

Bowery NG, Bettler B, Froestl W, Gallagher JP, Marshall F, Raiteri M, Bonner TI & Enna SJ. (2002). International Union of Pharmacology. XXXIII. Mammalian gamma-aminobutyric acid(B) receptors: structure and function. *Pharmacol Rev* **54,** 247-264.

Bowery NG, Hill DR, Hudson AL, Doble A, Middlemiss DN, Shaw J & Turnbull M. (1980). (-)Baclofen decreases neurotransmitter release in the mammalian CNS by an action at a novel GABA receptor. *Nature* **283,** 92-94.

Burda JE, Bernstein AM & Sofroniew MV. (2016). Astrocyte roles in traumatic brain injury. *Experimental Neurology* **275,** 305-315.

Burda JE & Sofroniew MV. (2014). Reactive gliosis and the multicellular response to CNS damage and disease. *Neuron* **81,** 229-248.

Calver AR, Medhurst AD, Robbins MJ, Charles KJ, Evans ML, Harrison DC, Stammers M, Hughes SA, Hervieu G, Couve A, Moss SJ, Middlemiss DN & Pangalos MN. (2000). The expression of GABA(B1) and GABA(B2) receptor subunits in the cNS differs from that in peripheral tissues. *Neuroscience* **100,** 155-170.

Chalifoux JR & Carter AG. (2011). GABAB receptor modulation of synaptic function. *Curr Opin Neurobiol* **21,** 339-344.

Charles AC, Merrill JE, Dirksen ER & Sanderson MJ. (1991). Intercellular signaling in glial cells: calcium waves and oscillations in response to mechanical stimulation and glutamate. *Neuron* **6,** 983-992.

Charles KJ, Deuchars J, Davies CH & Pangalos MN. (2003). GABA B receptor subunit expression in glia. *Mol Cell Neurosci* **24,** 214-223.

Chen R & Chung SH. (2014). Mechanism of tetrodotoxin block and resistance in sodium channels. *Biochem Biophys Res Commun* **446,** 370-374.

Cordelieres FP & Bolte S. (2014). Experimenters' guide to colocalization studies: finding a way through indicators and quantifiers, in practice. *Methods in cell biology* **123,** 395-408.

Couve A, Moss SJ & Pangalos MN. (2000). GABAB receptors: a new paradigm in G protein signaling. *Mol Cell Neurosci* **16,** 296-312.

Cupido A, Catalin B, Steffens H & Kirchhoff F. (2014). Surgical procedures to study microglial motility in the brain and in the spinal cord by in vivo two-photon laser-scanning microcopy. In *Confocal and Multiphoton Laser-Scanning Microscopy of Neuronal Tissue: Applications and Quantitative Image Analysis*, ed. Bakota L & Brandt R, pp. 37-50. Springer.

Ding F, O'Donnell J, Thrane AS, Zeppenfeld D, Kang H, Xie L, Wang F & Nedergaard M. (2013). alpha(1)-Adrenergic receptors mediate coordinated Ca2+ signaling of cortical astrocytes in awake, behaving mice. *Cell Calcium* **54,** 387-394.

Eng LF, Ghirnikar RS & Lee YL. (2000). Glial fibrillary acidic protein: GFAP-thirty-one years (1969-2000). *Neurochem Res* **25,** 1439-1451.

Eng LF, Vanderhaeghen JJ, Bignami A & Gerstl B. (1971). An acidic protein isolated from fibrous astrocytes. *Brain Res* **28,** 351-354.

Erlander MG, Tillakaratne NJ, Feldblum S, Patel N & Tobin AJ. (1991). Two genes encode distinct glutamate decarboxylases. *Neuron* **7,** 91-100.

Fritschy JM, Sidler C, Parpan F, Gassmann M, Kaupmann K, Bettler B & Benke D. (2004). Independent maturation of the GABA(B) receptor subunits GABA(B1) and GABA(B2) during postnatal development in rodent brain. *J Comp Neurol* **477,** 235-252.

Gaiarsa JL, Kuczewski N & Porcher C. (2011). Contribution of metabotropic GABA(B) receptors to neuronal network construction. *Pharmacol Ther* **132,** 170-179.

Grampp T, Notz V, Broll I, Fischer N & Benke D. (2008). Constitutive, agonist-accelerated, recycling and lysosomal degradation of GABA(B) receptors in cortical neurons. *Mol Cell Neurosci* **39,** 628-637.

Guo ZV, Hires SA, Li N, O'Connor DH, Komiyama T, Ophir E, Huber D, Bonardi C, Morandell K, Gutnisky D, Peron S, Xu NL, Cox J & Svoboda K. (2014). Procedures for behavioral experiments in head-fixed mice. *PLoS One* **9,** e88678.

Haller C, Casanova E, Müller M, Vacher CM, Vigot R, Doll T, Barbieri S, Gassmann M & Bettler B. (2004). Floxed allele for conditional inactivation of the GABAB(1) gene. *Genesis* **40,** 125-130.

Han J, Kesner P, Metna-Laurent M, Duan T, Xu L, Georges F, Koehl M, Abrous DN, Mendizabal-Zubiaga J, Grandes P, Liu Q, Bai G, Wang W, Xiong L, Ren W, Marsicano G & Zhang X. (2012). Acute cannabinoids impair working memory through astroglial CB1 receptor modulation of hippocampal LTD. *Cell* **148,** 1039-1050.

Haydon PG. (2009). Astrocytic purines regulate sleep homeostasis and memory loss following sleep deprivation. *Journal of Neurochemistry* **109,** 265-265.

Hirrlinger PG, Scheller A, Braun C, Quintela-Schneider M, Fuss B, Hirrlinger J & Kirchhoff F. (2005). Expression of reef coral fluorescent proteins in the central nervous system of transgenic mice. *Mol Cell Neurosci* **30,** 291-303.

Hösli L, Hösli E, Redle S, Rojas J & Schramek H. (1990). Action of baclofen, GABA and antagonists on the membrane potential of cultured astrocytes of rat spinal cord. *Neurosci Lett* **117,** 307-312.

Jahn HM, Kasakow CV, Helfer A, Michely J, Verkhratsky A, Maurer HH, Scheller A & Kirchhoff F. (2018). Refined protocols of tamoxifen injection for inducible DNA recombination in mouse astroglia. *Sci Rep* **8,** 5913.

Kang J, Jiang L, Goldman SA & Nedergaard M. (1998). Astrocyte-mediated potentiation of inhibitory synaptic transmission. *Nat Neurosci* **1,** 683-692.

Kaupmann K, Huggel K, Heid J, Flor PJ, Bischoff S, Mickel SJ, McMaster G, Angst C, Bittiger H, Froestl W & Bettler B. (1997). Expression cloning of GABA(B) receptors uncovers similarity to metabotropic glutamate receptors. *Nature* **386,** 239-246.

Kaupmann K, Malitschek B, Schuler V, Heid J, Froestl W, Beck P, Mosbacher J, Bischoff S, Kulik A, Shigemoto R, Karschin A & Bettler B. (1998). GABA(B)-receptor subtypes assemble into functional heteromeric complexes. *Nature* **396,** 683-687.

Kim YS & Yoon BE. (2017). Altered GABAergic Signaling in Brain Disease at Various Stages of Life. *Exp Neurobiol* **26,** 122-131.

Kislin M, Mugantseva E, Molotkov D, Kulesskaya N, Khirug S, Kirilkin I, Pryazhnikov E, Kolikova J, Toptunov D, Yuryev M, Giniatullin R, Voikar V, Rivera C, Rauvala H & Khiroug L. (2014). Flat-floored air-lifted platform: a new method for combining behavior with microscopy or electrophysiology on awake freely moving rodents. *J Vis Exp*, e51869.

Lee M, McGeer EG & McGeer PL. (2011a). Mechanisms of GABA release from human astrocytes. *Glia* **59,** 1600-1611.

Lee M, Schwab C & McGeer PL. (2011b). Astrocytes are GABAergic cells that modulate microglial activity. *Glia* **59,** 152-165.

Luisier F, Blu T & Unser M. (2010). Fast interscale wavelet denoising of Poisson-corrupted images. *SignalProcessing* **10,** 415-427.

Lüscher C, Jan LY, Stoffel M, Malenka RC & Nicoll RA. (1997). G protein-coupled inwardly rectifying K+ channels (GIRKs) mediate postsynaptic but not presynaptic transmitter actions in hippocampal neurons. *Neuron* **19,** 687-695.

Madisen L, Zwingman TA, Sunkin SM, Oh SW, Zariwala HA, Gu H, Ng LL, Palmiter RD, Hawrylycz MJ, Jones AR, Lein ES & Zeng H. (2010). A robust and high-throughput Cre reporting and characterization system for the whole mouse brain. *Nat Neurosci* **13,** 133-140.

Madison RD, Sofroniew MV & Robinson GA. (2009). Schwann cell influence on motor neuron regeneration accuracy. *Neuroscience* **163,** 213-221.

Maitre M, Humbert JP, Kemmel V, Aunis D & Andriamampandry C. (2005). [A mechanism for gamma-hydroxybutyrate (GHB) as a drug and a substance of abuse]. *Med Sci (Paris)* **21,** 284-289.

Margeta-Mitrovic M, Mitrovic I, Riley RC, Jan LY & Basbaum AI. (1999). Immunohistochemical localization of GABA(B) receptors in the rat central nervous system. *J Comp Neurol* **405,** 299-321.

Mariotti L, Losi G, Sessolo M, Marcon I & Carmignoto G. (2016). The inhibitory neurotransmitter GABA evokes long-lasting Ca(2+) oscillations in cortical astrocytes. *Glia* **64,** 363-373.

Martin SC, Russek SJ & Farb DH. (2001). Human GABA(B)R genomic structure: evidence for splice variants in GABA(B)R1 but not GABA(B)R2. *Gene* **278,** 63-79.

Metzger D & Chambon P. (2001). Site- and time-specific gene targeting in the mouse. *Methods* **24,** 71-80.

Middeldorp J & Hol EM. (2011). GFAP in health and disease. *Prog Neurobiol* **93,** 421-443.

Mori T, Tanaka K, Buffo A, Wurst W, Kühn R & Götz M. (2006). Inducible gene deletion in astroglia and radial glia--a valuable tool for functional and lineage analysis. *Glia* **54,** 21-34.

Mullis KB & Faloona FA. (1987). Specific synthesis of DNA in vitro via a polymerase-catalyzed chain reaction. *Methods Enzymol* **155,** 335-350.

Nakai J, Ohkura M & Imoto K. (2001). A high signal-to-noise Ca(2+) probe composed of a single green fluorescent protein. *Nat Biotechnol* **19,** 137-141.

Nedergaard M, Ransom B & Goldman SA. (2003). New roles for astrocytes: redefining the functional architecture of the brain. *Trends Neurosci* **26,** 523-530.

Nett WJ, Oloff SH & McCarthy KD. (2002). Hippocampal astrocytes in situ exhibit calcium oscillations that occur independent of neuronal activity. *J Neurophysiol* **87,** 528-537.

Nilsson M, Eriksson PS, Rönnbäck L & Hansson E. (1993). GABA induces Ca2+ transients in astrocytes. *Neuroscience* **54,** 605-614.

Nilsson M, Hansson E & Rönnbäck L. (1992). Agonist-evoked Ca2+ transients in primary astroglial cultures--modulatory effects of valproic acid. *Glia* **5,** 201-209.

Nimmerjahn A, Mukamel EA & Schnitzer MJ. (2009). Motor behavior activates Bergmann glial networks. *Neuron* **62,** 400-412.

Niwa H, Yamamura K & Miyazaki J. (1991). Efficient selection for high-expression transfectants with a novel eukaryotic vector. *Gene* **108,** 193-199.

Oka M, Wada M, Wu Q, Yamamoto A & Fujita T. (2006). Functional expression of metabotropic GABAB receptors in primary cultures of astrocytes from rat cerebral cortex. *Biochem Biophys Res Commun* **341,** 874-881.

Pagano A, Rovelli G, Mosbacher J, Lohmann T, Duthey B, Stauffer D, Ristig D, Schuler V, Meigel I, Lampert C, Stein T, Prezeau L, Blahos J, Pin J, Froestl W, Kuhn R, Heid J, Kaupmann K & Bettler B. (2001). C-terminal interaction is essential for surface trafficking but not for heteromeric assembly of GABA(b) receptors. *J Neurosci* **21,** 1189-1202.

Paukert M, Agarwal A, Cha J, Doze VA, Kang JU & Bergles DE. (2014). Norepinephrine controls astroglial responsiveness to local circuit activity. *Neuron* **82,** 1263-1270.

Perea G, Gómez R, Mederos S, Covelo A, Ballesteros JJ, Schlosser L, Hernández-Vivanco A, Martín-Fernández M, Quintana R, Rayan A, Díez A, Fuenzalida M, Agarwal A, Bergles DE, Bettler B, Manahan-Vaughan D, Martín ED, Kirchhoff F & Araque A. (2016). Activity-dependent switch of GABAergic inhibition into glutamatergic excitation in astrocyte-neuron networks. *Elife* **5**.

Perea G, Navarrete M & Araque A. (2009). Tripartite synapses: astrocytes process and control synaptic information. *Trends Neurosci* **32,** 421-431.

Petroff OA. (2002). GABA and glutamate in the human brain. *Neuroscientist* **8,** 562-573.

Pfaff T, Malitschek B, Kaupmann K, Prézeau L, Pin JP, Bettler B & Karschin A. (1999). Alternative splicing generates a novel isoform of the rat metabotropic GABA(B)R1 receptor. *Eur J Neurosci* **11,** 2874-2882.

Pologruto TA, Sabatini BL & Svoboda K. (2003). ScanImage: flexible software for operating laser scanning microscopes. *Biomedical engineering online* **2,** 13.

Princivalle A, Regondi MC, Frassoni C, Bowery NG & Spreafico R. (2000). Distribution of GABA(B) receptor protein in somatosensory cortex and thalamus of adult rats and during postnatal development. *Brain Res Bull* **52,** 397-405.

Ren JQ, Aika Y, Heizmann CW & Kosaka T. (1992). Quantitative analysis of neurons and glial cells in the rat somatosensory cortex, with special reference to GABAergic neurons and parvalbumin-containing neurons. *Exp Brain Res* **92,** 1-14.

Runquist M & Alonso G. (2003). Gabaergic signaling mediates the morphological organization of astrocytes in the adult rat forebrain. *Glia* **41,** 137-151.

Saab AS, Neumeyer A, Jahn HM, Cupido A, Šimek AA, Boele HJ, Scheller A, Le Meur K, Götz M, Monyer H, Sprengel R, Rubio ME, Deitmer JW, De Zeeuw CI & Kirchhoff F. (2012). Bergmann glial AMPA receptors are required for fine motor coordination. *Science* **337,** 749-753.

Scemes E & Giaume C. (2006). Astrocyte calcium waves: what they are and what they do. *Glia* **54,** 716-725.

Schmidt E, Oheim M. (2018). Two-photon imaging induces brain heating and calcium microdomain hyper-activity in cortical astrocytes. *bioRxiv*.

Schmidt MJ & Mirnics K. (2015). Neurodevelopment, GABA system dysfunction, and schizophrenia. *Neuropsychopharmacology* **40,** 190-206.

Schuler V, Lüscher C, Blanchet C, Klix N, Sansig G, Klebs K, Schmutz M, Heid J, Gentry C, Urban L, Fox A, Spooren W, Jaton AL, Vigouret J, Pozza M, Kelly PH, Mosbacher J, Froestl W, Käslin E, Korn R, Bischoff S, Kaupmann K, van der Putten H & Bettler B. (2001). Epilepsy, hyperalgesia, impaired memory, and loss of pre- and postsynaptic GABA(B) responses in mice lacking GABA(B(1)). *Neuron* **31,** 47-58.

Serrano A, Haddjeri N, Lacaille JC & Robitaille R. (2006). GABAergic network activation of glial cells underlies hippocampal heterosynaptic depression. *J Neurosci* **26,** 5370-5382.

Thrane AS, Rangroo Thrane V, Zeppenfeld D, Lou N, Xu Q, Nagelhus EA & Nedergaard M. (2012). General anesthesia selectively disrupts astrocyte calcium signaling in the awake mouse cortex. *Proc Natl Acad Sci U S A* **109,** 18974-18979.

Vigot R, Barbieri S, Bräuner-Osborne H, Turecek R, Shigemoto R, Zhang YP, Luján R, Jacobson LH, Biermann B, Fritschy JM, Vacher CM, Müller M, Sansig G, Guetg N, Cryan JF, Kaupmann K, Gassmann M, Oertner TG & Bettler B. (2006). Differential compartmentalization and distinct functions of GABAB receptor variants. *Neuron* **50,** 589-601.

Vives V, Alonso G, Solal AC, Joubert D & Legraverend C. (2003). Visualization of S100B-positive neurons and glia in the central nervous system of EGFP transgenic mice. *J Comp Neurol* **457,** 404-419.

Volterra A, Liaudet N & Savtchouk I. (2014). Astrocyte Ca^{2+} signalling: an unexpected complexity. *Nat Rev Neurosci* **15,** 327-335.

von Bartheld CS, Bahney J & Herculano-Houzel S. (2016). The search for true numbers of neurons and glial cells in the human brain: A review of 150 years of cell counting. *J Comp Neurol* **524,** 3865-3895.

Von Blankenfeld G, Trotter J & Kettenmann H. (1991). Expression and Developmental Regulation of a GABAA Receptor in Cultured Murine Cells of the Oligodendrocyte Lineage. *Eur J Neurosci* **3,** 310-316.

Wang F, Smith NA, Xu Q, Goldman S, Peng W, Huang JH, Takano T & Nedergaard M. (2013). Photolysis of Caged Ca2+ But Not Receptor-Mediated Ca2+ Signaling Triggers Astrocytic Glutamate Release. *Journal of Neuroscience* **33,** 17404-17412.

Wang X, Lou N, Xu Q, Tian G-F, Peng WG, Han X, Kang J, Takano T & Nedergaard M. (2006). Astrocytic Ca2+ signaling evoked by sensory stimulation in vivo. *Nature Neuroscience* **9,** 816-823.

Wu C & Sun D. (2015). GABA receptors in brain development, function, and injury. *Metab Brain Dis* **30,** 367-379.

Xu J & Wojcik WJ. (1986). Gamma aminobutyric acid B receptor-mediated inhibition of adenylate cyclase in cultured cerebellar granule cells: blockade by islet-activating protein. *J Pharmacol Exp Ther* **239,** 568-573.

Yang Y, Liu N, He Y, Liu Y, Ge L, Zou L, Song S, Xiong W & Liu X. (2018). Improved calcium sensor GCaMP-X overcomes the calcium channel perturbations induced by the calmodulin in GCaMP. *Nat Commun* **9,** 1504.

Yoon BE, Woo J & Justin Lee C. (2012). Astrocytes as GABA-ergic and GABA-ceptive Cells. *Neurochem Res*.

Zhang Y, Chen K, Sloan SA, Bennett ML, Scholze AR, O'Keeffe S, Phatnani HP, Guarnieri P, Caneda C, Ruderisch N, Deng S, Liddelow SA, Zhang C, Daneman R, Maniatis T, Barres BA & Wu JQ. (2014). An RNA-sequencing transcriptome and splicing database of glia, neurons, and vascular cells of the cerebral cortex. *J Neurosci* **34,** 11929-11947.

8. APPENDIX I

8.1. Co-localization of GABA$_{B1}$ mRNA and protein in different brain regions and cell types
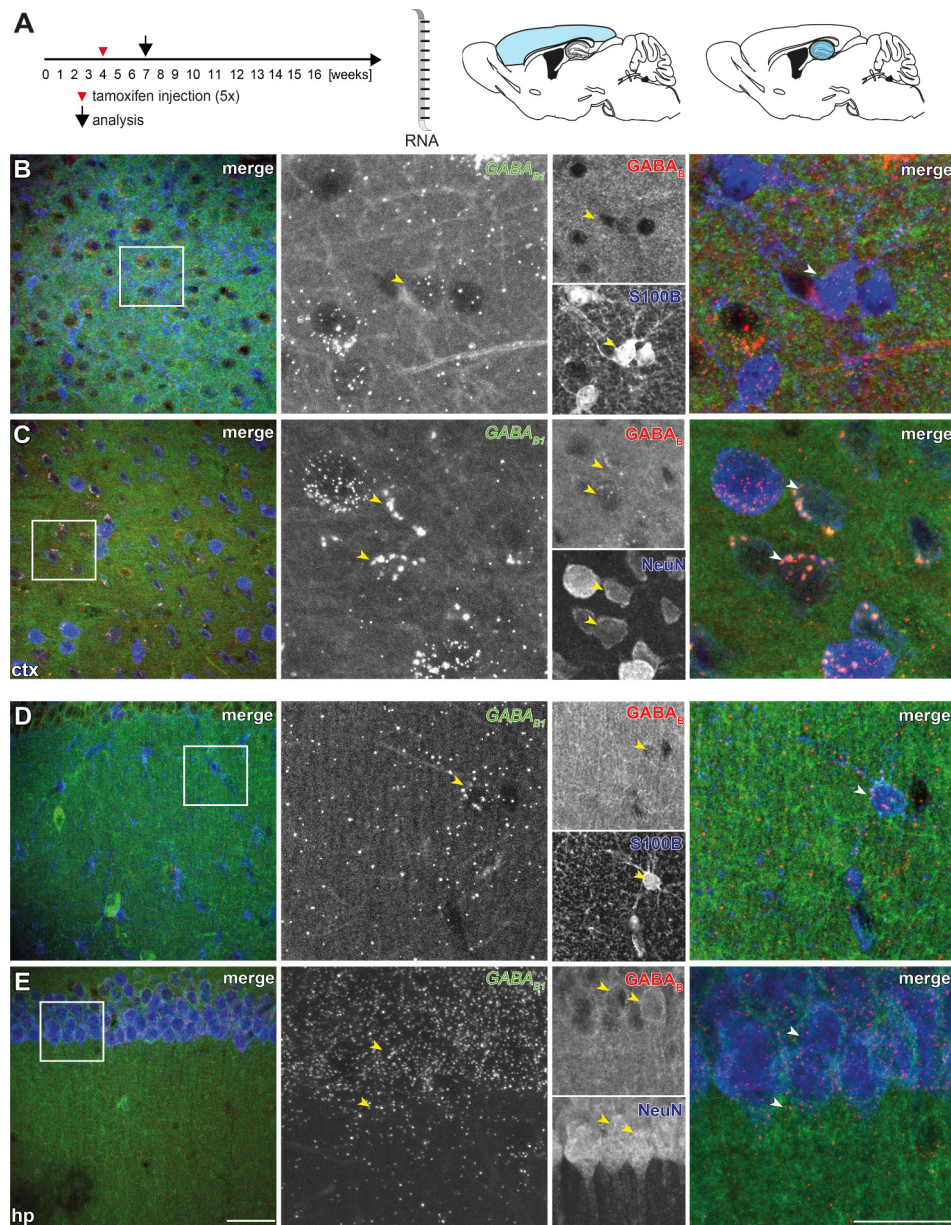
Figure 36: Overlay of GABA$_{B1}$ mRNA and GABA$_{B1}$ protein different cell types

A: Tamoxifen injection (5x) with four weeks and analysis with seven weeks. B: Co-expression of the GABA$_{B1}$ mRNA and GABA$_{B1}$ protein on astrocytes positive for S100B, indicated by arrow heads. C: Co-expression of the GABA$_{B1}$ mRNA and GABA$_{B1}$ in NeuN positive neurons, indicated by triangle. D-E: Expression of GABA$_{B1}$ mRNA and GABA$_{B1}$ subunit in hippocampal astrocytes and neurons. Bars indicate 10 µm (overview) and 20 µm (enlaregement), respectively.

8.2 Reduced GFAP expression in cKO animals
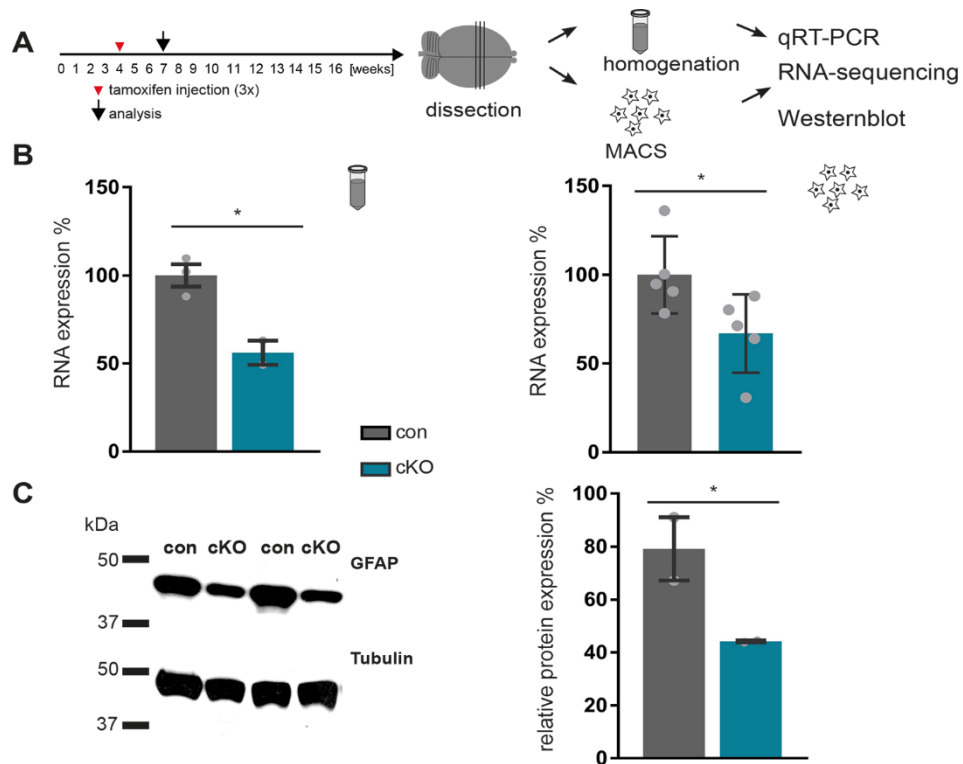
Figure 37: GFAP expression is reduced on mRNA and protein level

A: Tamoxifen injection (5x) with four weeks, analysis (qRT-PCR and Western blot) seven weeks. B: Reduction of GFAP mRNA in brain homogenates and in MAC-sorting isolated astrocytes in cKO. C: Protein expression of GFAP (47.79 kDa) in con and cKO. The quantitative analysis of the Western blot showed a reduction in the GFAP protein expression. Tubulin (48 kDa) was used as internal control.
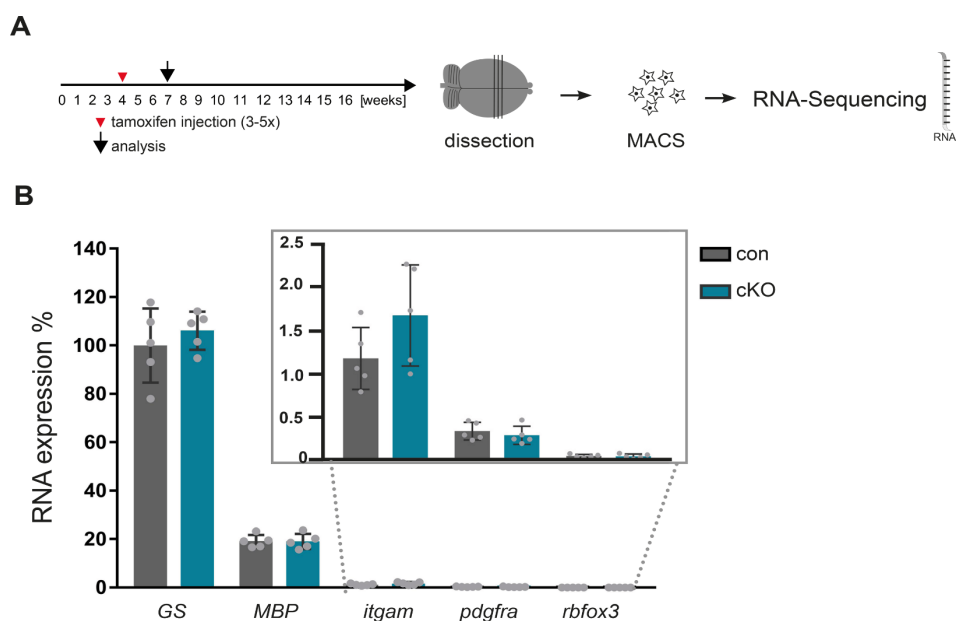
Figure 38: Purity of MAC-sorted astrocytes analyzed by NGS sequencing

A: Tamoxifen injection (5 times) with four weeks, analysis by NG sequencing on Mac-sorted astrocytes with seven weeks. B: Highest RNA expression for astrocytic marker GS (glutamine synthetase), low mRNA expression of non-glia markers; oligodendrocytes (MBP), microglia (itgam), NG2 cells (pdgfra) and neurons (rbfox3) No difference comapring cKO and con. Data were normalized to the mean of GS control (n= 5 aimals).

8.3 Example of the Ca^{2+} signal analysis with MSparkles
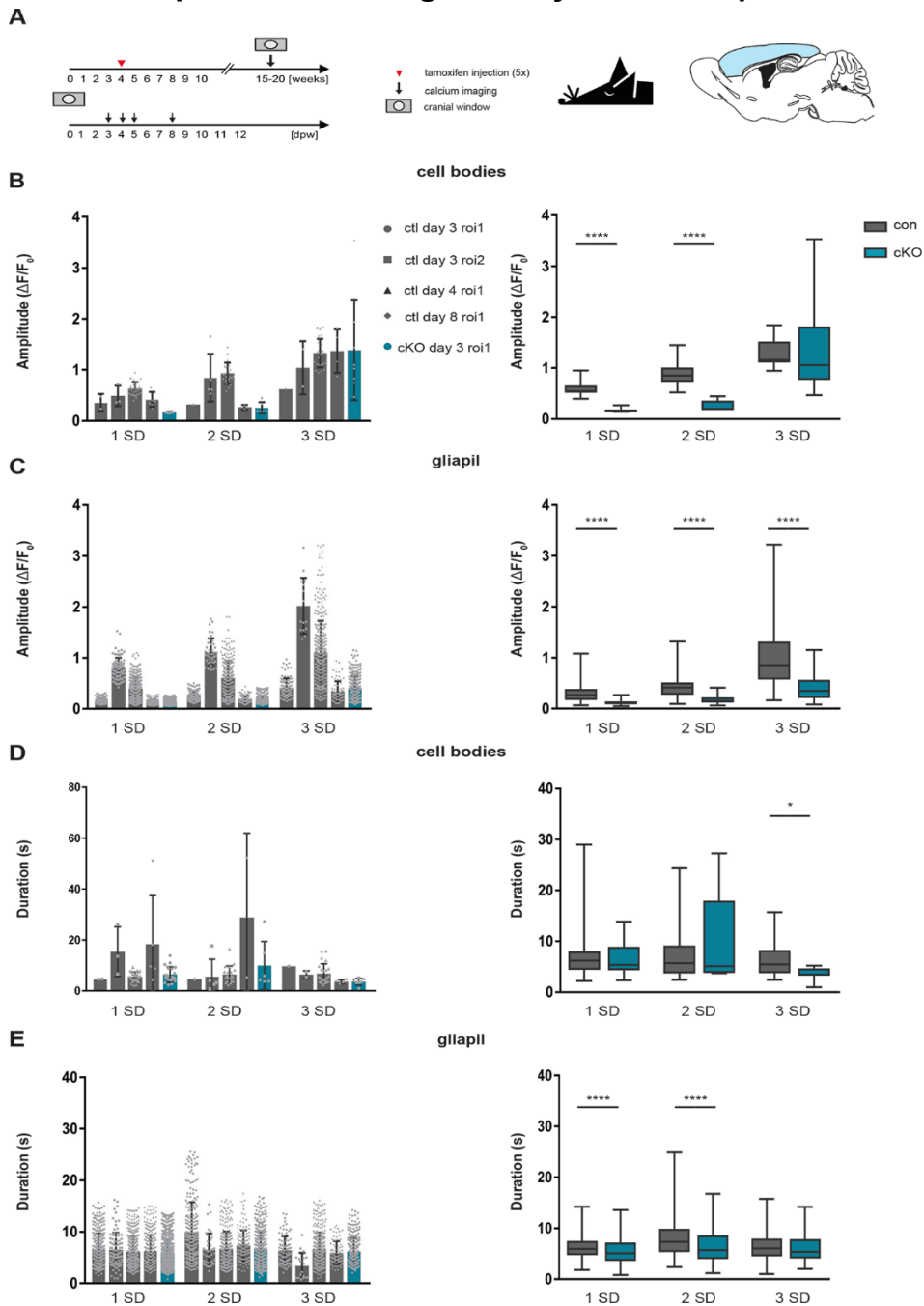
Figure 39: Example of Ca^{2+} data

A: Experimental design B-C: Individual representation of each FOV in the cell somata and gliapil. Gray dots represents one detected signal with MSparkles. Left,summary of these data sets. D-E: Individual representation of each FOV in the cell somata and gliapil. Gray dots represents one detected signals with MSparkles. Left, summary of these data sets (n= 3 animals and 5 FOVs).

8.4   Heat maps of the analyzed Ca²⁺ data
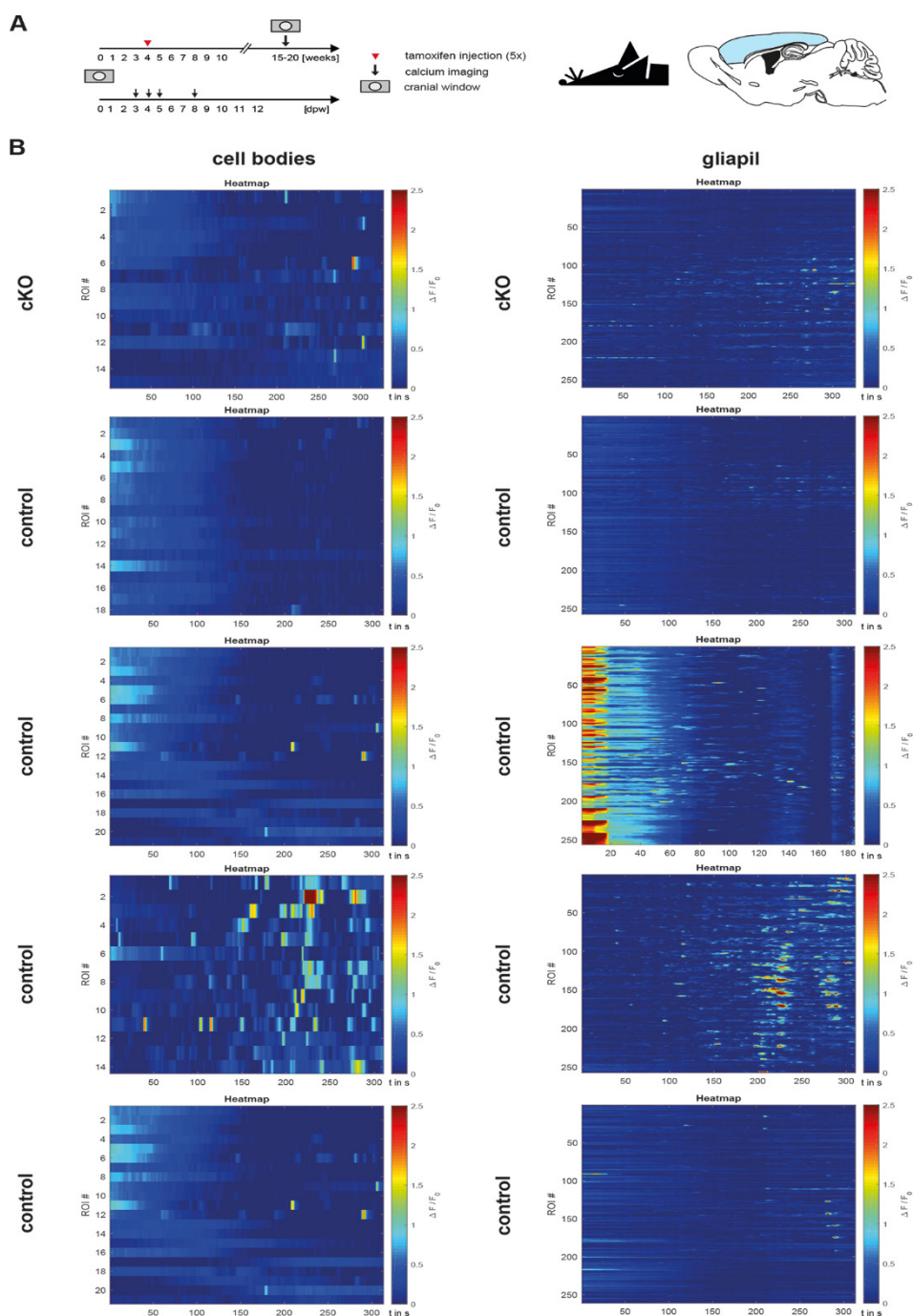
Figure 40: Heat maps of cKO and control anesthetized animals

A: Experimental design B: Heat maps of all FOVs, which were included in the analysis, separated in cell bodies and gliapil. Variability of the Ca^{2+} signals in the gliapil and cell bodies in cKO and con animals. Number of ROIs and time in second (s) was indicated. Signal amplitude ($\Delta F/F_0$) was color coded.
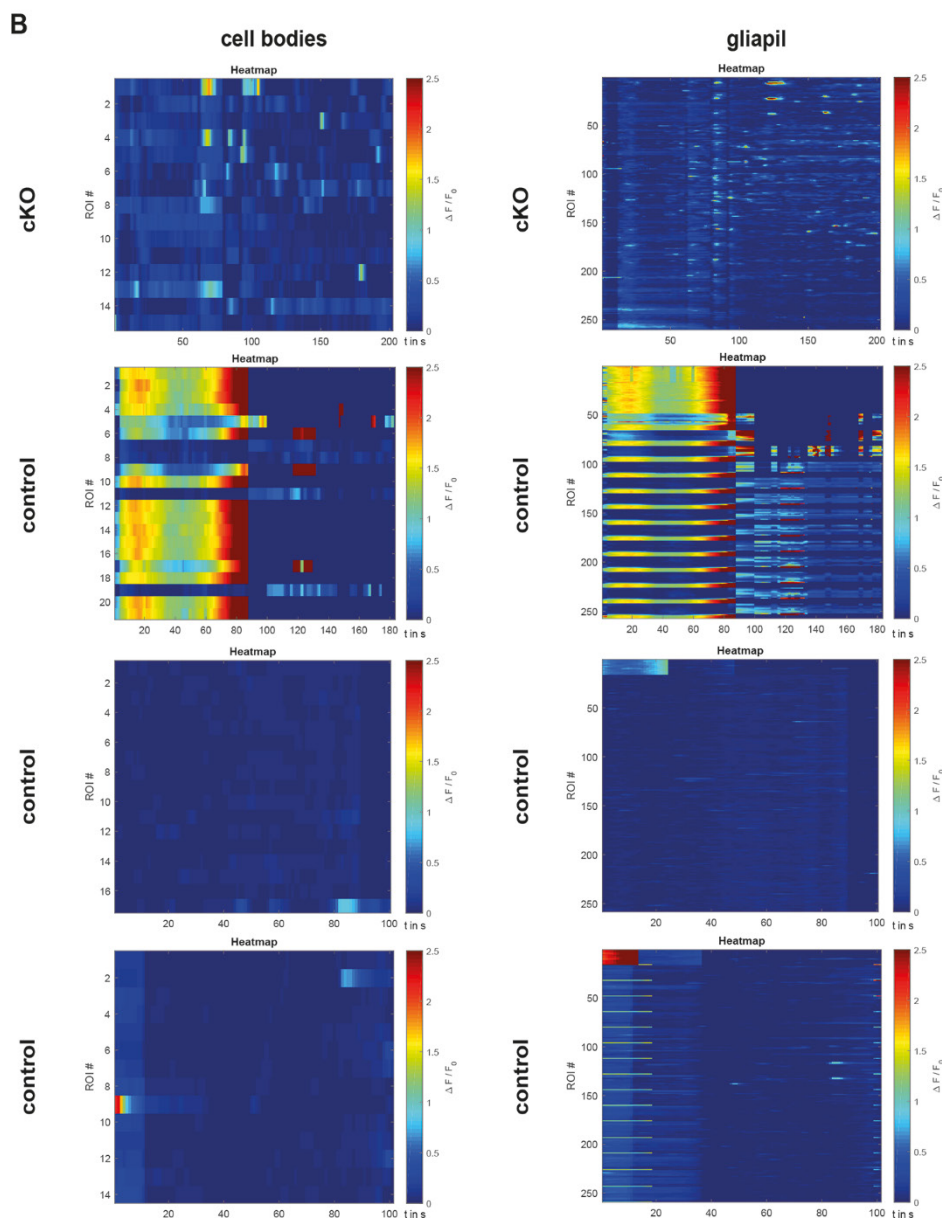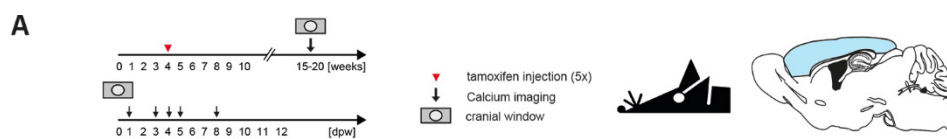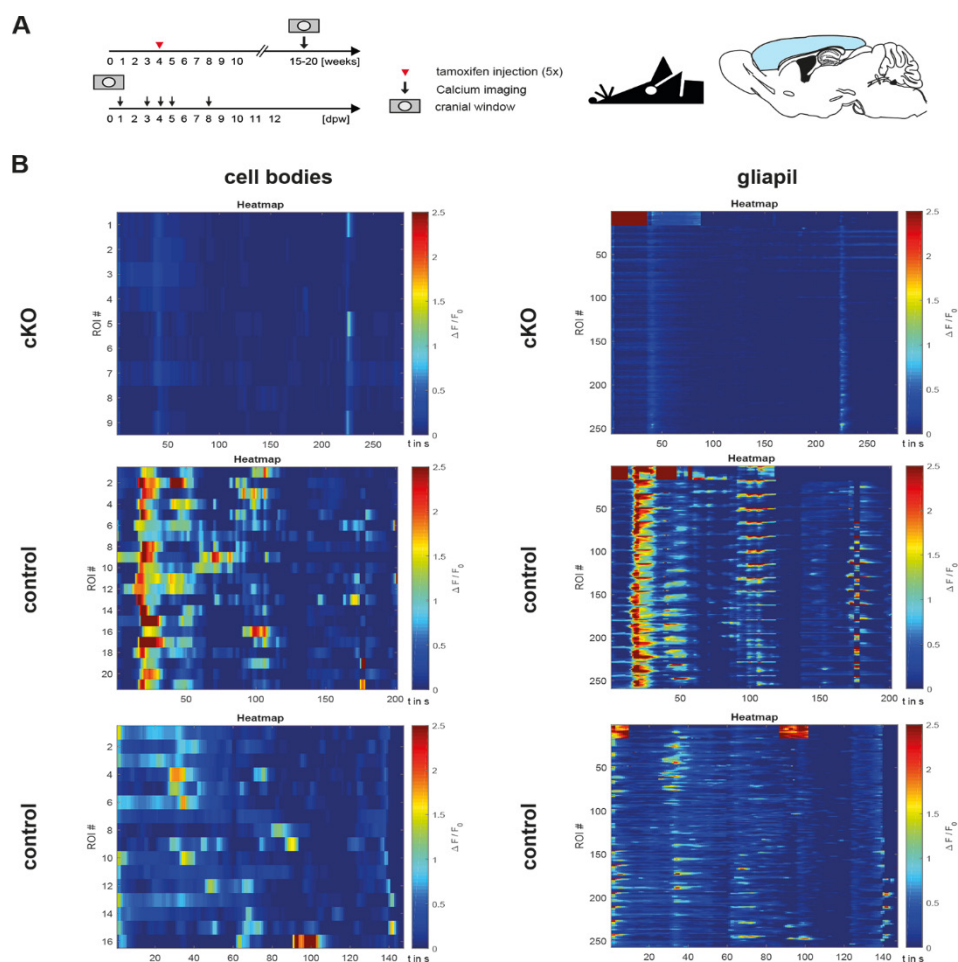
Figure 41: Heat maps of cKO and control animals in awake status

A: Experimental design B: Heat maps of all FOVs, which were included in the analysis, separated in cell bodies and gliapil. Variability of the Ca^{2+} signals in the gliapil and cell bodies in cKO and con animals. Number of ROIs and time in second (s) was indicated. Signal amplitude ($\Delta F/F_0$) was color coded.

Figure 42: Heat maps of anesthetized animals with tamoxifen injection at 7 weeks

A: Experimental design B: Heat maps of all FOVs, which were included in the analysis, separated in cell bodies and gliapil. Variability of the Ca^{2+} signals in the gliapil and cell bodies in cKO and con animals. Number of ROIs and time in second (s) was indicated. Signal amplitude ($\Delta F/F_0$) was color coded.

A

B
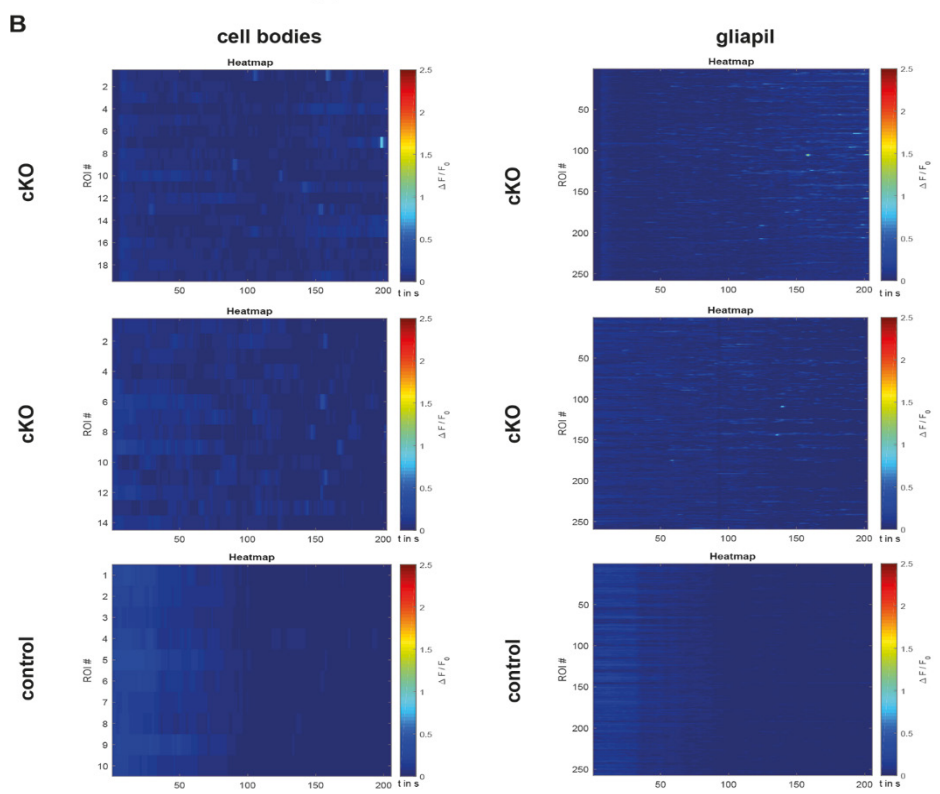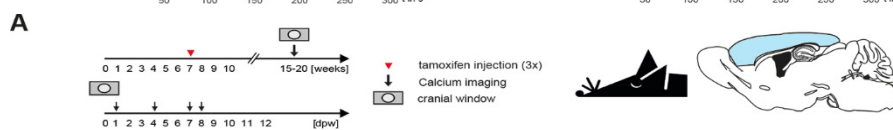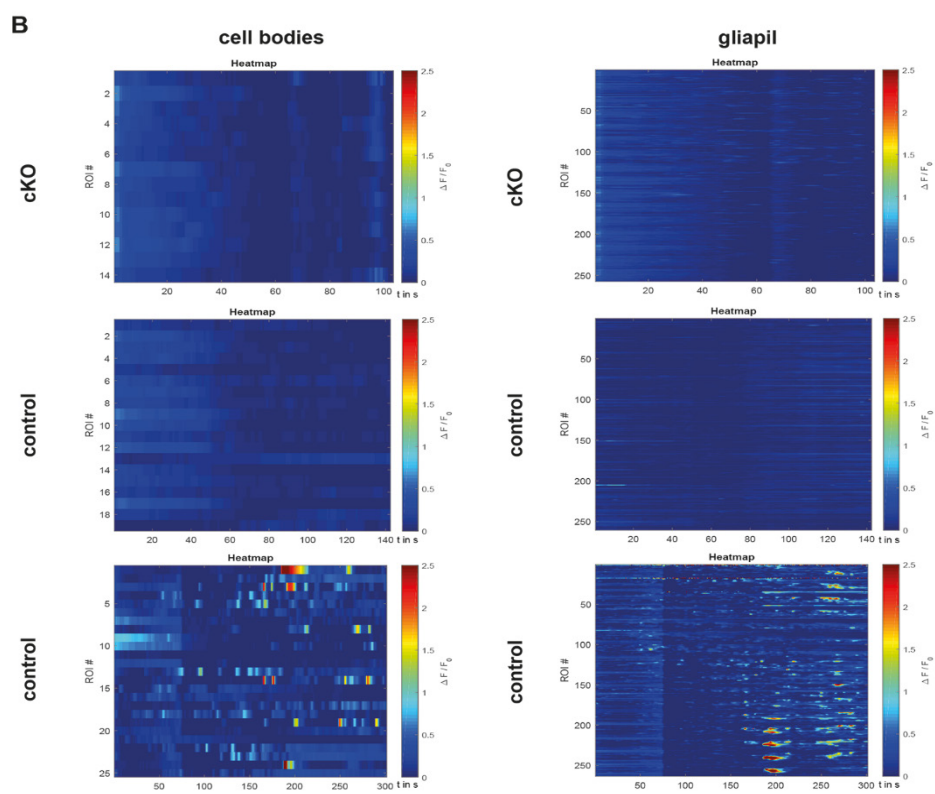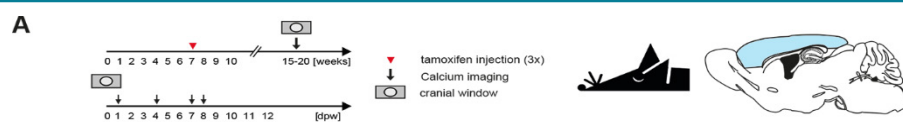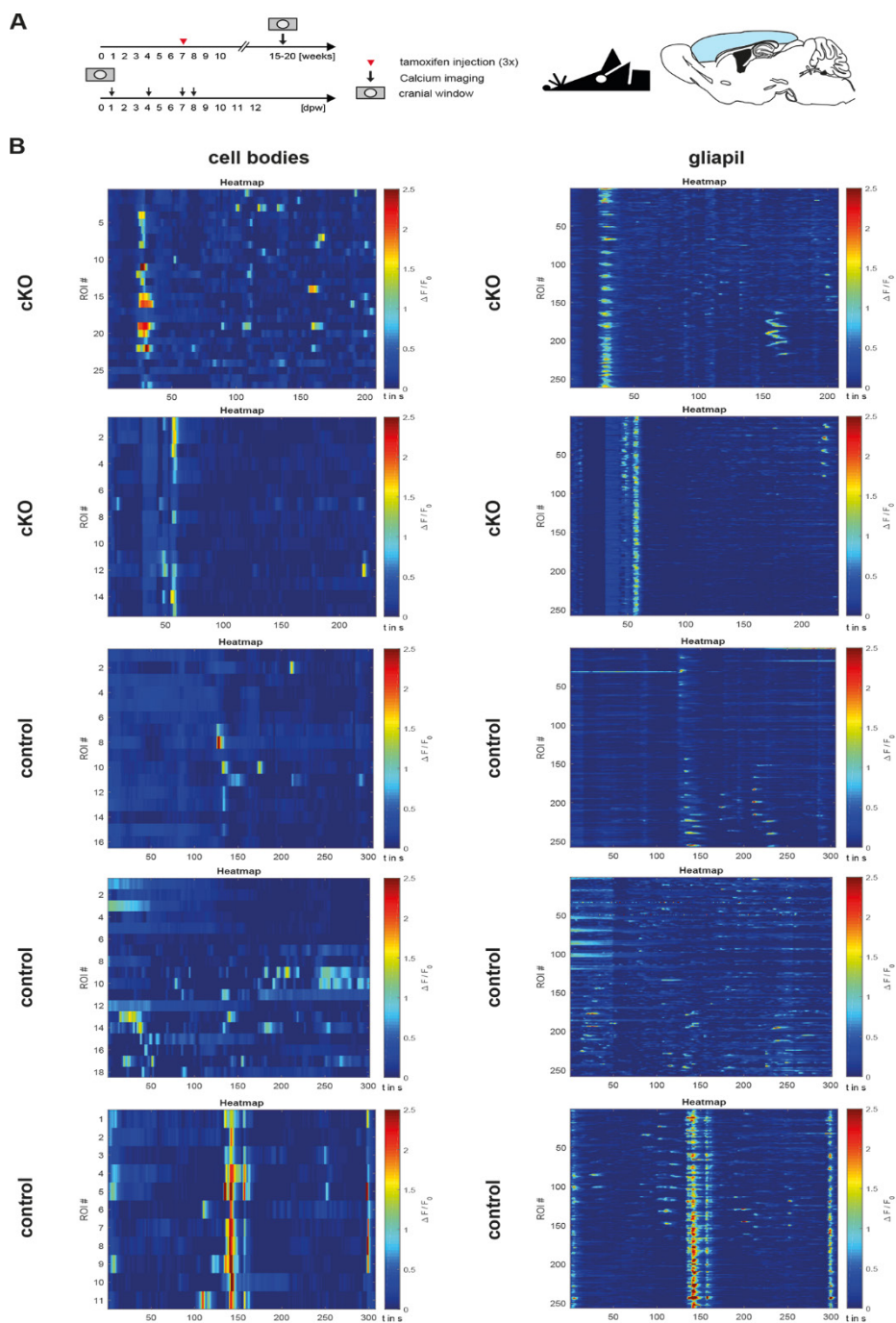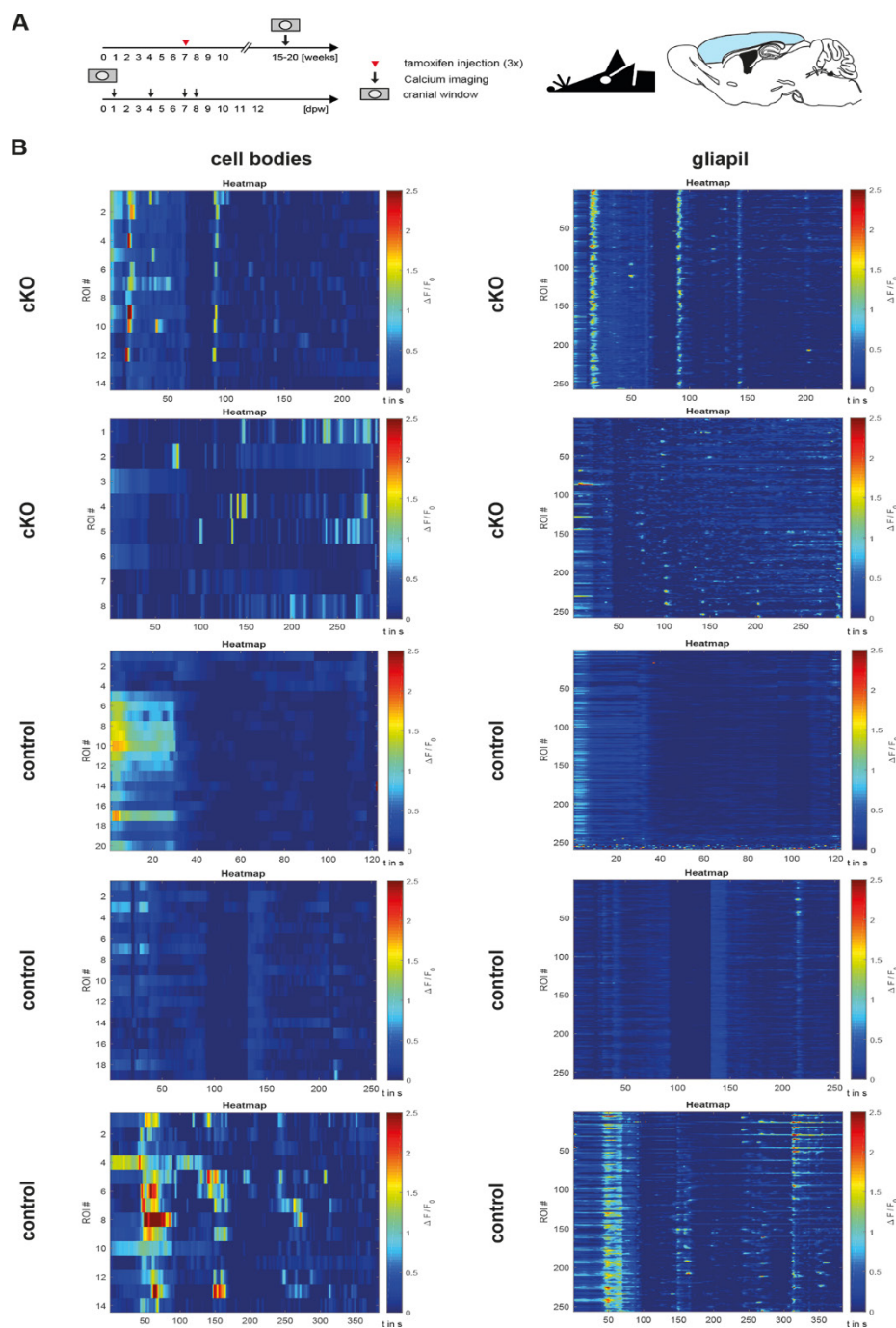
Figure 43: Heat maps of awake animals

A: Experimental design B: Heat maps of all FOVs, which were included in the analysis, separated in cell bodies and gliapil. Variability of the Ca^{2+} signals in the gliapil and cell bodies in cKO and con animals. Number of ROIs and time in second (s) was indicated. Signal amplitude ($\Delta F/F_0$) was color coded.

8.5 Changes in the Ca^{2+} signal properties compared anesthetized to awake animals
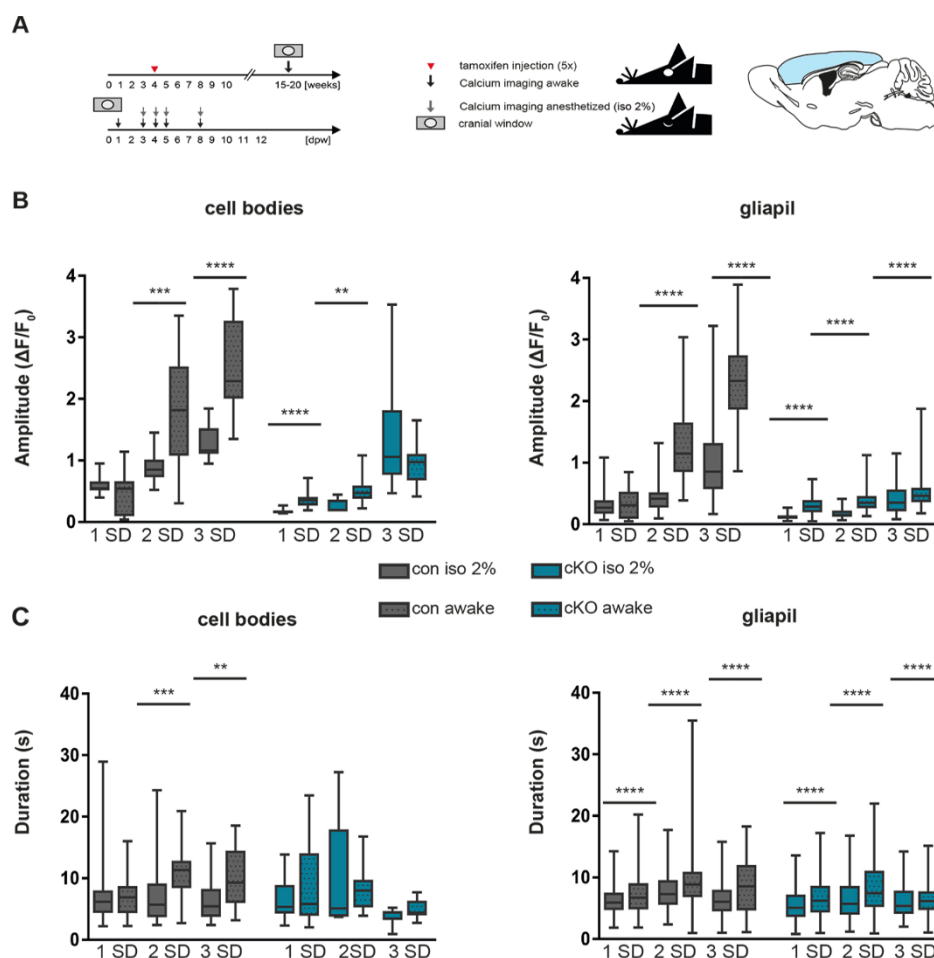
Figure 44: Larger and longer signals in awake cKO and con animals

A: Experimental design B: Higher amplitude of medium and large somatic Ca^{2+} signals in awake control animals. The amplitude of small and medium signals was increased in cKO. In the gliapil the signal amplitude was increased in control and cKO animals in all three groups (except control 1SD). C: The duration was longer in awake animals in the gliapil. Only control somatic medium and large Ca^{2+} signals were longer (n= 7 animals and 12 FOVs).
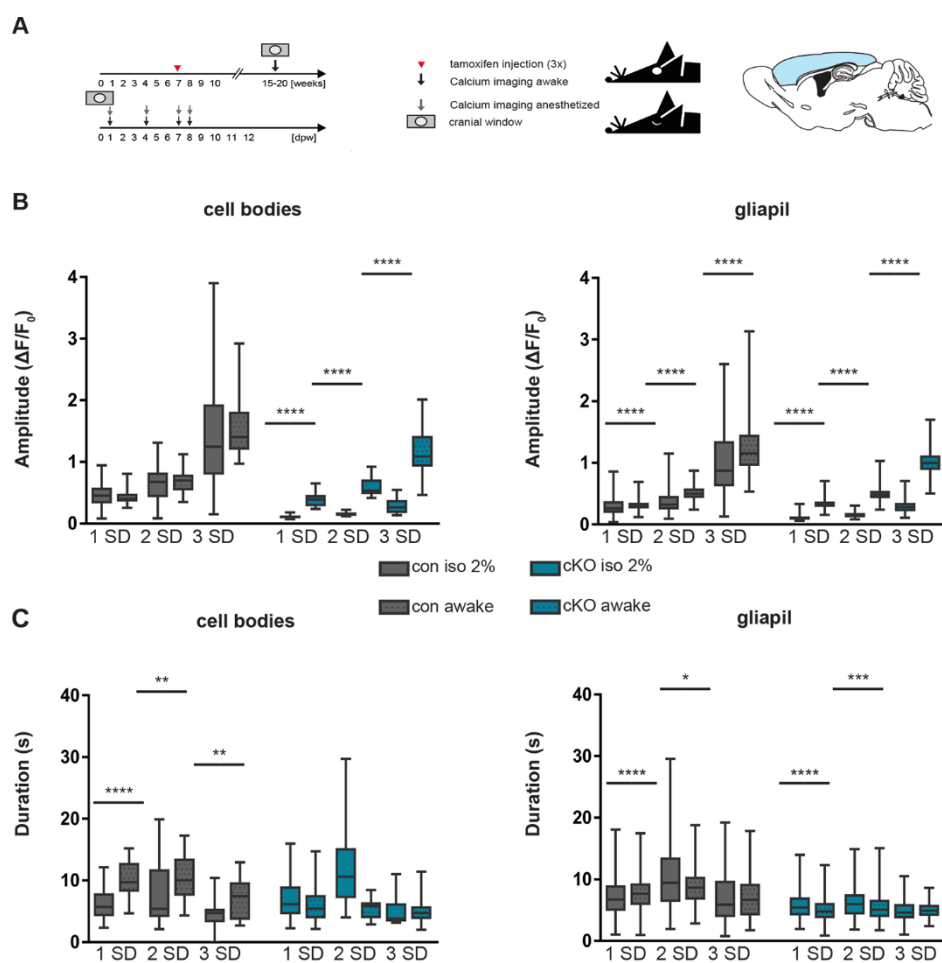
Figure 45: Larger and longer Ca²⁺ signals without anesthesia

A: Experimental design B: An increase in the signal amplitude of all somatic Ca^{2+} signals in awake cKO animals. In the gliapil the signal amplitude was increased in control and cKO animals in all three groups. C: Longer somatic signals in control animals . In the gliapil small and medium signals of cKO and control animals were prolonged (n= 6 animals and 14 FOVs).

8.6 Statistical values

Table 7: Statistical values for figure 5-17 and 34-38

	Mean	SD	p		Mean	SD	p
Figure 5B				**Figure 15B**			
bs con	101.6	10.8	0.04	con	70.34	7.42	0.018
bs cKO	75.1	1.34		cKO	41.01	1.04	
cb con	100.3	3.97	0.045	**Figure 15C**			
cb cKO	85.98	4.35		con 4-10w	61.03	1.54	<0.0001
ctx con	100.5	5.52	0.019	cKO 4-10w	27.06	1.05	
ctx cKO	75.46	5.95		**Figure 15C**			
hp con	100.5	4.29	0.0041	con p13,14-7w	58.08	2.99	0.0013
hp cKO	71.46	7.02		cKO p13,14-7w	27.04	3.89	
opt. N con	100.1	1.93	<0.0001	**Figure 15C**			
opt. N cKO	62.16	3.96		con 4-10w	61.03	1.54	<0.0001
Figure 5C				cKO 4-10w	27.06	1.05	
ctx con	106.1	40.79	0.055	**Figure 15C**			
ctx cKO	41.97	7.24		con 4-16w	63.86	1.54	<0.0001
Figure 6B				cKO 4-16w	27.29	0.97	
cb 4w con	100.4	4.78	0.30	**Figure 15C**			
cb 4w cKO	89.26	8.70		con 4,7,10-13w	60.38	2.70	0.0002
cb 4,7,10w con	100.3	5.78	0.08	cKO 4,7,10-13w	31.04	1.78	
cb 4,7,10w cKO	86.89	3.64		**Figure 15C**			
Figure 6C				con GFAP il	422.4	132.9	0.01
cb 4w con	100.0	12.38	<0.0001	cKO GFAP il	216.4	112.2	
cb 4w cKO	44.99	7.77		**Figure 18C**			
Figure 11D				Con	887.15	89.15	0.043
con (overlap)	85.00	1.05	<0.0001	cKO	989.3	99.15	
cKO (overlap)	73.66	1.29		**Figure 38C**			
Con (M2)	52.22	3.59	0.0009	glrb con	100	7.84	0.55
cKO (M2)	32.84	3.24		glrb cKO	97.28	5.87	
Figure 12B				grin1 con	100	20.01	0.76
ctx 4w con	103.8	14.99	0.50	grin1 cKO	91.15	19.5	
ctx 4w cKO	92.52	5.17		gria4 con	100	9.0	0.52
ctx 4,7,10w con	100.9	9.79	0.36	gria4 cKO	120	16.16	
ctx 4,7,10w cKO	90.16	6.23		p2y1r con	100	6.6	0.95
Figure12C				p2y1r cKO	93.84	21.77	
ctx 4w con	100.0	16.47	<0.0001	**Figure 38B**			
ctx 4w cKO	30.01	3.28		slc6a1 con	100	10.44	0.62
Figure 34D				slc6a1 cKO	103.3	10.64	
kcnj2 con	100	30.55	0.0025	gad2 con	100	31.92	0.45
kcnj2 cKO	168.8	17.93		gad2 cKO	82.35	37.02	
scn1a con	100	54.77	0.1	gabaarap con	100	9.4	0.0006

scn1a cKO	165	48.73		gabaarap cKO	55.44	15.6	
s100b con	100	11.72	0.017	gabaa b con	100	35.99	0.038
s100b cKO	135.5	24.05		gabaa b cKO	52.91	22.86	
GFAP con	100	9.74	0.04	gabbr1 con	100	7.36	<0.0001
GFAP cKO	66.88	9.87		gabbr1 cKO	30.01	1.47	
Figure 38E				gabb2 con	100	10.49	0.0014
syt10 con	99.5	5.34	0.01	gabbr2 cKO	38.18	3.48	
syt10 cKO	54.66	4.64		**Figure 38B**			
vti1b con	100	16.52	0.03	GS con	100.0	15.37	0.44
vti1b cKO	70.53	20.54		GS cKO	106.1	7.8	
syt14 con	100.3	2.3	0.06	MBP con	19.14	2.63	0.96
syt14 cKO	51.49	17.63		MBP cKO	19.05	3.10	
snapin con	100	11.38	0.02	itgam con	1.18	0.35	0.144
snapin cKO	120	12.35		itgam cKO	1.67	0.58	
Figure 37B				pdgfra con	0.34	0.10	0.48
con	100.0	6.39	0.02	pdgfra cKO	0.29	0.10	
cKO	56.11	6.85		rbfox3 con	0.056	0.01	0.86
Figure 37B				rbrfox3 cKO	0.053	0.02	
con	100.0	21.72	0.043				
cKO	66.88	22.09					
Figure 37C							
con	79.41	11.9	0.031				
cKO	44.1	1.19					

Table 8: Statistical values for figure 19-29

Fig. 19B	25%ile	median	75%ile	p	Fig. 19B	25%ile	median	75%ile	p
1SD base	0.3336	0.5965	0.8676	0.5	1SD base	0.345	0.409	0.4826	0.0025
1SD bac	0.6453	0.7433	0.8278		1SD bac	0.3323	0.383	0.4351	
2SD base	1.137	1.137	1.137	0.47	2SD base	0.505	0.5743	0.681	0.44
2SD bac	0.4952	0.9067	1.203		2SD bac	0.4959	0.5666	0.6697	
3SD base	0.9239	1.716	1.73	0.41	3SD base	0.7032	0.8627	1.059	0.065
3SD bac	1.582	1.782	1.843		3SD bac	0.7432	0.9277	1.137	
Fig. 19C	**25%ile**	**median**	**75%ile**	**p**	**Fig. 19C**	**25%ile**	**median**	**75%ile**	**p**
1SD base	3.896	5.445	5.871	0.07	1SD base	4.709	5.556	7.649	<0.0001
1SD bac	6.058	9.446	17.63		1SD bac	8.344	12.83	19.52	
2SD base	5.35	5.35	5.35	0.055	2SD base	4.767	5.973	8.075	<0.0001
2SD bac	7.333	9.123	17.84		2SD bac	7.805	9.69	13.1	
3SD base	8.082	13.95	19.08	0.76	3SD base	7.979	9.815	12.49	0.27
3SD bac	7.026	14.98	19.07		3SD bac	7.596	8.945	11.24	
Fig. 20B	**25%ile**	**median**	**75%ile**	**p**	**Fig. 20B**	**25%ile**	**median**	**75%ile**	**p**
1SD base	0.3317	0.5756	0.8194	0.58	1SD base	0.2614	0.2949	0.3405	0.15
1SD bac	0.3997	0.5701	0.9742		1SD bac	0.2459	0.2935	0.3419	
2SD base	0.8112	1.278	1.454	0.54	2SD base	0.3144	0.3553	0.399	0.0021

	25%ile	median	75%ile	p		25%ile	median	75%ile	p
2SD bac	0.6051	0.8347	1.522		2SD bac	0.2673	0.331	0.3772	
3SD base	1.685	2.501	2.958	0.28	3SD base	0.2618	0.5204	0.6661	<0.0001
3SD bac	0.9216	1.373	1.824		3SD bac	0.191	0.2499	0.337	
Fig. 20C	**25%ile**	**median**	**75%ile**	**p**	**Fig. 20C**	**25%ile**	**median**	**75%ile**	**p**
1SD base	3.625	4.489	5.353	0.07	1SD base	6.573	10.37	16.14	0.54
1SD bac	7.272	9.27	15.95		1SD bac	7.065	10.77	12.85	
2SD base	8.478	10.77	12.48	0.09	2SD base	6.178	8.331	11.23	<0.0001
2SD bac	11.77	17.81	37.63		2SD bac	11	17.9	30.4	
3SD base	6.583	7.543	12.67	>0.999	3SD base	7.05	9.033	11.22	<0.0001
3SD bac	6.658	10.13	13.61		3SD bac	8.991	12.24	23.32	

Fig. 22B	**25%ile**	**median**	**75%ile**	**p**	**Fig. 22C**	**25%ile**	**median**	**75%ile**	**p**
1SD base	0.243	0.3194	0.5623	0.0016	1SD base	0.7265	0.935	1.04	<0.0001
1SD CGP	1.339	2.183	2.577	0.0079	1SD CGP	0.3419	0.4915	1.104	<0.0001
1SD bac	1.409	1.832	2.009	0.94	1SD bac	0.5598	0.7259	0.8738	0.08
2SD base	0.4734	0.9233	2.486	0.22	2SD base	0.7072	0.8759	1.176	<0.0001
2SD CGP	0.3677	0.4203	2.006	0.39	2SD CGP	1.107	1.526	1.968	0.18
2SD bac	1.783	2.366	2.696	0.03	2SD bac	0.4385	0.6631	1.657	<0.0001
3SD base	0.1567	0.6775	1.107	0.2	3SD base	0.8156	0.9937	1.244	<0.0001
3SD CGP	0.9957	0.9957	0.9957	0.2	3SD CGP	1.55	2.461	2.874	<0.0001
3SD bac	1.52	1.52	1.52	0.8	3SD bac	1.428	2.303	3.1	0.68
Fig. 22C	**25%ile**	**median**	**75%ile**	**p**	**Fig.22C**	**25%ile**	**median**	**75%ile**	**p**
1SD base	5.484	9.529	9.944	0.6	1SD base	5.848	8.927	12.29	<0.0001
1SD CGP	9.772	25.06	31.98	0.2	1SD CGP	5.71	7.976	12.62	0.42
1SD bac	1.629	5.262	11.79	0.03	1SD bac	5.597	7.333	9.892	0.0006
2SD base	31.73	33.28	36.33	0.2	2SD base	5.89	10.22	16.6	<0.0001
2SD CGP	12.17	17.65	33.21	0.4	2SD CGP	7.282	12.94	20.32	<0.0001
2SD bac	2.164	4.455	29.64	0.2	2SD bac	5.748	8.198	11.13	<0.0001
3SD base	0	12.99	25.98	>0.999	3SD base	7.111	12.58	18.61	<0.0001
3SD CGP	2.723	32.57	62.42	0.66	3SD CGP	5.13	10.82	14.65	<0.0004
3SD bac	2.825	6.207	13.84	0.8	3SD bac	3.379	5.632	7.336	<0.0001
Fig. 23B	**25%ile**	**median**	**75%ile**	**p**	**Fig.23B**	**25%ile**	**median**	**75%ile**	**p**
1SD base	0.7131	0.8239	2.403	0.25	1SD base	0.9002	1.052	1.271	0.0005
1SD CGP	1.41	1.96	2.08	0.22	1SD CGP	1.018	1.165	1.344	0.0002
1SD bac	0.4426	0.5928	0.9327	0.03	1SD bac	1.002	1.169	1.351	0.91
2SD base	0.5704	1.07	1.984	0.88	2SD base	1.473	1.67	1.84	0.019
2SD CGP	0.4976	1.497	2.094	0.97	2SD CGP	1.324	1.554	1.766	0.0036
2SD bac	0.5829	1.036	1.489	0.68	2SD bac	1.513	1.744	2.173	<0.0001
3SD base	1.064	1.461	2.664	0.35	3SD base	2.197	2.559	2.988	<0.0001
3SD CGP	1.185	1.645	2.053	0.97	3SD CGP	2.135	2.491	2.92	0.64
3SD bac	2.047	2.047	2.047	0.7	3SD bac	2.402	2.897	3.574	<0.0001
Fig. 23C	**25%ile**	**median**	**75%ile**	**p**	**Fig.23C**	**25%ile**	**median**	**75%ile**	**p**
1SD base	6.076	9.386	13.02	>0.99	1SD base	5.926	7.327	9.208	<0.0001
1SD CGP	9.581	19.29	22.68	0.09	1SD CGP	8.707	12.72	16.69	<0.0001
1SD bac	6.241	7.07	24.83	>0.99	1SD bac	8.588	14.29	23.66	0.0049

2SD base	10.37	12.12	25.82	0.88	2SD base	7.138	9.272	12.47	<0.0001
2SD CGP	7.986	17.75	29.85	0.73	2SD CGP	11.69	16.05	21.33	<0.0001
2SD bac	12.49	13.86	15.23	>0.99	2SD bac	8.972	13.95	20.95	0.058
3SD base	12.07	18.04	42.25	0.06	3SD base	8.896	13.91	21.15	<0.0001
3SD CGP	1.148	2.432	11.57	0.01	3SD CGP	11.73	16.23	24.42	0.001
3SD bac	1.074	1.092	14.89	0.78	3SD bac	4.462	7.371	12.65	<0.0001

Fig. 25B	media	75%ile	p	Fig.25B	25%ile	media	75%ile	p
1SD con	0.549	0.6599	<0.0001	1SD con	0.1725	0.269	0.3897	<0.0001
1SD cKO	0.163	0.1818		1SD cKO	0.0893	0.111	0.142	
2SD con	0.853	1.013	<0.0001	2SD con	0.2723	0.414	0.5191	<0.0001
2SD cKO	0.194	0.3623		2SD cKO	0.1207	0.152	0.2214	
3SD con	1.161	1.522	<0.0001	3SD con	0.5716	0.855	1.319	<0.0001
3SD cKO	1.059	1.816		3SD cKO	0.2106	0.351	0.5638	
Fig. 25C	**media**	**75%ile**	**p**	**Fig.25C**	**25%ile**	**media**	**75%ile**	**p**
1SD con	6.188	8.023	0.62	1SD con	0.5158	0.549	0.6599	<0.0001
1SD cKO	5.339	8.913		1SD cKO	0.1491	0.163	0.1818	
2SD con	5.719	9.162	0.74	2SD con	0.7294	0.853	1.013	<0.0001
2SD cKO	5.116	17.96		2SD cKO	0.1794	0.194	0.3623	
3SD con	5.46	8.285	0.029	3SD con	1.107	1.161	1.522	0.33
3SD cKO	3.456	4.647		3SD cKO	0.7653	1.059	1.816	
Fig. 26B	**media**	**75%ile**	**p**	**Fig. 26B**	**25%ile**	**media**	**75%ile**	**p**
1SD con	0.541	0.6622	0.038	1SD con	0.0883	0.309	0.5279	0.36
1SD cKO	0.354	0.4037		1SD cKO	0.1936	0.285	0.3901	
2SD con	1.82	2.526	<0.0001	2SD con	0.8489	1.15	1.652	<0.0001
2SD cKO	0.470	0.593		2SD cKO	0.2633	0.348	0.4578	
3SD con	2.287	3.267	<0.0001	3SD con	1.862	2.327	2.747	<0.0001
3SD cKO	0.976	1.104		3SD cKO	0.359	0.460	0.5929	
Fig. 26C	**media**	**75%ile**	**p**	**Fig. 26C**	**25%ile**	**media**	**75%ile**	**p**
1SD con	6.881	8.748	0.93	1SD con	4.83	6.708	9.034	0.049
1SD cKO	5.809	14.04		1SD CKO	4.31	6.231	8.649	
2SD con	11.35	12.84	0.02	2SD con	6.818	8.85	10.91	0.0037
2SD cKO	8.01	9.754		2SD cKO	5.204	7.452	11.1	
3SD con	9.284	14.49	0.002	3SD con	4.657	8.538	12	<0.001
3SD cKO	4.382	6.353		3SD cKO	4.73	6.138	7.765	
Fig. 28B	**media**	**75%ile**	**p**	**Fig. 28B**	**25%ile**	**media**	**75%ile**	**p**
1SD con	0.452	0.5803	<0.0001	1SD con	0.1725	0.269	0.3897	<0.0001
1SD cKO	0.104	0.1267		1SD cKO	0.0893	0.111	0.142	
2SD con	0.673	0.8279	<0.0001	2SD con	0.2723	0.414	0.5191	<0.0001
2SD cKO	0.143	0.1804		2SD cKO	0.1207	0.152	0.2214	
3SD con	1.247	1.935	<0.0001	3SD con	0.5716	0.855	1.319	<0.0001
3SD cKO	0.260	0.3813		3SD cKO	0.2106	0.351	0.5638	
Fig. 28C	**media**	**75%ile**	**p**	**Fig. 28C**	**25%ile**	**media**	**75%ile**	**p**
1SD con	5.706	7.911	0.55	1SD con	4.882	6.725	9.06	<0.0001
1SD cKO	6.148	9.035		1SD cKO	4.15	5.434	7.093	
2SD con	5.427	11.82	0.008	2SD con	6.356	9.41	13.54	<0.0001

	media	75%ile	p
2SD cKO	10.62	15.24	
3SD con	4.751	5.429	0.79
3SD cKO	3.825	6.283	
Fig. 29B	**media**	**75%ile**	**p**
1SD con	0.401	0.4843	0.013
1SDcKO	0.345	0.4287	
2SD con	0.703	0.7941	<0.0001
2SD cKO	0.530	0.7159	
3SD con	1.405	1.816	<0.0001
3SD cKO	1.089	1.421	
Fig. 29C	**media**	**75%ile**	**p**
1SD con	9.729	12.84	<0.0001
1SD cKO	5.522	7.099	
2SD con	10	13.56	<0.0001
2SD cKO	5.899	6.476	
3SD con	7.47	9.706	0.010
3SD cKO	4.753	5.828	

	25%ile	media	75%ile	p
2SD cKO	4.314	5.994	7.567	
3SD con	3.885	5.878	9.782	<0.0001
3SD cKO	3.673	4.605	5.991	
Fig. 29B	**25%ile**	**media**	**75%ile**	**p**
1SD con	0.2614	0.306	0.3536	0.7
1SD cKO	0.2859	0.330	0.3733	
2SD con	0.4314	0.498	0.5845	<0.0001
2SD cKO	0.4286	0.484	0.5492	
3SD con	0.9486	1.156	1.454	<0.0001
3SD cKO	0.8862	0.997	1.122	
Fig. 29C	**25%ile**	**media**	**75%ile**	**p**
1SD con	5.855	7.689	9.347	<0.0001
1SD cKO	3.705	4.775	6.195	
2SD con	6.724	8.643	10.43	<0.0001
2SD cKO	3.895	5.086	6.713	
3SD con	4.142	6.64	9.299	<0.0001
3SD cKO	4.047	4.914	5.898	

Table 9: p-values for Figure 21

	1SD base con vs cKO	2SD base con vs cKO	3SD base con vs cKO	1SD bac con vs cKO	2SD bac con vs cKO	3SD bac con vs cKO
Fig. 22B	>0.99	0.8	0.25	0.43	0.87	0.85
Fig. 22B	<0.0001	<0.0001	<0.0001	<0.0001	<0.0001	<0.0001
Fig. 22C	0.8	0.09	0.35	>0.99	0.14	0.42
Fig. 22C	<0.0001	<0.0001	0.17	<0.0001	<0.0001	<0.0001

Table 10: p-values for Figure 24

	1SD base con vs cKO	2SD base con vs cKO	3SD base con vs cKO	1SD CGP con vs cKO	2SD CGP con vs cKO	3SD CGP con vs cKO
Fig.24B	0.015	>0.99	0.07	0.012	0.133	0.7
Fig.24B	<0.0001	<0.0001	<0.0001	<0.0001	0.0004	0.0004
Fig.24C	0.9	0.11	0.51	0.37	0.53	0.4
Fig.24C	0.0011	0.72	0.07	<0.0001	<0.0001	0.0012

	1SD bac con vs cKO	2SD bac con vs cKO	3SD bac con vs cKO
Fig.24B	0.42	0.33	0.8
Fig.24B	<0.0001	<0.0001	<0.0001
Fig.24C	0.41	0.7	0.38
Fig.24C	<0.0001	0.0009	<0.0001

Table 11: p-values for Figure 32-33

	1SD con 4w vs 7w Iso2%	2SD con 4w vs 7w Iso2%	3SD con 4w vs 7w Iso2%	1SD cKO 4w vs 7w Iso2%	2SD cKO 4w vs 7w Iso2%	3SD cKO 4w vs 7w Iso2%
Fig. 32B	0.001	0.0003	0.71	<0.0001	0.008	<0.0001
Fig. 32B	0.96	0.0002	0.23	<0.0001	0.022	<0.0001
Fig. 32C	0.61	0.7	0.10	0.5	0.17	0.26
Fig. 32C	<0.0001	<0.0001	0.54	0.0038	0.81	<0.0001
	1SD con 4w vs 7w awake	2SD con 4w vs 7w awake	3SD con 4w vs 7w awake	1SD cKO 4w vs 7w awake %	2SD cKO 4w vs 7w awake	3SD cKO 4w vs 7w awake
Fig. 33B	0.15	<0.0001	<0.0001	0.18	0.007	0.05
Fig. 33B	0.88	<0.0001	<0.0001	<0.0001	<0.0001	<0.0001
Fig. 33C	<0.0001	0.84	0.04	0.21	0.005	0.91
Fig. 33C	<0.0001	0.39	<0.0001	<0.0001	<0.0001	<0.0001

Table 12: p-values for figure 45-46

	1SD con Iso2% vs awake	2SD con Iso2% vs awake	3SD con Iso2% vs awake	1SD cKO Iso2% vs awake	2SD cKO Iso2% vs awake	3SD cKO Iso2% vs awake
Fig. 45B	0.17	0.0006	<0.0001	<0.0001	0.013	0.37
Fig. 45B	0.437	<0.0001	<0.0001	<0.0001	<0.0001	<0.0001
Fig. 45C	0.76	0.0009	0.008	0.40	0.44	0.16
Fig. 45C	<0.0001	<0.0001	<0.0001	<0.0001	<0.0001	0.005
Fig. 46B	0.37	0.33	0.16	<0.0001	<0.0001	<0.0001
Fig. 46B	<0.0001	<0.0001	<0.0001	<0.0001	<0.0001	<0.0001
Fig. 46C	<0.0001	0.0027	0.0098	0.20	0.20	0.45
Fig.46C	<0.0001	0.01	0.56	<0.0001	0.0002	0.21

9. APPENDIX II

9.1 Publications

1. Huang W, Bai X, **Stopper L**, Catalin B, Catarrozzi L, Scheller A, Kirchhoff F. During development NG2 glial cells of the spinal cord are restricted to the oligodendrocyte lineage, but generate astrocytes upon acute injury. Neuroscience. Volume 385, August 2018, Pages 154-16

2. **Stopper L**, Bălşeanu T, Cătălin B, Rogoveanu O, Mogoanta L, Scheller A. Microglia morphology in the physiological and diseased brain – from fixed tissue to in vivo conditions. Rom J Morphol Embryol 2018 April, 59(1):7–12.

3. Cătălin B**, Stopper L,** Bălşeanu T, Scheller A**.** The *in situ* morphology of microglia is highly sensitive to the mode of tissue fixation**.** J Chem Neuroanat. 2017 Dec;86:59-66.

4. Perea G, Gomez R, Mederos S, Ballesteros ACJJ, **Schlosser L**, A Hernandez-Vivanco, Martın-Fernandez M, Quintana R, Rayan A, Dıez A, Fuenzalida M, Agarwal A, Bergles DE, Bettler B, Manahan-Vaughan D, Martın ED, Kirchhoff F, Araque A. Activity-dependent switch of GABAergic inhibition into glutamatergic excitation in astrocyte-neuron networks. Elife. 2016 Dec 24;5.

9.2 Poster presentation

1. **Schlosser L,** Jahn H, Scheller A, Kirchhoff F (2013). Analysis of $GABA_B$ receptor deletion in mouse astrocytes. Poster presentation at the XI European Conference on Glial Cells in Health and Disease Berlin, Germany.

2. **Schlosser L**, Jahn H, Bai X, Scheller A, Kirchhoff F (2015) Deletion of $GABA_B$ receptors in astrocytes. Poster presentation at the XII European Conference on Glial Cells in Health and Disease Bilbao, Spain.

3. **Schlosser L** (2015) Analysis of Analysis of astrocyte-specific and inducible $GABA_B$ receptor deletion in the mouse brain. Oral presentation at the 3rd DAAD-CAPES workshop in Campinas, Brazil.

4. **Schlosser L**, Jahn H, Bai X, Scheller A, Kirchhoff F (2016) Ca2+ signals in awake mice-role of G-protein coupled receptors in glia. Poster presentation at the 1st YoungGlia meeting Tokyo, Japan.

5. **Schlosser L**, Jahn H, Bai X, Caudal LC, Stopper G, Scheller A, Kirchhoff F (2016) Study of astrocyte-specific and inducible $GABA_B$ receptor deletion in the mouse brain, Oral presentation at 12th Göttingen Meeting of the German Neuroscience Society, Göttingen, Germany

6. **Schlosser L**, Bai X, Caudal LC, Stopper G, Scheller A, Kirchhoff F (2017) Study of astrocyte-specific and inducible GABAB receptor deletion in the mouse brain Poster presentation at the XIII European Conference on Glial Cells in Health and Disease Edinburgh, United Kingdom.

Einen ganz großen Danke an meine Mädels, Anna, Anna, Kaddi und Anke. Für euer Verständnis und eure Unterstützung in der Schlussphase dieser Arbeit. Aber auch für die wundervolle Zeit in Saarbrücken. Besonders danke möchte ich Nora: wir kennen uns seid fast 25 Jahren und du warst einer der Menschen auf die ich mich immer verlassen konnte. Catrin, meine gute Seele. Danke für alles, besonders für die regelmäßigen Schokoladenkekse in der letzten Phase der Arbeit.

Ein ganz großer Dank geht an meine Familie. Ihr habt diese Arbeit erst möglich gemacht und mich immer unterstützt. Ihr habt mir immer den Rücken freigehalten und versucht meine Arbeit zu verstehen.

Zu guter Letzt, geht mein Danke an meinen liebsten Menschen und Ehemann Gebhard. Du bist mein Gegenstück und ohne dich wäre so vieles nicht möglich gewesen. Außerdem hast du MSparkles möglich gemacht, auch wenn der Weg dahin nicht einfach war. Einfach nur Danke.